QUANTITATIVE PREDICTION AND INTERPRETATION OF INFRARED SPECTRA

By

STEVEN CHIN

A DISSERTATION PRESENTED TO THE GRADUATE SCHOOL
OF THE UNIVERSITY OF FLORIDA IN
PARTIAL FULFILLMENT OF THE REQUIREMENTS
FOR THE DEGREE OF DOCTOR OF PHILOSOPHY

UNIVERSITY OF FLORIDA

1984

ACKNOWLEDGEMENTS

I would like to express my deepest gratitude to Dr. Person, without whom this work would not have been possible. He has been everything I could possible hope for in an advisor, and more. His patience, understanding and guidance have been the primary inspiration for this work.

I would also like to express my thanks to Drs. Tony Ford and Krystyna Szczepaniak, with both of whom I was fortunate to have many stimulating discussions.

I am also grateful to all the past and present members of this research group for their friendship over the years. Each of you, in your own special way have made an important contribution to this work.

Partial financial support from NSF Research Grant No. CHE81-01131 is gratefully acknowledged, as is a supplemental fellowship from the Graduate School at the University of Florida. In addition, support of some of the computation time from the College of Liberal Arts and Sciences at the University of Florida, and from the Northeast Regional Data Center is gratefully acknowledged.

Finally, I would like to thank Ms. Pam Victor for making the extra effort that was needed to put this thesis in its final typed form.

TABLE OF CONTENTS

		Page
ACKNOWLEDGEMENTS		ii
ABSTRACT		v
CHAPTER		
1	INTRODUCTION	1
2	THEORY	18
	2.1 Coordinate Systems	18
	2.2 Normal Coordinate Analysis	22
	2.3 Infrared Intensity Analysis	25
	2.4 Transformation to Different Coordinate Systems	29
	2.4.1 Internal Force Constants	30
	2.4.2 Atomic Polar Tensors	32
	2.4.3 The $\bar{S}$ Coordinates	33
	2.5 Experimental Infrared Intensities	35
	2.6 Theoretical Infrared Intensities	36
	2.7 Characteristic Invariants of Atomic Polar Tensors	39
	2.8 Quantum Mechanical Interpretation of Atomic Polar Tensors: The Charge, Charge Flux, Overlap Theory (CCFO)	44
3	THE WATER MONOMER	54
	3.1 Calculation Procedure	55
	3.2 The Predicted Spectra for the Water Monomer	58
4	THE LINEAR WATER DIMER	72
	4.1 The Predicted Spectrum for the Linear Dimer	75
	4.2 Intensity Analysis for Linear Pair of Water Molecules	83
	4.3 Frequency Analysis for the Linear Pair of Water Molecules	94
	4.4 Further Calculations on Weaker and Stronger Interacting Linear Pairs of Water Molecules	102

Page

CHAPTER

5 THE CYCLIC WATER WATER COMPLEX 122

5.1 Intensity Analysis for the Cyclic Complex.. 130
5.2 Frequency Analysis for the Cyclic Complex.. 139
5.3 Further Calculations on the Cyclic Complex at Different Interaction Distances 147
5.4 Comparisons Between Linear and Cyclic Complexes 158

6 THE IN-PLANE BIFURCATED WATER-WATER COMPLEX 161

6.1 The Predicted Spectrum for the Bifurcated Water-Water Complex (R = 2.89 A°) 162
6.2 Additional Calculations on the Bifurcated Water-Water Complex 175

7 THE $O^M \cdot H_2O \cdot O^M$ COMPLEX, M = 0, -1, -2 179

7.1 Intensity Theory for Charged Species 180
7.2 The $O^M \cdot H_2O \cdot O^M$ Complex 184
7.3 Intensity Analysis for the $O^M \cdot H_2O \cdot O^M$ Complex 186
7.4 Frequency Analysis for the $O^M \cdot H_2O \cdot O^M$ Complexes 198
7.5 Model for the Infrared Spectra of Beta-Alumina 206

8 IONIZED WATER, H_2O^+ 210

9 GENERAL COMMENTS AND FINAL SUMMARY 223

9.1 Comments on the Charge Flux, Charge, and Overlap Tensors 226
9.2 Other Applications for These Calculations.. 234

APPENDIX

A SUMMARY OF PROGRAMS 238

B NORMAL COORDINATE TRANSFORMATION MATRICES 245

C REDUNDANT INTERNAL COORDINATES 247

REFERENCES 251

BIOGRAPHICAL SKETCH 257

Abstract of Dissertation Presented to the Graduate School of the University of Florida in Partial Fulfillment of the Requirements for the Degree of Doctor of Philosophy

QUANTITATIVE PREDICTION AND INTERPRETATION OF INFRARED SPECTRA

By

Steven Chin

April 1984

Chairman: Willis B. Person
Major Department: Chemistry

Ab initio quantum mechanical calculations at the self consistent field level have been performed for interacting water molecules to predict their infrared spectra. These calculations have been made using Gaussian 76 and a 4-31G basis set. The calculated ab initio force field has been used to predict the fundamental absorption frequencies and the corresponding normal coordinate transformation. This normal coordinate transformation has then been used in conjunction with Atomic Polar Tensors (APTs) that were also found in the ab initio calculation to predict the absolute integrated intensities for these fundamental normal vibrations.

The role that the chemical environment plays in the predicted spectra for interacting water molecules has been

investigated by analyzing the predicted spectra for different assumed orientations of the "complex" at various assumed intermolecular distances, and by varying the electron donating properties of the electron donor. The former effect was investigated by predicting spectra for water pairs in the linear, cyclic, and bifurcated configurations, at varying intermolecular distances. The latter effect was studied by calculating the spectra for water complexed with two oxygen atoms which have varying charge ($O^M \cdot H_2O \cdot O^M$, where M = 0, -1, or -2) where the oxygen atoms with the larger negative charge are stronger electron donors. Finally, the spectrum for ionized water, H_2O^+, is also predicted.

These calculations indicate that both the frequencies and intensities of the vibrations for water interacting with its environment are predicted to be strongly dependent upon the nature of this environment. The predicted spectra for these water molecules in different chemical environments are then compared with the predicted spectrum for isolated monomeric water, and also experimental spectra when available. The vibrational changes from isolated water to the interacting water molecule in these different environments are then analyzed and discussed to provide some insight into the effect of intermolecular interactions on the vibrational spectrum of the interacting molecule.

CHAPTER 1
INTRODUCTION

The infrared spectrum of a molecule is an extremely rich and valuable source of information. For many years it has been used in both the qualitative and quantitative analysis of chemical compounds. The concept of group frequencies (1), and its use in the identification of molecular compounds is one of the most fundamental and fruitful applications of infrared spectroscopy. As a result, most experimental spectroscopists, and theoreticians working with them, traditionally placed great emphasis on the locations of the band centers, or absorption frequencies. In recent years, however, there has also been an increased interest not only on the fundamental infrared absorption frequencies, but also on the absolute integrated intensities (2,3). Specifically, there has been a great deal of interest in the parameterization and interpretation of infrared intensities. The use of electro-optical intensity parameters (EOPs) (4,5) has been pioneered by the Soviet workers (6), while the use of Atomic Polar Tensors (APTs) was first introduced by Biarge, Herranz, and Morcillo (7), and later reformulated by Person and Newton (8) and used in conjunction with quantum mechanical calculations of signs of $(\partial P/\partial Q)$s. Both methods have had good success in the parameterization of infrared intensities (9). The APT

method is particularly useful in quantum mechanical calculations and therefore has been adopted here.

The success of the quantum mechanical calculations of APTs offers hope that in the future the prediction of infrared intensity parameters may be almost routine. Using these intensity parameters, the absolute integrated intensities can be predicted, provided that the normal coordinate transformation is well known. The normal coordinate transformation can be easily obtained from the force field of the molecule by performing a normal coordinate analysis (10,11). Unfortunately, the available experimental data are usually not sufficient to determine completely an accurate vibrational force field. For this reason quantum mechanical calculations of vibrational force fields have become increasingly more popular (12-16). These calculations, coupled with the calculation of APTs, have made possible the completely ab initio prediction of infrared spectra (including both band frequencies and absolute intensities).

These predictions are useful for several reasons. They can be extremely helpful in assigning complicated spectra (17), especially spectra for relatively large (> 10 atoms) molecules. A second application of these types of calculations concern chemical systems which cannot be isolated in pure form and packaged in a bottle. These systems include radicals and ions (18) frozen in rare-gas matrices, reaction intermediates observed by time-resolved spectroscopy or observed on catalytic surfaces, molecular fragments existing

in flames and plasma, small molecular compounds that are believed to exist in space, and dimers or other intermolecular complexes that are found in rare-gas matrices or supersonic expansions. In recent years there has been an increased interest in the application of vibrational spectroscopy towards characterizing these unstable and hard to isolate molecular species. However, this task is made much more difficult by the absence of spectroscopic standards and standard spectra. Therefore, any spectral determination of the concentration of these transient species must rely on a separate estimate of its intensities. The development of ab initio calculations of these intensities appears to be well suited for making these estimates. Additionally, the spectral patterns predicted by these calculations (including both wavenumbers and intensities) can be qualitatively used as a direct confirmation of the spectral assignment for the species, especially in the absence of standard spectra. The calculated intensities would be especially valuable in the case that the observed wavenumbers of the unstable species could not be compared with those of a structurally similar stable molecule; or in the opposite situation where the observed wavenumbers matched equally well with more than one structure. In situations such as these the correct assignment must match the predicted wavenumbers as well as the predicted intensity pattern.

There are very encouraging developments in the ab initio predictions of infrared spectra of unstable or hard-to-isolate

molecular species. However, these methods must be further tested if one is to be able to routinely predict reliable spectra for these types of species. Therefore, we have used the ab initio method to predict and interpret spectra of some of these types of species.

The water dimer has been the subject of many experimental (19-29), and theoretical (30-41) investigations. One reason for this interest is that it is thought to be a prototype model for liquid water, which is of paramount importance in the life of biological systems. A second reason is that the water dimer is a classic example of a donor-acceptor complex, in this case, specifically a hydrogen bonded complex. The water dimer represents a unique example of a hydrogen bonded system because one water molecule is the electron donor and another is the electron acceptor.

The importance of vibrational spectroscopy in the study of H-bonded systems is well documented (42,43). The infrared spectra of such complexed species exhibit characteristic spectral changes when compared with that of the corresponding isolated molecules and with the spectra of other complexes. The comparisons among these spectra are valuable sources of information concerning the properties and characteristics of these systems.

The hydrogen bond interaction can be described as an intermolecular interaction through a hydrogen atom. Typically, the interaction is of the type RAH--B, where RAH is an electron acceptor, B is an electron donor molecule, and the hydrogen bond is the H--B interaction. When water is

both the electron acceptor and the donor, A-H is the O-H bond of one water molecule, and the electron donor B is the oxygen atom in the other water molecule. In the water dimer, this interaction is slightly more complicated by the presence of two O-H bonds. In the isolated molecule, these two bonds are symmetrically equivalent, and therefore are strongly coupled to form two stretching vibrations, a symmetric stretch and an asymmetric stretch. In the complex the symmetry is reduced in relation to the isolated monomer, the O-H bonds are no longer symmetric, and the coupling between these two bonds is reduced. In general, the forces governing intramolecular coupling are much stronger than those governing hydrogen bonding. Therefore, this reduction in coupling between the two O-H bonds is important to consider in analyzing complexes involving water molecules.

For H-bonded complexes, the vibration most perturbed by the interaction is the symmetric stretch. This band undergoes a shift to lower energy, and an increase in intensity. The similarities and differences between these two changes in the spectra of H-bonded systems are vital to our understanding of these complexes.

The frequency shift is usually thought to originate in a weakening of the A-H bond as the H-bond is formed. This in turn is believed to be due primarily to two effects: the polarization effect, where the donor molecular polarizes electron density from the A-H bond into the non-bonding region of the A atom, where it no longer compensates for the A-H nuclear repulsion; and the electron transfer effect, where the donor molecule donates electron density into the antibonding

orbitals of the acceptor molecules, thereby weakening the bond. Regardless, the net result is that the A-H bond is weakened, and so the frequency shifts towards lower energy. This effect can be analyzed by calculating the internal force constants for the complex.

The intensity enhancement is well known experimentally, but not as well understood. The electrostatic polarization and charge-transfer effects just mentioned cannot individually account for the great enhancement in the intensity. Zilles and Person (39) have recently applied a quantum mechanical model of the APTs in order to interpret the intensity enhancement for the water dimer. They have found that the largest single most important contribution to the intensity enhancement is from the increase in charge flows in the complex compared to the monomer. This interpretation can be taken one step further by attempting to compare the nature of these charge flows in the linear dimer with those in other systems involving water as the electron acceptor.

Furthermore, the reduction in coupling between the two O-H bonds usually creates some mixing between the symmetric stretching vibrations and both the bending and assymetric stretching vibrations. So, in effect, it is no longer strictly a symmetric stretching vibration, but a mixture of all three vibrations. Naturally, a consequence of this mixing is that the normal vibrations in the complex are no longer the same vibrations as those in the isolated molecule. The intensities, as well as the frequencies, are strongly dependent upon the form

of the normal vibrations. The effect of these changes on both the frequencies and intensities are also important to understanding the spectral changes present in the complex, and these effects will be examined in detail.

The experimental studies of the infrared spectrum of the water dimer are quite varied with respect to the interpretation of the results. Most of these results have been previously summarized (41 and references cited therein). The most generally accepted interpretation of the infrared spectrum is that of Tursi and Nixon (19). They have assigned the six high frequency modes of the water dimer in a nitrogen matrix. Their assignment is consistent with a linear structure (see Fig. 1.1) for the dimer, and is accepted by many as the correct interpretation for the dimer. Other workers prefer the cyclic (see Fig. 1.2) structure (20,21,24), while still others postulate the existence of the bifurcated structure (see Fig. 1.3) (26).

Most theoretical calculations support the linear structure as the most stable geometry for the water dimer (31,34). Zilles and Person (39) have used the experimental force field of Tursi and Nixon (19) for this linear structure and quantum mechanical APTs to predict and interpret the infrared intensities of the linear dimer. To expand and further develop our understanding of the infrared spectra of interacting molecules we have used ab initio quantum mechanical calculations to predict the vibrational force fields and APTs for not only the linear configuration, but also the cyclic and the bifurcated

Figure 1.1 Geometrical orientation for the linear water dimer. The assumed intramolecular parameters are:

R $(H_1\text{-}O_3)$ = .950 A°	R $(H_4\text{-}O_5)$ = .958 A°
R $(H_2\text{-}O_3)$ = .950 A°	R $(O_5\text{-}H_6)$ = .950 A°
θ $(H_1\text{-}O_3\text{-}H_2)$ = 112°	$\theta(H_4\text{-}O_5\text{-}H_6)$ = 111.3°

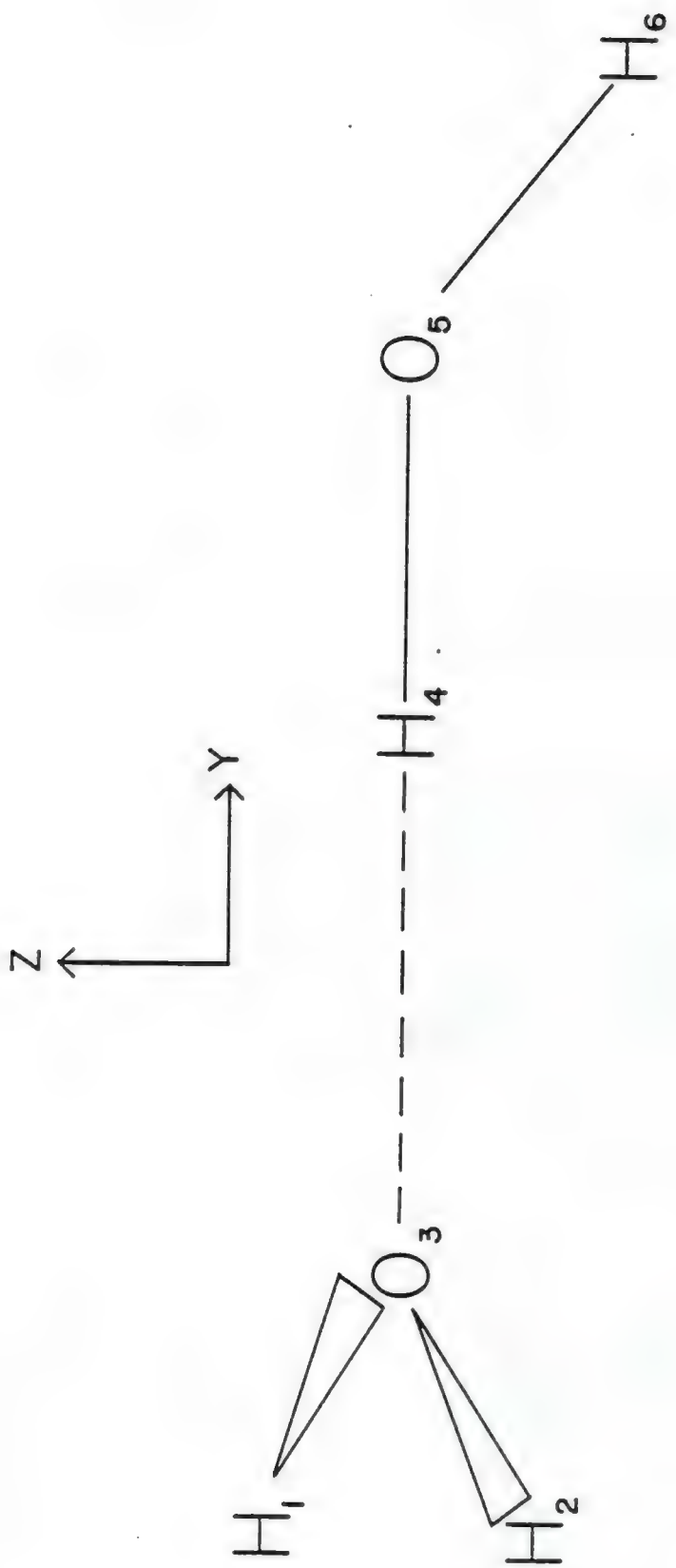
H6
O5
H4
Y
Z
O3
H1
H2

Figure 1.2 Geometrical orientation for the cyclic configuration of a pair of interacting water molecules. The assumed intramolecular parameters are:

$$R\ (H_2\text{-}O_1) = R\ (H_5\text{-}O_1) = R\ (H_4\text{-}O_3) = R\ (H_6\text{-}O_3) = .951\ A^\circ$$

$$\theta\ (H_5\text{-}O_1\text{-}H_2) = \theta\ (H_1\text{-}O_3\text{-}H_6) = 111.2^\circ$$

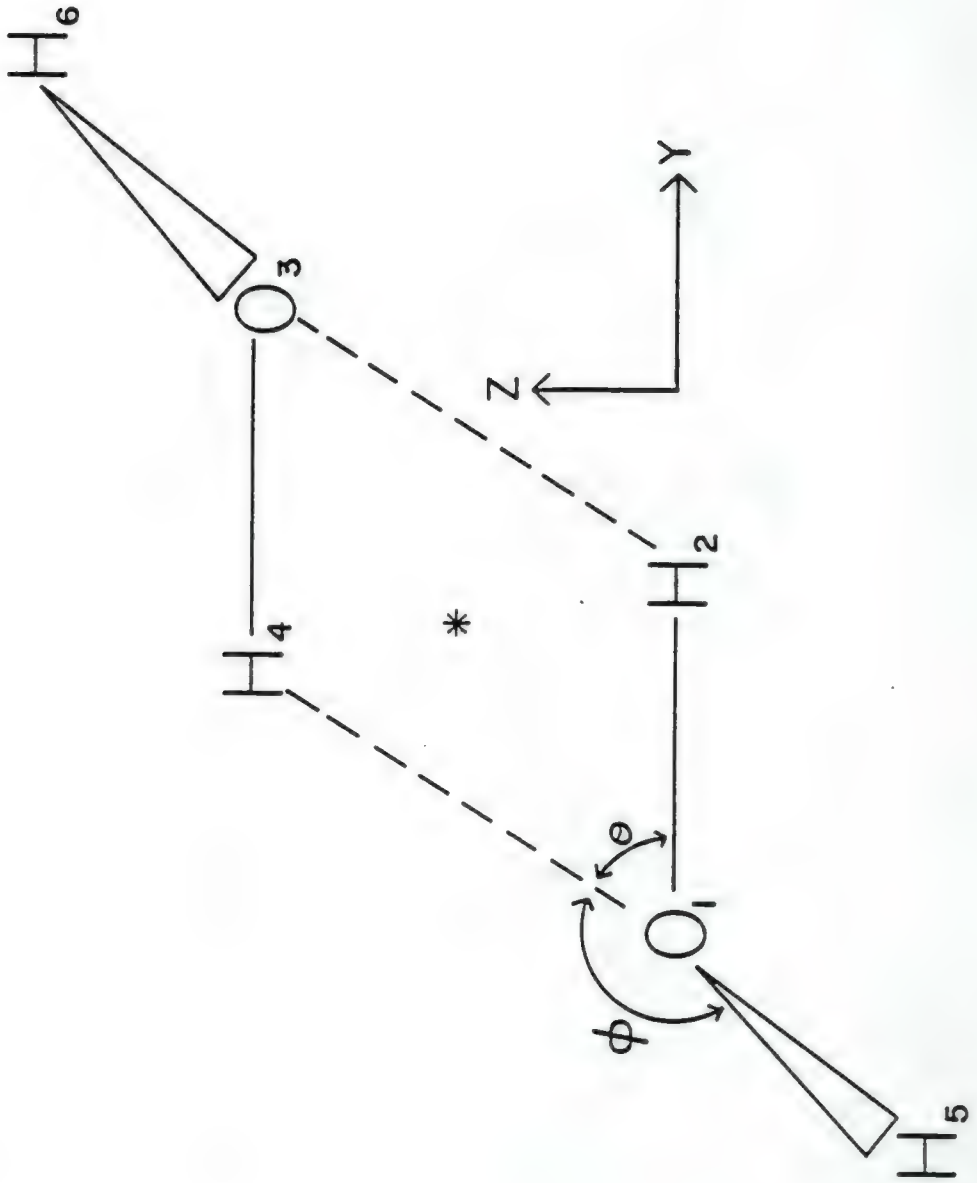
H6
O3
Y
Z
H2
H4
*
θ
O1
φ
H5

Figure 1.3 Geometrical orientation for the bifurcated configuration of a pair of interacting water molecules. The assumed intramolecular parameters are:

$$R\ (H_1\text{-}O_2) = R\ (H_3\text{-}\ O_2) = R\ (H_4\text{-}O_5) = R\ (H_6\text{-}O_5) = .951\ A^\circ$$

$$\theta\ (H_1\text{-}O_2\text{-}H_3) = \theta\ (H_4\text{-}O_5\text{-}H_6) = 111.2^\circ$$

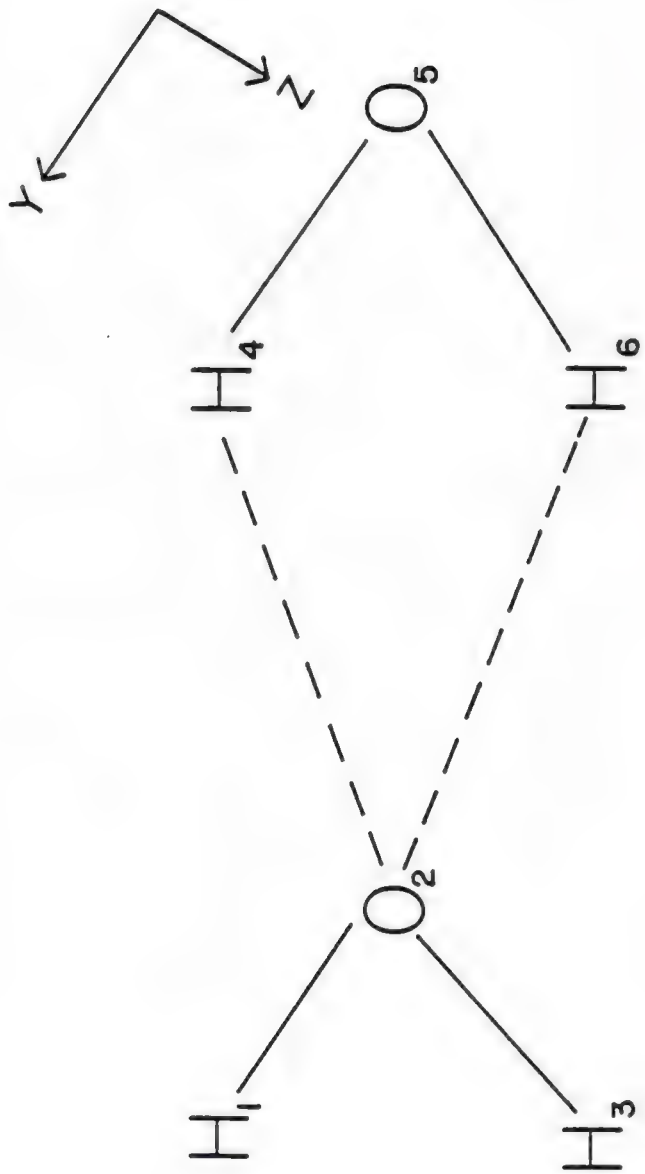
Z
Y
O5
H4
H6
O2
H1
H3

structures. We will examine the spectra predicted for these three different configurations and discuss the differences among them, as well as the differences between our calculations and those of Zilles and Person (39). In addition, we have tried to simulate the extremum, namely complete electron donation, by calculating the spectrum of H_2O^+.

Finally, the infrared spectrum of a model for water isolated in a beta-alumina complex has been calculated. Water, as an impurity in beta-alumina, is important to the electrical conductivity and mechanical strength properties of beta-alumina (44). This in turn is important towards the use of beta-alumina as solid electrolyte in the sodium-sulfur battery. Until recently, the nature of the hydration reaction of beta-alumina was not known. Bates and coworkers (45) have determined that the water molecules diffuse into the conduction layers and form strong electrostatic bonds with the mobile cations, thereby affecting the properties of the beta-alumina. Infrared spectroscopy is used as a tool to probe the kinetics and thermodynamics of the reaction of water with beta-alumina. Therefore, before attempting to use the infrared spectrum as a probe for other properties, it is important to first understand the structure and vibrational properties of hydrated beta-alumina. Bates and coworkers have recently determined the crystal structure and vibrational spectrum of hydrated beta-alumina (44). The water molecules are located in the crystal so that they are strongly hydrogen-bonded to the oxygen atoms of the aluminate ion (see Fig. 1.4).

Figure 1.4 Geometrical orientation for the $O^{M} \cdot H_2O \cdot O^{M}$ complexes, M = 0, -1, -2. The assumed intramolecular parameters are:

$$R\ (H_2\text{-}O_3) = R\ (H_4\text{-}O_3) = .991\ A^\circ$$

$$\theta\ (H_2\text{-}O_3\text{-}H_4) = 114^\circ$$

$$R(O_1\text{-}H_2) = R(O_5\text{-}H_4) = 1.671\ A^\circ$$

$$\theta(O_3\text{-}H_2\text{-}O_1) = (O_5\text{-}H_4\text{-}O_3) = 159.3^\circ$$

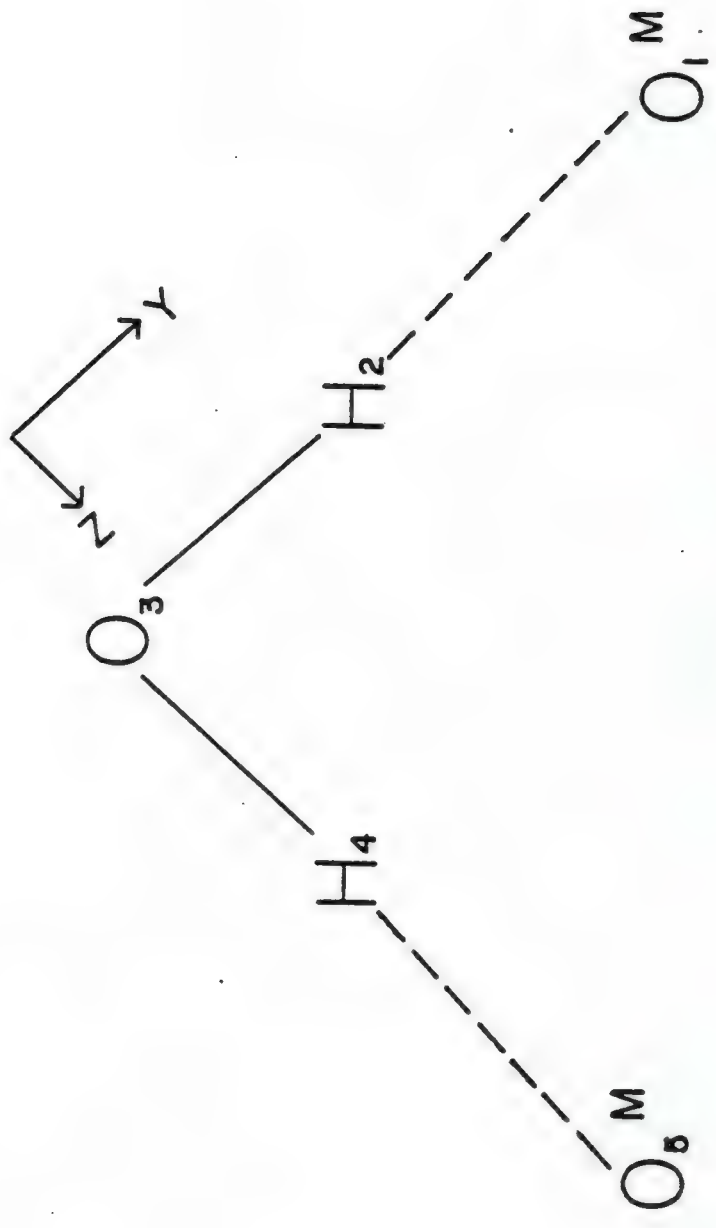
O_1^M
H_2
Y
Z
O_3
H_4
O_5^M

Consequently, this is a good system to use to expand our studies on hydrogen bonded water molecules.

The quantum mechanical calculation of the spectrum of hydrated beta-alumina takes on importance for several reasons. First, it offers the opportunity to verify (or dispute) the experimental spectrum and the interpretation of this spectrum. Secondly, it represents a different example of an intermolecular interaction involving a water molecule. It offers the opportunity to investigate the role that the electron donor plays in intermolecular interactions. And lastly, it is a challenge to our ability to simulate a complicated chemical system by using a rather simple model.

A summary of the calculational procedure developed for this work, along with a review of both normal coordinate analysis and infrared intensity analysis, is given in Chapter 2. The results of these calculations on isolated water monomers and the linear, cyclic, and bifurcated forms of a pair of interacting water molecules are presented in Chapters 3, 4, 5, and 6 respectively. The importance of some of the effects just discussed, such as coupling between O-H bonds, weakening of the O-H bond, charges flows, and the mixing of normal coordinates, are discussed with respect to each of the systems calculated. The predicted spectrum for our model of water isolated in a beta-alumina complex is given in Chapter 7, and the predicted spectrum for H_2O^+ is presented in Chapter 8. A final summary and suggestions for future calculations are presented in Chapter 9.

CHAPTER 2
THEORY

The theory of both normal coordinate analysis (10,11,46) and infrared intensity analysis (2,3,41,47,48) is well known and described fully elsewhere. We have developed a slightly different approach to analyze simultaneously the normal coordinated and infrared intensities. This method will be discussed in detail, including the similarities and differences with the more traditional procedures.

2.1 Coordinate Systems

A polyatomic molecule of N atoms has 3N degrees of freedom. Of these 3N degrees of freedom some are rigid body motions (translations and rotations) and some are elastic body motions (vibrations). The analysis of the molecular vibrations is best done in a coordinate system which allows the maximum separation of the overall motions into translations, rotations, and vibrations. This problem has been discussed in the past (11,49,50), and amounts to choosing a coordinate system such that the interactions between vibrations and the translations and rotations are minimized. The necessary coordinate system is a molecule fixed coordinate system which translates and rotates along with the molecule. These conditions require that there is no component of either

translation or rotation present in a vibration, are are known as the Eckart-Sayvetz conditions (11).

The Eckart-Sayvetz conditions provide explicit definitions for the translations and rotations of a molecule. They are given below in terms of mass-weighted principal cartesian coordinates (11).

$$\rho_1 = \frac{1}{M_o^{1/2}} \sum_\alpha m_\alpha^{1/2} q_{x_\alpha}$$

$$\rho_2 = \frac{1}{M_o^{1/2}} \sum_\alpha m_\alpha^{1/2} q_{y_\alpha}$$

$$\rho_3 = \frac{1}{M_o^{1/2}} \sum_\alpha m_\alpha^{1/2} q_{x_\alpha}$$

$$\rho_4 = \sum_\alpha \left(\frac{m_\alpha}{I_{xx}}\right)^{1/2} (y_\alpha^o q_{z_\alpha} - z_\alpha^o q_{y_\alpha}) \qquad (1)$$

$$\rho_5 = \sum_\alpha \left(\frac{m_\alpha}{I_{yy}}\right)^{1/2} (z_\alpha^o q_{x_\alpha} - x_\alpha^o q_{z_\alpha})$$

$$\rho_6 = \sum_\alpha \left(\frac{m_\alpha}{I_{zz}}\right)^{1/2} (x_\alpha^o q_{y_\alpha} - y_\alpha^o q_{x_\alpha})$$

Here ρ_1, ρ_2, ρ_3, ρ_4, ρ_5, and ρ_6 represent translation and rotation in the x, y, and z directions, respectively, M_o is the total mass of the molecule, m_α is the mass of atom , x_α^o, y_α^o, and z_α^o are the principal cartesian coordinates for atom α, q_{x_α}, q_{y_α}, and q_{z_α} are the mass weighted principal cartesian coordinates for atom α, and I_{xx}, I_{yy}, and I_{zz} are the moments of inertia along the principal cartesian axes, or the principal moments of inertia.

The remaining vibrational coordinates should reflect these constraints, and at the same time form a complete, nonredundant, vector representation of the vibrational subspace. The calculations can be further simplified by utilizing the symmetry of the molecule and by requiring that all the coordinates be orthogonal to each other. The resulting coordinate system is a mass-weighted, molecule-fixed, symmetry-adapted, principal cartesian coordinate system, hereafter denoted as the $\bar{S}$ coordinates.

The transformation from mass-weighted principal cartesian coordinates $\bar{q}$ to $\bar{S}$ coordinates can be written in matrix notation as

$$\bar{S} = \underline{U}\,\bar{q} \tag{2a}$$

where $\underline{U}$ is an orthogonal transformation matrix and $\bar{q}$ is the column vector representation of the mass-weighted principal cartesian coordinates. The matrix $\underline{U}$ can be constructed via a Gram-Schmidt orthogonalization (51) of the irreducible representations of the cartesian coordinates to the Eckart-Sayvetz conditions. The linear combinations of the principal cartesian coordinates which reduce as the irreducible representations of the point group of the molecule can be found by following the prescription given in Cotton (52). These linear combinations are then made orthogonal to the Eckart-Sayvetz conditions, giving the $\underline{U}$ matrix.

Since $\underline{U}$ is constructed as an orthogonal matrix, its inverse is simply $\underline{U}^{+}$ where $\underline{U}^{+}$ represents the transpose of $\underline{U}$.

Equation 2a can now be rewritten as

$$\bar{q} = \underline{U}^{+}\bar{S} \tag{2b}$$

where all the symbols have their previously defined meanings. Equation 2b can now be applied in the method of finite differences (53) in order to calculate the force constants and dipole derivatives in $\bar{S}$ coordinates. The values of $\bar{S}$ are incremented by a specific amount, usually $\pm 0.01\ u^{\frac{1}{2}}$ A°, and equation 2b is used to calculate the values at $\bar{q}$ of these displaced values of $\bar{S}$.

The Gaussian 76 ab initio molecular orbital program (54) is then used to calculate the energies and dipole moments for the equilibrium geometry and also at appropriate displacements from equilibrium. The force constants are derived by assuming a pure quadratic potential, and then calculating the second derivatives of this potential function. Mathematically, these constants can be calculated by using the following equations (from (53))

$$F_{xx} = \frac{E(x_o+\Delta x) + E(x_o-\Delta x) - 2E(x_o)}{\Delta x^2} \tag{3}$$

$$F_{xy} = \frac{(E(x_o+\Delta x, y_o+\Delta y) - E(x_o+\Delta x, y_o) - E(x_o, y_o+\Delta y) + E(x_o, y_o)}{\Delta x \Delta y} \tag{4}$$

where F_{xx} represents a diagonal force constant, F_{xy} an off-diagonal force constant, $E(x_o)$ the energy at the equilibrium configuration, $E(x_o+\Delta x)$ and $E(x_o-\Delta x)$ the energies at the positive and negative displacements of coordinate x from

equilibrium respectively, $E(x_o+\Delta x, y_o+\Delta y)$ the energy at the simultaneous positive displacement of both coordinate x and y, and Δx the numerical value of the displacement of coordinate x. The dipole derivatives are approximated by averaging the displacements at the positive and negative distortions, to account in part for the nonlinearity of the dipole moment.

$$\frac{\partial P_\alpha}{\partial x} \cong \frac{\Delta P_\alpha}{\Delta x} = \left(\frac{P_\alpha(x_o+\Delta x) - P_\alpha(x_o)}{2\Delta x} + \frac{P_\alpha(x_o-\Delta x) - P_\alpha(x_o)}{2\Delta x} \right) = \frac{P_\alpha(x_o+\Delta x) - P_\alpha(x_o-\Delta x)}{2\Delta x} \tag{5}$$

Here $P_\alpha(x_o)$ represents the permanent equilibrium dipole moment in the α = x, y, or z direction, $P_\alpha(x_o+\Delta x)$ and $P_\alpha(x_o-\Delta x)$ represent these same components of the dipole moment at the positive and negative displacements of coordinate x respectively, and Δx is the displacement of coordinate x.

2.2 Normal Coordinate Analysis

After the force constants have been calculated, the next step is to derive the vibrational frequencies and the nature of the normal vibrations (or the normal coordinate transformation). For a harmonic oscillator the solution of Newton's equations of motion gives the secular equation (11),

$$|\underline{GF} - \underline{E\Lambda}| = 0 \tag{6}$$

where $\underline{F}$ is the potential energy matrix, $\underline{G}$ is the inverse kinetic energy matrix, $\underline{E}$ is the identity matrix and $\underline{\Lambda}$ is the eigenvalue matrix. The solution to this system of homogeneous linear equations gives the eigenvalues, or normal

frequency paramaters $\underline{\Lambda}$, and the eigenvectors, or column vector representations of the normal coordinates, also known as the normal coordinate transformation matrix, $\underline{L}$.

If the potential energy matrix is represented in mass-weighted cartesian coordinates, then the $\underline{G}$ matrix becomes the identity matrix (11). Equation 6 can be rewritten as

$$\underline{K}\ \underline{\ell} = \underline{\ell}\ \underline{\Lambda} \tag{7}$$

where $\underline{K}$ represents the matrix of force constants in mass-weighted cartesian coordinates, $\underline{\ell}$ is the eigenvector matrix in these coordinates, and $\underline{\Lambda}$ is the diagonal eigenvalue matrix. The values of $\underline{\Lambda}$ are related to the vibrational frequencies by

$$\nu_i(cm^{-1}) = \lambda_i^{\frac{1}{2}} \left(\frac{md}{u^{-1}_A}\right) * \left(\frac{1}{2\pi c}\right) \text{ or } \nu_i = 1303.1*\lambda_i^{\frac{1}{2}} \tag{8}$$

and the matrix $\underline{\ell}$ is the orthogonal normal coordinate transformation which transforms from normal coordinates to mass-weighted cartesian coordinates

$$\overline{q} = \underline{\ell}\ \overline{Q} \tag{9}$$

where $\overline{Q}$ is the vector of normal coordinates. Thus in mass-weighted cartesian coordinates solving the secular equation reduces to finding the matrix $\underline{\ell}$ which diagonalizes the potential energy matrix, $\underline{K}$.

$$\underline{\ell}^{+}\underline{K}\ \underline{\ell} = \underline{\Lambda} \tag{10}$$

Therefore the force constants calculated in $\overline{S}$ coordinates must

be transformed to force constants in mass-weighted cartesian coordinates $\underline{K}$. The force constants in $\bar{S}$ coordinates, $\underline{K}$, can be easily transformed to mass-weighted cartesians using the $\underline{U}$ matrix. Since this matrix is orthogonal its inverse is simply equal to $\underline{U}^{+}$. In mass-weighted cartesians the potential and kinetic energies are equal to

$$2T = \dot{\bar{q}}^{+}\underline{G}^{-1}\dot{\bar{q}} \tag{11}$$

$$2V = \bar{q}^{+}\underline{K}\,\bar{q} \tag{12}$$

respectively, where $\dot{\bar{q}}$ represents differentiation with respect to time, and $\underline{G}^{-1}$ is actually the identity matrix, $\underline{E}$, since the potential energy is now expressed in mass-weighted cartesian coordinates.

In $\bar{S}$ coordinates the potential and kinetic energy can be written as

$$2T = \dot{\bar{S}}^{+}\,\underline{G}^{-1}\,\dot{\bar{S}} \tag{13}$$

$$2V = \bar{S}^{+}\,\underline{K}\,\bar{S} \tag{14}$$

where $\underline{G}$ is the inverse kinetic energy matrix in $\bar{S}$ coordinates and $\underline{K}$ is the potential energy matrix in $\bar{S}$. Since

$$\bar{S} = \underline{U}\,\bar{q} \text{ and } \bar{S}^{+} = \bar{q}^{+}\underline{U}^{+} \tag{15}$$

equation 13 and 14 can be rewritten as

$$2T = \dot{\bar{q}}^{+}\,\underline{U}^{+}\,\underline{G}^{-1}\,\underline{U}\,\dot{\bar{q}} \tag{16}$$

$$2V = \bar{q}^{+}\,\underline{U}^{+}\,\underline{K}\,\underline{U}\,\bar{q} \tag{17}$$

By comparing equations 12 and 17 the transformation from $\underline{K}$ to $\underline{K}$ can be written as

$$\underline{K} = \underline{U}^{+} \underline{K} \underline{U} \tag{18}$$

The secular equation can now be solved in terms of mass-weighted cartesian coordinates using equation 10.

Here $\underline{\ell}^{+}$ is a matrix of dimension 3N by 3N, and each row of this matrix represents one of the 3N normal modes. Six (or five for linear molecules) of these modes are the translations and rotations, and the remaining modes are the fundamental vibrations. Each row of $\underline{\ell}^{+}$ consists of N (3 by 1) vectors corresponding to the motion of each atom N in that particular normal coordinate. By analyzing the corresponding vectors for each atom we can determine what motions constitute that particular normal vibration. This will be discussed in more detail later. The matrix $\underline{\Lambda}$ is a diagonal one containing the eigenvalues of the secular equation. Six of these eigenvalues correspond to the translations and rotations of the molecule, and are therefore of value zero. The remaining values give the vibrational frequencies via equation 8.

2.3 Infrared Intensity Analysis

The absolute infrared intensity of the ith vibrational mode of a molecular is proportional to the square of the dipole moment derivative with respect to motion along the ith normal coordinate. In units of km/mole this becomes (2)

$$A_i \text{ (km/mole)} = 974.9 \, d_i \left| (\partial P / \partial Q_i) \right|^2 \tag{19}$$

where d_i is the degeneracy of the ith mode, and $(\partial P/\partial Q_i)$ is given in units of $e \cdot u^{\frac{1}{2}}$ where e is the atomic unit of charge, equal to 1.602×10^{-19}C. If the value of the dipole moment derivative with respect to the normal coordinate is known, then the intensity for that mode can be easily calculated with equation 19. The problem of infrared intensity analysis then reduces to evaluating and interpreting this derivative.

As stated previously, the method of finite differences can be used to approximate the dipole moment derivatives. By using equation 5, the dipole moment derivatives in $\overline{S}$ coordinates can be calculated. Since the normal coordinate transformation is given in terms of mass-weighted cartesians, then the dipole moment derivatives must be transformed to this same coordinate system in order to utilize this normal coordinate transformation to calculate the intensities. This transformation is written as

$$\underline{P_q} = \underline{P_S}\ \underline{U} \tag{20}$$

where $\underline{P_q}$ is the 3x3N matrix of the dipole derivatives in mass-weighted cartesians and $\underline{P_S}$ is the corresponding 3x3N matrix of dipole derivatives in $\overline{S}$. The first six (or five for linear molecules) columns represent the dipole derivatives with respect to the three translational and three rotational motions respectively. These values can be calculated from the charge of the molecule (q_e), the mass of molecule (M_o), the principal moments of inertia (I_{xx}, I_{yy}, and I_{zz}) and the vector components of the permanent dipole moment P_x, P_y, and P_z. These relations are

given by King (55) and have recently been reformulated by Rogers and Hillman (56), and are summarized below in columns one through six. The remaining columns of this matrix, $\underline{P_S}$, are calculated using equation 5, and represent the dipole derivatives with respect to the vibrational $\bar{S}$ coordinates. The three rowsof this matrix represent differentiation of one of each of the three vector components of the dipole moment; either P_x, P_y, or P_z.

$$\underline{P_S} = \begin{pmatrix} \frac{q_e}{M_o^{1/2}} & 0 & 0 & 0 & \frac{P_z^o}{I_{yy}^{1/2}} & \frac{-P_y^o}{I_{zz}^{1/2}} & \frac{\Delta P_x}{\Delta S_7} \cdots\cdots & \frac{\Delta P_x}{\Delta S_{3N}} \\ 0 & \frac{q_e}{M_o^{1/2}} & 0 & \frac{-P_z^o}{I_{xx}^{1/2}} & 0 & \frac{P_x^o}{I_{zz}^{1/2}} & \frac{\Delta P_y}{\Delta S_7} \cdots\cdots & \frac{\Delta P_y}{\Delta S_{3N}} \\ 0 & \frac{q_e}{M_o^{1/2}} & \frac{P_y^o}{I_{xx}^{1/2}} & \frac{-P_x^o}{I_{yy}^{1/2}} & 0 & \frac{\Delta P_z}{\Delta S_7} \cdots\cdots & \frac{\Delta P_z}{\Delta S_{3N}} & \end{pmatrix} \tag{21}$$

The matrix $\underline{P_q}$ consists of the dipole moment derivatives in mass-weighted cartesian coordinate space. By removing the mass dependence the derivatives in cartesian coordinates are obtained

$$\underline{P_x} = \underline{P_q}\ \underline{M}^{1/2} \tag{22}$$

where $\underline{P_x}$ is composed of the juxtaposition of the Atomic Polar Tensors (APTs) (57) for the N atoms in the molecule, and $\underline{M}^{1/2}$ is a diagonal matrix represented by the triplet sets of the square root of the masses of the atoms in the molecule. The

$\underline{P_x}$ matrix has the general form (3 x 3N)

$$\underline{P_x} = \begin{pmatrix} \frac{\partial P_x}{\partial X_A} & \frac{\partial P_x}{\partial Y_A} & \frac{\partial P_x}{\partial Z_A} & \cdots\cdots\cdots\cdots & \frac{\partial P_x}{\partial X_N} & \frac{\partial P_x}{\partial Y_N} & \frac{\partial P_x}{\partial Z_N} \\ \frac{\partial P_y}{\partial X_A} & \frac{\partial P_y}{\partial Y_A} & \frac{\partial P_y}{\partial Z_A} & \cdots\cdots\cdots\cdots & \frac{\partial P_y}{\partial X_N} & \frac{\partial P_y}{\partial Y_N} & \frac{\partial P_y}{\partial Z_N} \\ \frac{\partial P_z}{\partial X_A} & \frac{\partial P_z}{\partial Y_A} & \frac{\partial P_z}{\partial Z_A} & \cdots\cdots\cdots\cdots & \frac{\partial P_z}{\partial X_N} & \frac{\partial P_z}{\partial X_N} & \frac{\partial P_z}{\partial Z_N} \end{pmatrix} \qquad (23)$$

The APTs will be discussed in more detail later.

The transformation from $\underline{P_q}$ to $\underline{P_Q}$, and in essence the absolute integrated intensities, can be accomplished with the $\underline{\ell}$ matrix

$$\underline{P_Q} = \underline{P_q}\ \underline{\ell} \qquad (24)$$

where $\underline{P_Q}$ is the matrix of dipole moment derivatives in normal coordinate space. This matrix is also 3 by 3N, with the first five or six columns corresponding to the dipole derivatives with respect to the translations and rotations. The values of these derivatives are all zero since there is no component of vibration in a pure translation or rotation, and hence no intensity or frequency for these modes. Each of the next (3N-6) columns corresponds to the dipole derivatives with respect to one of the (3N-6) vibrational normal modes. The derivative of one of the three vector components of the dipole moment P_x, P_y, and P_z are again each responsible for one of the three rows of this matrix. This matrix has the following representation

$$\underline{P_Q} = \begin{pmatrix} 0 & 0 & 0 & 0 & 0 & 0 & \frac{\partial P_x}{\partial Q_7} & \cdots\cdots & \frac{\partial P_x}{\partial Q_{3N}} \\ 0 & 0 & 0 & 0 & 0 & 0 & \frac{\partial P_y}{\partial Q_7} & \cdots\cdots & \frac{\partial P_y}{\partial Q_{3N}} \\ 0 & 0 & 0 & 0 & 0 & 0 & \frac{\partial P_z}{\partial Q_7} & \cdots\cdots & \frac{\partial P_z}{\partial Q_{3N}} \end{pmatrix} \quad (25)$$

The absolute integrated intensity for the ith mode is simply proportional to the sum of the squares of the vector components of the dipole moment derivatives for the ith column. The actual value of the absolute intensity in km/mole is found using equation 19, where the following relationship is now true

$$\left|\frac{\partial P}{\partial Q_i}\right|^2 = \left(\left(\frac{\partial P_x}{\partial Q_i}\right)^2 + \left(\frac{\partial P_y}{\partial Q_i}\right)^2 + \left(\frac{\partial P_z}{\partial Q_i}\right)^2\right) \quad (26)$$

2.4 Transformation to Different Coordinate Systems

The $\overline{S}$ coordinates are very convenient for the calculations of frequencies and intensities. However, the detailed analyses of the frequencies and intensities are best accomplished in two different coordinate systems. The frequency parameters are most easily analyzed in terms of force constants in internal coordinates and the intensity parameters will be discussed in terms of dipole derivatives with respect to space fixed cartesian coordinates, or APTs. Therefore, the frequency and intensity parameters in $\overline{S}$ coordinates must be transformed to the corresponding parameters in internal and cartesian coordinates respectively.

2.4.1 Internal Force Constants

As chemists, we have a desire to interpret the absorption frequencies in terms of molecular structure. Therefore, the necessary frequency parameters should be related to the molecular geometry. The most useful frequency parameters are thus the force constants in internal coordinates (10,11).

The internal displacement coordinates are changes in bond lengths and bond angles of a molecule. For most applications five coordinates -- bond stretching, angle bending, torsional motion, out-of-plane bending (wagging), and linear bending--are sufficient to describe completely all of the vibrational motions (10,11). For more unusual situations other specific internal coordinates can be defined by following the prescription of Califano (11). More detailed information on internal coordinates can be found in references 10 and 11.

The internal coordinates are related to the cartesian coordinates by

$$R_k = \left(\frac{\partial R_k}{\partial X_i}\right) X_i \quad \text{where} \quad \begin{matrix} k = 1, 2 \ldots (3N-6) \\ i = 1, 2, 3 \ldots (3N) \end{matrix} \tag{27a}$$

or in matrix notation

$$\bar{R} = \underline{B}\, \bar{X} \tag{27b}$$

where $\underline{B}$ is a (3N-6) by 3N matrix with typical element defined as $(\partial R_k / \partial X_i)$ and $\bar{R}$ is the column vector representation of internal coordinates. The $\underline{B}$ matrix is a function solely of the molecular geometry, and formulas for the calculation of its matrix elements for the five most common type of internal

coordinates have been derived (11). The $\underline{A}$ matrix transforms the internal coordinates back to cartesian coordinates

$$\overline{X} = \underline{A}\ \overline{R} \tag{28}$$

where $\underline{A}$ is apparently the inverse of $\underline{B}$. However, since the $\underline{B}$ matrix is not a square matrix, but rather a rectangular one, it does not have an inverse, and the $\underline{A}$ matrix is calculated via the $\underline{G}$ matrix (58).

In internal coordinates

$$\underline{G} = \underline{B}\ \underline{M}^{-1}\ \underline{B}^{+} \tag{29}$$

where $\underline{M}^{-1}$ is a (3N by 3N) diagonal matrix of the reciprocal masses. The "inverse" of $\underline{B}$ is then obtained by (47)

$$\underline{B}^{-1}\ \underline{G} = \underline{B}^{-1}\ \underline{B}\ \underline{M}^{-1}\ \underline{B}^{+} \tag{30}$$

$$\underline{B}^{-1} = \underline{M}^{-1}\ \underline{B}^{+}\ \underline{G}^{-1} \tag{31}$$

$$\underline{A} = \underline{M}^{-1}\ \underline{B}^{+}\ \underline{G}^{-1} \tag{32}$$

At this point is it appropriate to mention that $\underline{A}$ in equation 32 can be calculated only if the $\underline{G}$ matrix is a square non-singular matrix. This in turn means that there cannot be any redundancies defined in the $\underline{B}$ matrix elements. This is often a problem if one wishes to fully utilize the symmetry of the molecule. The methods of dealing with this problem will be discussed later; suffice it to say there that the problem exists and must be resolved.

The relationship between the force constants in mass-weighted cartesian coordinates $\underline{K}$ and in internal coordinates

$\underline{F}_i$ is now given by

$$\underline{F}_i = \underline{A}^+ \underline{K} \underline{A} \tag{33}$$

where $\underline{A}^+$ is the transpose of the $\underline{A}$ matrix, and $\underline{F}_i$ is the force constant matrix in internal coordinates.

2.4.2 Atomic Polar Tensors

The APT has been defined in the first three columns of equation 23 above, and equation 20 calculates the APTs in principal cartesian coordinates. However, usually the principal cartesian coordinate system is not ideally oriented for the interpretation of infrared intensities. This arises in part because the actual values of the polar tensor elements depend upon the orientation of the axis system used. Therefore, the bond coordinate system is usually the best system for analyzing the APTs. The transformation of the APT from one coordinate system to any other system is done by rotating the axis system. As the axis system is rotated, the values of the polar tensors change according to the rotation performed. The new values of these tensors can be calculated by performing the appropriate tensor rotations on these tensors. The matrices for the rotation of the axis system by the angle θ about either the X, Y, and Z axes respectively are (from (59))

$$R_X = \begin{pmatrix} 1 & 0 & 0 \\ 0 & \cos\theta & -\sin\theta \\ 0 & \sin\theta & \cos\theta \end{pmatrix} \quad R_y = \begin{pmatrix} \cos\theta & 0 & \sin\theta \\ 0 & 1 & 0 \\ -\sin\theta & & \cos\theta \end{pmatrix} \quad R_Z = \begin{pmatrix} \cos\theta & -\sin\theta & 0 \\ \sin\theta & \cos\theta & 0 \\ 0 & 0 & 1 \end{pmatrix} \tag{34}$$

where the sign of the angle θ is determined by viewing along the rotation axis from the positive direction. If the old axis system must be rotated in a clockwise direction to transform to the new coordinate system, then the angle is positive, and if the old axis system must be rotated in a counter-clockwise direction to transform to the new coordinate system, then the angle is negative. The rotation matrices defined in equation 34 are the ones usually used for the rotation of a cartesian axis system (59). The transformation for tensors is given by

$$\underline{T}' = \underline{R_\alpha}\ \underline{T}\ \underline{R_\alpha}^{+} \qquad \alpha = x,\ y,\ \text{or}\ z \qquad (35)$$

where $\underline{T}'$ is in the new coordinate system, and $\underline{T}$ is the tensor in the old coordinate system.

2.4.3 The $\overline{S}$ Coordinates

We have just seen the advantages of interpreting the predicted frequencies in terms of internal force constants and the predicted intensities in terms of APTs. Why, you may ask, have we chosen to perform the actual calculations in $\overline{S}$ coordinates? This question is discussed below.

The transformation from cartesian coordinates to $\overline{S}$ coordinates is performed by the orthogonal matrix $\underline{U}$ (see equation 2a). The orthogonality of $\underline{U}$ makes the reverse transformation matrix, from $\overline{S}$ coordinates to $\overline{q}$ coordinates, simply the transpose of $\underline{U}$, $\underline{U}^{+}$ (see equation 2b). In internal coordinates the analogous equation to equation 2a is equation 27. The reverse transformation is then performed by equation 28. However,

since the $\underline{B}$ matrix in equation 27 is not square, the $\underline{A}$ matrix in equation 28 cannot be obtained by simple inversion of $\underline{B}$, but must be obtained using equation 32. Equation 32 requires that all of the redundancies which are often necessary to completely describe the vibrational degrees of freedom using only the previously defined five internal coordinates be removed. The method of finite differences requires the transformation given by either equation 2b or equation 28. In internal coordinates equation 28 is often not easily obtained because the redundancy cannot be removed in any unique manner. Therefore, we avoid the problem with redundant coordinates by using equation 2b, or the $\overline{S}$ coordinates.

The cartesian coordinates used in the definition of the APT also avoid the redundancy problem. However, these coordinates do not utilize the symmetry of the molecule, nor do they explicitly separate the vibrational degrees of freedom from the translations and rotations. This means that in cartesian coordinates there are 3N coordinates rather than 3N-6, and the symmetry of the molecule cannot be used to simplify the problem. This greatly increases the computational effort necessary to predict the infrared spectrum. Therefore, since the $\overline{S}$ coordinates explicitly separate the vibrations from the translations and rotations, and utilize the symmetry of the molecules, they are preferred to cartesian coordinates.

2.5 Experimental Infrared Intensities

The experimental absolute infrared band intensity is given by (60)

$$A_i(\text{km/mole}) = \left(\frac{1}{100\ c\ell}\right)\int_{\text{band}} \ln(I_o/I)\ d\nu_i \qquad (36)$$

where A_i is the absolute integrated molar absorption coefficient or intensity for the ith fundamental mode in k/mole, c is the sample concentration in moles/liter, ℓ is the pathlength in cm, I_o is the intensity of the incident light in the absence of the sample, I is the intensity of the transmitted light after passing through the sample, ν_i is the wavenumber of the band in cm^{-1}, and the integration is performed over the entire band region. The factor of 100 converts A_i into the units of km/mole. In these units a very strong band would have an intensity of around 1000 km/mole, while a very weak band would have a value of 0.10 km/mole (57).

The alternate definition of the experimental integrated absolute band intensity uses integration over $\ln\nu_i$ instead of Γ_i (60). This quantity is given as the symbol $_i$ and is defined as

$$\Gamma_i(\text{cm}^2/\text{mole}) = \left(\frac{1}{c\ell}\right)\int_{\text{band}} \ln(I_o/I)\ d(\ln\nu_i) \qquad (37)$$

where all the symbols have their previously defined meanings and units. The definition of Γ_i is preferred for many purposes (61,62), but most spectrometers record spectra linear in wavenumbers, so integration over ν_i is much easier to measure

experimentally. As a result, A_i is the more commonly reported value. The difference between A_i and Γ_i is not too severe, however, the two quantities being related through

$$A_i \cong \Gamma_i \nu_i \tag{38}$$

Here ν_i is the band center in cm^{-1}, A_i is the intensity in km/mole and Γ_i measures the intensity in cm^2/mole.

The quantities A_i measure the total vibrational strength for a transition from the ground vibrational state to an excited vibrational state ($v_i = 0 \Rightarrow v_i = 1$) (60). Theoretically, the most important quantity related to this strength is the transition dipole moment $\mu_{mn}(i)$ (from (57))

$$\mu_{mn}(i) = \int \psi_m^* \hat{P} \psi_n \, d\tau \tag{39}$$

where the transition occurs from state m to state n, $\hat{P}$ is the dipole moment operator, ψ_m is the wavefunction for vibrationally excited state m, and ψ_n is the wavefunction for the initial state n.

2.6 Theoretical Infrared Intensities

The absolute intensity of an infrared absorption band is related to the theoretical quantity $\mu_{mn}(i)$ by (60)

$$A_i = \left(\frac{8\pi^3 N_{av} \nu_i}{3hc} \right) \left| \mu_{mn}(i) \right|^2 d_i \tag{40}$$

where N_{av} is Avagadro's number, ν_i is the wavenumber of the absorption band, h is Planck's constant, c is the speed of light, and d_i is the degeneracy of the ith vibration. If the

vibrations are harmonic so that ψ_m and ψ_n in equation 39 are harmonic oscillator wavefunctions, then equation 40 becomes (60)

$$A_i(\text{km/mole}) = \left(\frac{N_{av}\pi d_i}{3c^2}\right)\left(\frac{\partial P}{\partial Q_i}\right)^2 \qquad (41)$$

where $(\partial P/\partial Q_i)$ is the dipole moment charge with respect to motion along the ith normal coordinate. If the proper constants are substituted into equation 41, then that equation can be simplified (57) to

$$A_i(\text{km/mole}) = 974.9\ |(\partial P/\partial Q_i)|^2\ di \qquad (42)$$

where $(\partial P/\partial Q_i)$ has units of $e \cdot u^{-\frac{1}{2}}$, where e is the atomic unit of charge ($1\ e = 1.602 \times 10^{-19}$C) and u is the atomic mass unit. The units are $e \cdot u^{\frac{1}{2}}$ for $(\partial P/\partial Q_i)$ when the value of P is expressed in e A (where 1 e A = 4.8 Debye) and the normal coordinates Q are in units of A $u^{\frac{1}{2}}$.

Equation 42 indicates that the intensity for the ith mode depends on the form of the ith normal coordinate. Unfortunately, the normal coordinates are strongly dependent upon the molecule in question. They usually involve motion of all the atoms in the molecule simultaneously, and the amplitudes of motion depend also on the masses of the atoms. The interpretation and parameterization of infrared intensities in terms of these quantities are not easily accomplished because of the dependence of the form of the normal coordinates on the molecule in question. This dependence makes it difficult to compare these derivatives $(\partial P/\partial Q)$ among different

molecules. Instead, it appears to be more useful to attempt to use the fact that the atoms in a molecule are connected by bonds, and that these atoms (in similar chemical environments) should exhibit similar properties within different molecules.

The most natural coordinate system to use to try to interpret the absolute intensities are the cartesian coordinates. These coordinates are uniquely defined for every atom in the molecule, and are not dependent upon the geometry of the molecule. They can be oriented in the same direction in any molecule, thereby offering the possibility of directly comparing parameters among different molecules. This is necessary if we hope to be able to interpret intensities in terms of chemical structure. The transformation from normal coordinates to cartesian coordinates can be derived using the chain rule of differentiation

$$\frac{\partial P}{\partial X_j} = \sum_i \left(\frac{\partial P}{\partial Q_i} \right) \left(\frac{\partial Q_i}{\partial X_j} \right) \tag{43}$$

$$\frac{\partial P}{\partial X_j} = \sum_i \left(\frac{\partial P}{\partial Q_i} \right) L^+_{ij} \tag{44}$$

where $(\partial P/\partial Q_i)$ are derivatives of the dipole moment with respect to normal coordinates Q_i, $(\partial P/\partial Q_j)$ are these same derivatives with respect to cartesian coordinates X_j, and $(\partial Q_i/\partial X_j)$ is the derivative of the normal coordinate with respect to a cartesian coordinate. This last derivative is one of the elements in the normal coordinate transformation matrix. This matrix is given the representation $\underline{L}^+$, and represents the transformation from cartesian coordinate to normal coordinates

$$\bar{Q} = \underline{L}^{+} \bar{X} \qquad (45)$$

The concept of the dipole derivatives in cartesian coordinates, or the Atomic Polar Tensor (APT), was introduced in 1961 by Biarge, Herranz, and Morcillo (7), and later reformulated by Person and Newton (8). The matrix of APTs for any particular molecule (termed $\underline{P_x}$) is 3 by 3N and consists of the juxtaposition of N 3 by 3 second rank tensors, one for each atom in the molecule. Each element of the Nth APT is defined as $(\partial P_\alpha / \partial x_j)$, where P_α is the αth component (either x, y or z) of the total dipole moment, and x_j is the direction of the displacement of the jth coordinate (also either x, y, or z). More detailed discussions on the formalism of the APT are available in the literature, (2,3,7,8,41,47,48). However, it should be remembered that the APT is simply a more easily interpretable representation of the dipole derivatives in normal coordinates.

2.7 Characteristic Invariants of Atomic Polar Tensors

The actual values of the elements of the APT depend, of course, on the orientation of the axis system used. For this reason it is imperative that the coordinate system being used always be reported along with the APT in order to properly interpret the APT. We begin our discussion of how to interpret the APT by starting with those properties which are invariant to the axis system utilized.

The mechanics of molecular vibrations impose two important conditions on the APTs. These conditions, and also the other invariant properties of the APT, will be briefly discussed here. A more thorough discussion is available elsewhere (55,63-65).

The translational symmetry of the dipole moment requires that the APTs for a molecule sum to a diagonal tensor; each element in this tensor is equal to the total charge in the molecule. From (55)

$$\sum_N [\underline{\nabla}_N(\vec{P})]^+ = q_e \underline{E} \qquad (46)$$

where the summation runs over all the atoms in a molecule, $\underline{\nabla}_N$ is the cartesian gradient operator ($\partial/\partial x$, $\partial/\partial y$, $\partial/\partial z$), which when applied to a vector quantity ($\vec{P}$, the dipole moment) gives a 3 by 3 tensor. $\underline{E}$ is the identity matrix whose only nonzero elements are ones along the diagonal. For a neutral molecule this reduces to the requirement that the elements of the APTs sum to zero, which is commonly expressed as the null condition

$$\sum_N [\nabla_N(P)]^+ = o \underline{E} \qquad (47)$$

A second important condition is an intensity sum rule first derived by Crawford (63). This sum rule is most easily derived following (55) through an analogy with the molecular kinetic energy T,

$$2T = (\frac{\partial T}{\partial \underline{\dot{X}}}) \underline{M}^{-1} (\frac{\partial T}{\partial \underline{\dot{X}}})^+ \qquad (48a)$$

$$2T = \sum_N \left(\frac{1}{M_N}\right) \left(\left(\frac{\partial T}{\partial \dot{x}_N}\right)^2 + \left(\frac{\partial T}{\partial \dot{y}_N}\right)^2 + \left(\frac{\partial T}{\partial \dot{z}_N}\right)^2 \right) \qquad (48)$$

where $\dot{x}$, $\dot{y}$ and $\dot{z}$ represent differentiation with respect to time. The momenta in cartesian space ($\partial T/\partial \dot{X}$) can be transformed to moment in normal coordinate space using the chain rule of differentiation.

$$\left(\frac{\partial T}{\partial \dot{X}}\right) = \left(\frac{\partial T}{\partial \dot{Q}}\right)\left(\frac{\partial \dot{Q}}{\partial \dot{X}}\right) + \left(\frac{\partial T}{\partial \dot{\omega}}\right)\left(\frac{\partial \dot{\omega}}{\partial \dot{X}}\right) + \left(\frac{\partial T}{\partial \dot{X}_O}\right)\left(\frac{\partial \dot{X}_O}{\partial \dot{X}}\right) \qquad (49)$$

where ω represents rotational motion, and X_O translational motion. In these coordinate the kinetic energy takes on the form

$$2T = \sum_i \left(\frac{\partial T}{\partial \dot{Q}_i}\right)^2 + \sum_\alpha \left[\left(\frac{1}{I_{\alpha\alpha}}\right)\left(\frac{\partial T}{\partial \omega_\alpha}\right)^2 + \frac{1}{M_O}\left(\frac{\partial T}{\partial \dot{X}_{O\alpha}}\right)^2 \right] \qquad (50)$$

The relationship between equation 49 and the corresponding equation for the dipole derivatives is obvious

$$\left(\frac{\partial P}{\partial X}\right) = \left(\frac{\partial P}{\partial Q}\right)\left(\frac{\partial Q}{\partial X}\right) + \left(\frac{\partial P}{\partial \omega}\right)\left(\frac{\partial \omega}{\partial X}\right) + \left(\frac{\partial P}{\partial X_O}\right)\left(\frac{\partial X_O}{\partial X}\right) \qquad (51)$$

Their equivalence is complete because in the harmonic oscillator approximation $\partial \dot{Q}/\partial \dot{X} = \partial Q/\partial X$ and $\partial \dot{\omega}/\partial \dot{X} = \partial \omega/\partial X$. Therefore an expression analogous to equations 48b and 50 for the kinetic energy can be written for the dipole derivatives

$$\sum_N \frac{1}{M_N}\left(\left(\frac{\partial \bar{P}}{\partial x_N}\right)^2 + \left(\frac{\partial \bar{P}}{\partial y_N}\right)^2 + \left(\frac{\partial \bar{P}}{\partial z_N}\right)^2 \right) = \sum_i \left(\frac{\partial \bar{P}}{\partial Q_i}\right)^2 + \sum_\alpha \left[\left(\frac{1}{I_{\alpha\alpha}}\right)\left(\frac{\partial \bar{P}}{\partial \omega_\alpha}\right)^2 + \left(\frac{1}{M_O}\right)\left(\frac{\partial \bar{P}}{X_{O\alpha}}\right)^2 \right] \qquad (52)$$

The above equation can be simplified by summation over the three components of the dipole moment P_x, P_y, P_z, giving the intensity sum rule

$$\sum_i \left(\frac{\partial \bar{P}}{\partial Q_i}\right)^2 + \Omega = \sum_N \frac{1}{M_N}\left(\left(\frac{\partial \bar{P}}{\partial x_N}\right)^2 + \left(\frac{\partial \bar{P}}{\partial y_N}\right)^2 + \left(\frac{\partial \bar{P}}{\partial z_N}\right)^2\right) \tag{53}$$

or, by using equation 42 and multiplying both sides of equation 53 by the appropriate constants

$$\sum_i A_i + \Omega = \left(\frac{N_{av}\pi}{3c^2}\right) \sum_N \left(\frac{1}{M_N}\right) \chi_N^2 \tag{54}$$

where χ_N defines the "effective charge" according to King

$$\chi_N^2 = \frac{1}{3}\left(\left(\frac{\partial \bar{P}}{\partial x_N}\right)^2 + \left(\frac{\partial \bar{P}}{\partial y_N}\right)^2 + \left(\frac{\partial \bar{P}}{\partial z_N}\right)^2\right) = \frac{1}{3}\left(\underline{P_x}^N + \underline{P_x}^N\right) \tag{55}$$

The term Ω defines the translational and rotational corrections in equation 54

$$\Omega = \left(\frac{N_{av}\pi}{3c^2}\right)\left(\frac{P_x^2+P_y^2}{I_{zz}} + \frac{P_y^2+P_z^2}{I_{xx}} + \frac{P_z^2+P_x^2}{I_{yy}} + \frac{3q_e^2}{M_o}\right) \tag{56}$$

where the first three terms in the brackets of equation 56 represent the contributions to the dipole moment derivatives due to rotation of the axis system, and the last term is the correction due to translation. This last term arises only when the permanent total charge q_e on the molecule is not equal to zero.

For any molecule the LHS of equation 53 is invariant to a similarity transformation. Therefore the quantities on the RHS of this equation must also be invariant to similarity transform. This is equivalent to stating that the sum of the square of the elements of the APT for atom N is invariant to axis rotation.

The importance of the effective charge as defined in equation 55 is twofold. First, it is invariant to a similarity transformation, and therefore is not dependent upon the axis system defined. Ideally, these quantities should then be transferable from an atom in one molecule to the same atom in another molecule (as long as this atom is in similar chemical environments in both molecules). Secondly, the effective charge is important because from equation 54 we can now see that the effective charge for an atom (normalized by the recripocal of the mass for that atom) measures the contribution of that atom to the total intensity sum for the molecule.

A second quantity useful in characterizing APTs is the mean dipole moment $\bar{p}_N$. From (55)

$$\bar{p}^N = \frac{1}{3} \text{ Trace } (\underline{P_x}^N) = \frac{1}{3}\left(\frac{\partial P_x}{\partial x_N} + \frac{\partial P_y}{\partial y_N} + \frac{\partial P_z}{\partial z_N}\right) \qquad (57)$$

The trace of any tensor is invariant to a similarity transform, so the mean dipole moment is also invariant.

The last invariant property of the APT is related to the two previously defined invariant properties according to

$$\beta_N^2 = \frac{9}{2}(\chi_N^2 - \bar{p}^{N2}) \qquad (58)$$

where β_N^2 is defined as the anisotropy. It measures the deviation of the APT from the constant diagonal tensor, $\bar{p}^N\underline{E}$ (55).

2.8 Quantum Mechanical Interpretation of Atomic Polar Tensors: The Charge, Charge Flux, Overlap Theory (CCFO)

The charge-charge flux-overlap (CCFO) model was first introduced by King (55,66,67) and is related to the equilibrium charge, charge flux concepts of Decius (68). The reader is referred to the original references, and also some more recent work illustrating the application of this model in interpreting infrared intensities (13,39,41,56,69) for a more detailed description of this model. Here only a brief outline of the more important concepts of this model will be discussed.

The exact quantum mechanical definition of the dipole moment within the LCAO-MO method is as follows (41)

$$\langle\bar{p}\rangle = \sum_A [Q_A \overline{R_A} - \sum_B \sum_{\mu_A} \sum_{\nu_B} D_{\mu_B\nu_B} \langle \mu_A | \overline{r_A} | \nu_B \rangle] \qquad (59)$$

where μ_A represents the orbitals on atom A, ν_B represents the orbitals on atom B, $\overline{r_A}$ is the position vector of electron 1 with respect to nucleus A, $D_{\mu_A\nu_B}$ is the density matrix element between orbital μ_A on atom A and orbital ν_B on atom A, and Q_A is the gross atomic charge on atom A. The electronic position vector may be defined as specifying the position of an electron, and may be expressed as

$$\bar{r}_1 = \overline{R_A} + \overline{r_A} \qquad (60)$$

where $\overline{R_A}$ is the position vector of nucleus A and $\bar{r}_1$ is the electron position vector.

Q_A is the gross atomic charge on atom A and is given by

$$Q_A = Z_A - \sum_B \sum_{\mu_A} \sum_{\nu_B} D_{\mu_A \nu_B} S_{\mu_A \nu_B} \tag{61}$$

The term $D_{\mu_A \nu_B}$ is the density matrix element which is defined as

$$D_{\mu_A \nu_B} = 2 \sum_{i=1}^{n} c_{\mu_A i} c_{\nu_B i} \tag{62}$$

and $S_{\mu_A \nu_B}$ is the overlap integral

$$S_{\mu_A \nu_B} = \langle \mu_A | \nu_B \rangle \tag{63}$$

For simplicity, equation 58 can be rewritten as

$$\overline{p} = \sum_A Q_A \overline{R_A} + \sum_{A,B} \overline{F}(A,B) \tag{64}$$

where $\overline{F}(A,B)$ is now given by

$$\overline{F}(A,B) = -\sum_{\mu_A, \nu_B} \sum D_{\mu_A \nu_B} \int \Phi_{\mu_A}(1) \overline{r}_A \Phi_{\nu_B}(1) d\tau_1 \tag{65}$$

The first term in equation 64 is obtained from the net charges located at the nuclear positions and can be assigned to a single atom. The second term is essentially a hybridization term which measures the contribution due to the displacement of charge away from the center of the nuclear position. This effect is proportional to the off-diagonal density matrix element between orbitals centered on atoms A and B and is therefore intrinsically associated with a pair of atoms (41).

The APT for atom A is derived by applying the gradient operator (with respect to the cartesian coordinates of atom A) to the dipole moment vector of the molecule

$$P_x^C = APT(C) = [\nabla_C(\bar{P})]^+ \tag{66}$$

Application of this equation to the quantum mechanical definition of the dipole moment gives (Equation 64)

$$P_x^C = \sum_A [\nabla_C(Q_A \overline{R_A})]^+ - \sum_A \sum_B [\nabla_C(\bar{F}(A,B))]^+ \tag{67a}$$

$$P_x^C = Q_C \underline{E} + \sum_A \overline{R_A}[\nabla_C(Q_A)]^+ - \sum_A \sum_B [\nabla_C(\bar{F}(A,B))]^+ \tag{67b}$$

$$= P^C(C) + P^C(CF) + P^C(O) \tag{67c}$$

Thus the APT can be broken down into three components, which are represented by the three terms on the RHS of equation 67b. These three components are the charge, charge flux, and overlap tensors respectively. The physical meaning for each of these tensors will be briefly outlined below.

The charge tensor is a diagonal tensor, each element being composed of the net atomic charge on the atom in question

$$Q_A = Z_A - N_A \tag{68}$$

where Q_A is the net atomic charge, N_A is the Mulliken population (70), and Z_A is the number of electrons in the neutral atom. The charge contribution to the APT is static, and involves only one atom A. The charge flux tensor is defined (41) as

$$P^{C}(CF) = \sum_{A} \bar{R}_A[\nabla_C(Q_A)]^{+} = \sum_{A} \bar{R}_A \left(\frac{N_A(\bar{X}_C^{o}-\Delta\bar{X}_C) - N_A(\bar{X}_C^{o}+\Delta\bar{X}_C)}{2\Delta X_C^{o}} \right)^{+} \quad (69)$$

where $N_A(\bar{X}_C^{o} + \Delta\bar{X}_C)$ is the Mulliken population for atom A after displacement of coordinate $\bar{X}_C^{o}$ for atom C along the positive direction, $N_A(\bar{X}_C^{o} - \Delta\bar{X}_C)$ is the Mulliken population of this same atom after displacement along this same coordinate in the negative direction, $\bar{R}_A$ is the vector describing the equilibrium cartesian coordinates of atom A, ΔX_C^{o} is the numerical value of the displacement of coordinate $\bar{X}_C^{o}$, and the summation runs over all atoms in the molecule. The vector $\bar{R}_A$ is then multiplied by transpose of the vector quantity given in parenthesis in equation 69 to give the charge flux tensor for atom C.

These quantities measure the contributions from each atom to the dipole moment change due to the redistribution of charge among all the atoms as one particular atom is displaced along one of its cartesian coordinates. In effect, these terms arise as a result of the changes in the atomic charges as one atom moves in either the x, y, or z direction. The contribution to the dipole moment change is obtained by "normalizing" the changes in the atomic charges by the respective atomic coordinates. This contribution can be considered as a "diatomic contribution" (41) because the quantities in equation 69 involve a pair of atoms A and C.

The last component of the APT is the overlap tensor. This is a "triatomic contribution" (41) involving atoms A,

B and C. Physically, the overlap tensor corresponds to the changes in hybridization between atoms A and B as atom C is displaced along one of its cartesian coordinates. The effects on the dipole moment derivatives come about due to the changes in the displacement of charge from the nuclear centers. This last tensor is usually obtained from the difference of the total APT and the sum of the charge, and charge-flux contributions.

$$P^C(\text{overlap}) = P_x^C - [P\ (\text{charge}) + P^C(\text{charge-flux})] \quad (70a)$$

$$P^C(O) = P_x{}^C - P^C(C) - P^C(CF) \quad (70b)$$

It can be shown by analogy with the total APT that each of the three component tensors also has invariant properties. For the charge tensor this is already obvious. The charge tensor is a constant diagonal tensor, therefore the trace and the sum of the squares of the diagonal elements are also invariant.

$$\left[\chi^N(C)\right]^2 = \frac{1}{3} \sum_i \left[P^N(C)_{ii}\right]^2 = Q_N^2 \quad (71)$$

$$\bar{P}^N(C) = \frac{1}{3}\ \text{Trace (Charge Tensor)} = \frac{1}{3} \sum_i P^N C_{ii} = Q_N \quad (72)$$

where $P^N(C)_{ii}$ is a diagonal term of the charge tensor for atom N, given by Q_N. The trace of the charge tensor is termed the mean atomic charge, while the sum of the squares of the elements in the charge tensor is called the effective atomic charge. The anisotropy of the charge tensor is by definition always equal to zero:

$$\beta(C)^{N} = 0 \tag{73}$$

The charge flux tensor has been defined in equation 69. Using this definition and the chain rule of differentiation, the following equation can be written

$$\left(\frac{\partial Q_A}{\partial X}\right) = \left(\frac{\partial Q_A}{\partial Q}\right)\left(\frac{\partial Q}{\partial X}\right) + \left(\frac{\partial Q_A}{\partial \omega}\right)\left(\frac{\partial \omega}{\partial X}\right) + \left(\frac{\partial Q_A}{\partial X_o}\right)\left(\frac{\partial X_o}{\partial X}\right) \tag{74}$$

where all the symbols have their previously defined meanings and where the last two terms go to zero because atomic charges are not dependent upon either translation or rotation. By comparing this with equations 51 and 52, the relationship given below can be written

$$\sum_N \frac{1}{M_N}\left(\left(\frac{\partial Q_A}{\partial x_N}\right)^2 + \left(\frac{\partial Q_A}{\partial y_N}\right)^2 + \left(\frac{\partial Q_A}{\partial z_N}\right)^2\right) = \sum_i \left(\frac{\partial Q_A}{\partial Q_i}\right)^2 \tag{75}$$

where it is obvious that the RHS of equation 75 is invariant to similarity transform, so therefore the LHS of this equation must also be invariant to similarity transform. If both sides of equation 75 are premultiplied by the quantity $R_A^2 = (x_A^2+y_A^2+z_A^2)$, then the following equation results

$$\sum_N \frac{1}{M_N}(x_A^2+y_A^2+z_A^2)\left(\left(\frac{\partial Q_A}{\partial x_N}\right)^2 + \left(\frac{\partial Q_A}{\partial y_N}\right)^2 + \left(\frac{\partial Q_A}{\partial z_N}\right)^2\right)$$
$$= \sum_i \left(\frac{\partial Q_A}{\partial Q_i}\right)^2 (x_A^2+y_A^2+z_A^2) \tag{76}$$

The quantity $(x_A^2+y_A^2+z_A^2)$ is the square of the distance of atom A from the origin, and this distance is invariant to

rotation of the axis system (similarity transform). Therefore, a product on the LHS of equation 76 is invariant to a similarity transform since both quantitites on the RHS of this equation are invariant. If the LHS of equation 76 is expanded, the following result is obtained

$$\text{LHS} = \sum_N \frac{1}{M_N} \left(x_A^2 \left(\frac{\partial Q_A}{\partial x_N} \right)^2 + x_A^2 \left(\frac{\partial Q_A}{\partial y_N} \right)^2 + x_A^2 \left(\frac{\partial Q_A}{\partial z_N} \right)^2 + y_A^2 \left(\frac{\partial Q_A}{\partial x_N} \right)^2 \right.$$

$$\left. y_A^2 \left(\frac{\partial Q_A}{\partial y_N} \right)^2 + y_A^2 \left(\frac{\partial Q_A}{\partial z_N} \right)^2 + z_A^2 \left(\frac{\partial Q_A}{\partial x_N} \right)^2 + z_A^2 \left(\frac{\partial Q_A}{\partial y_N} \right)^2 + z_A^2 \left(\frac{\partial Q_A}{\partial z_N} \right)^2 \right) \tag{77}$$

If we now sum the RHS of this equation over all atoms A, and add the resulting terms, we obtain the squares of the nine elements of the charge flux tensor for the Nth atom. Since we are summing invariant quantities, then the total sum is also invariant to axis rotation. Therefore, we conclude that the sum of the squares of the elements of the charge flux tensor is invariant to axis rotation. This invariant quality is analogous to the effective charge for the APT, and is termed the effective charge of the charge flux tensor, $\chi^N(CF)$.

$$\left(\chi^N(CF) \right)^2 = \sum_A \overline{R_A}^2 \left(\left(\frac{Q_A}{x_N} \right)^2 + \left(\frac{Q_A}{y_N} \right)^2 + \left(\frac{Q_A}{z_N} \right)^2 \right) \tag{78}$$

Furthermore, as is true for any tensor, the trace of the charge flux tensor for the N atom is invariant to axis rotation. As a result, the trace of the charge flux tensor becomes the second invariant property of that tensor.

$$\bar{P}^{N}(CF) = \frac{1}{3}\,[\text{Trace (Charge Flux)}] = \frac{1}{3}\sum_{i}\left(P^{N}(CF)\right)_{ii} \qquad (79)$$

where $\left(P^{N}(CF)\right)_{ii}$ is a diagonal element of the charge flux tensor for the Nth atom. The third invariant property of the charge flux tensor is derived from the previous two invariants and is termed the anisotropy $\beta^{N}(CF)$. It is expressed as

$$\left(\beta^{N}(CF)\right)^{2} = \frac{9}{2}\left(\left(\chi^{N}(CF)\right)^{2} - \left(\bar{P}^{N}(CF)\right)^{2}\right) \qquad (80)$$

A similar argument can also be made for the overlap tensor. Each term of the overlap tensor is defined in equation 67c, where $\bar{F}(A,B)$ is given in equation 65. An equation similar to equation 73 can be written for the overlap terms

$$\frac{\partial \bar{F}(A,B)}{\partial X} = \left(\frac{\partial \bar{F}(A,B)}{\partial Q}\right)\left(\frac{\partial Q}{\partial X}\right) + \left(\frac{\bar{F}(A,B)}{\partial \omega}\right)\left(\frac{\partial \omega}{\partial X}\right) + \left(\frac{\partial \bar{F}(A,B)}{\partial X_{o}}\right)\left(\frac{\partial X_{o}}{\partial X}\right) \qquad (81)$$

where as in the case of the charge flux tensor, the last two quantitites in equation 81 are equal to zero. This makes the correspondence between equation 74 and equation 81 exact, and the corresponding argument leads to the following result:

$$\sum_{N}\frac{1}{M_{N}}\left(\left(\left(\frac{\partial \bar{F}(A,B)}{\partial x_{N}}\right)^{2} + \left(\frac{\partial \bar{F}(A,B)}{\partial y_{N}}\right)^{2}\right) + \left(\frac{\partial \bar{F}(A,B)}{\partial z_{N}}\right)^{2}\right) = \sum_{i}\left(\frac{\partial \bar{F}(A,B)}{\partial Q_{i}}\right)^{2} \qquad (82)$$

Here the LHS of this equation is equivalent to the sum of the squares of the overlap tensor. Since the RHS of this equation is dependent only on the form of the normal coordinate and is independent of the axis system used, then the LHS also becomes

invariant to axis rotation. The sum of the squares of the overlap tensor is then invariant to axis rotation and is termed the effective overlap, defined here in the LHS of equation 82. Again, as is true for any tensor, the trace over the overlap tensor becomes the second invariant property of that tensor. The trace of the overlap tensor, described in an analogous way to the traces of the previous tensors, is termed the mean overlap, and is defined as

$$\bar{p}^N(O) = \frac{1}{3}\,[\text{Trace (overlap)}] = \sum_i \left(P^N(O)\right)_{ii} \qquad (83)$$

where $\left(P^N(O)\right)_{ii}$ is a diagonal element of the overlap tensor. Finally, the anisotropy of the overlap tensor is also invariant to axis rotation and is defined as

$$\left(\beta^N(O)\right)^2 = \frac{9}{2}\left(\left(\chi^N(O)\right)^2 - \left(\bar{p}^N(O)\right)^2\right) \qquad (84)$$

The three component tensors of the APT, namely the charge charge flux, and overlap tensors, each has its own invariants analogous to the total APT. The sum of the squares of all of the elements for each individual tensor is invariant to axis rotation. For the total APT this quantity is the "effective charge," for the charge tensor the "effective atomic charge," the charge-flux tensor gives the "effective charge flux," and the overlap tensor yields the "effective overlap." The relationship between the last three terms and the "effective charge" as defined by King and Mast (65) is given below

$$\chi^{N^2} = \chi^N(C)^2 + \chi^N(CF)^2 + \chi^N(O)^2 + \text{Residuals} \qquad (85)$$

where the residuals come about because the sum of the squares do not equal the square of the sum. These residuals are defined as follows:

$$\text{Residuals} = \sum_i \sum_j \Big[2\, {}^{N}P(C)_{ij}\, {}^{N}P(CF)_{ij} + 2\, {}^{N}P(C)_{ij}\, {}^{N}P(O)_{ij} + 2\, {}^{N}P(CF)_{ij}\, {}^{N}P(O)_{ij} \Big] \tag{86}$$

where the sum extends over all nine elements of the respective tensors.

The trace of the total APT has been previously defined as the mean dipole moment in equation 57. The trace of the charge, the charge flux, and the overlap tensors are defined as the mean atomic charge, the mean charge flux, and the mean overlap and are defined in equations 72, 79, and 82 respectively. The anisotropy for each tensor derives from the two previous invariants for each tensor, χ^N and $\bar{p}^N$, and is defined for the charge, charge flux, and overlap tensors in equation 73, 80, and 84 respectively. The significance of each of these terms will be discussed later.

CHAPTER 3
THE WATER MONOMER

The frequencies and intensities were calculated for water interacting with a number of different chemical environments. The different environments were chosen to simulate different experimental conditions. Among those investigated were water interacting with another water molecule in several different geometries. These orientations include the linear, the cyclic, and the bifurcated pair of interacting water molecules, as shown in Figures 1.1, 1.2, and 1.3 respectively. In addition, the spectrum of water isolated in a beta-alumina complex was modelled by performing calculations on H_2O interacting with O atoms, O^{-1} atoms, and O^{-2} atoms. Finally, the spectrum of ionized water, H_2O^+, was also calculated. The results calculated for these species were then compared with those results calculated for isolated water. The changes in the calculated spectral parameters relative to the isolated molecule were dependent on both the geometrical orientation and the chemical environment of the water molecule. Therefore, calculations were done first on the isolated water molecule, and then these results were compared with the results obtained for a water molecule that was allowed to interact with its environment.

3.1 Calculation Procedure

For water and all other molecules the force constants and dipole derivatives in $\bar{S}$ coordinates were calculated on the Amdahl 470 V/6-II computer of the Northeast Regional Data Center (NERDC) operating with OS MV/SP-JES2 Release 2 and using the Gaussian 76 system of ab initio molecular orbital programs (54). This program was modified to allow the calculation of the dipole moments of ions. This modification was first suggested by Rogers and Hillman (56), and permits the program to calculate the dipole moment for charged species in the same manner as done in the case of neutral molecules. The standard 4-31G basis set was used for all molecules (71). The integral threshold was set at 1.0×10^{-6}, and the convergence limit at 5.0×10^{-5}. These values are standard for use with Gaussian 76. There has been some work on the dependence of the calculated results on the values used for these limits (72), but this problem was not considered here. The molecular geometry was input using principal cartesian coordinates, and the density matrix for the converged set of wavefunctions was stored on the IBM 3380 disk pack at the NERDC, to be used as the initial guess wavefunction for the calculations at the displaced geometries. This procedure reduces the amount of computer time needed for the ab initio calculations on the displaced geometries. Typically, a calculation on the equilibrium geometry would take 20 iterations before convergence was met, while a calculation on a displacement geometry would only take three or four iterations if the density matrix

for the equilibrium geometry was used as the initial guess. Two programs, ORTHO and PUNCH, were written for the Amdahl 470 to set up the appropriate disk data sets at the NERDC for input to Gaussian 76. ORTHO writes the $\underline{U}$ transformation matrix to a 3380 disk pack. PUNCH uses this matrix as input and performs the matrix algebra described by equation 2b. This results in the calculation of the cartesian coordinates of the displaced geometries. These coordinates are then written to an IBM 3380 disk pack in the proper format for input to Gaussian 76. Finally, Gaussian 76 is used to calculate the energies and dipole moments of the equilibrium geometry and the displaced geometries. These results are then used in conjunction with equations 3, 4 and 5 to give the force constants and dipole derivatives in $\overline{S}$ coordinates.

These two programs were designed to complement each other, each program creating an IBM 3380 disk data set for use in the next program. This eliminates some of the errors that can occur if one has to type all the data into the computer by hand (either using cards or a remote terminal).

After the ab initio calculations were completed, the calculated force constants $\underline{K}$, and the calculated dipole derivatives $\underline{P}_S$, were transferred to an 8-inch floppy disk for use in the normal coordinate analysis. This analysis was performed on this laboratory's S-100 bus microcomputer. This system includes the CompuPro/Godbout 8085/8088 CPU integrated to operate with CP/M 2.2 (73) and CP/M 86. Two Shugart SA 801R disk drives for use with 8-inch floppy disks are used for data and

program storage. Other peripherals include a Televideo 910 terminal, Centronics 739 dot matrix printer, Hayes Stack Smartmodem 1200 (for connecting to the NERDC) and a Micro-angelo Graphics Subsystem. The graphics subsystem includes a 15-inch high resolution graphics screen (480 x 512) detachable keyboard and light pen. In addition, there is available 128K of S-100 static memory, of which 64K is accessible by the 8 bit 8085 CPU. Software which is currently used operates with the 8 bit processor (8085) and includes Microsoft FORTRAN 80, Microsoft BASIC 80, Microsoft BASIC COMPILER, and Microsoft muMATH/muSIMP 80 (74). All of the normal coordinate programs used here (see Appendix A for a brief description of each program) operates with the 8 bit 8085 CPU and 64K of S-100 static memory. A whole series of programs was written to perform the normal coordinate analysis. These programs were designed to be run in sequence; each program creates 8-inch floppy disk data sets for use in the following programs. The proper sequence of programs necessary to perform a complete normal coordinate analysis is given in Appendix A, along with the necessary data input for each program (either from an 8-inch disk data set or by the operator via the Televideo terminal). All of the programs were written in either Microsoft FORTRAN (74) or Microsoft BASIC (74). The library subroutines necessary to run the main programs are also listed in Appendix A.

3.2 The Predicted Spectra for the Water Monomer

A bond length of 0.951 A° and a bond angle of 111.2° was used for the calculation on the isolated water molecule. The numbering of the atoms and the orientation of the principal cartesian axis system used in these calculations is shown in Table 3.1. This geometry corresponds to the absolute minimum on the potential curve (theoretical geometry) for the *ab initio* SCF calculation of isolated water with the 4-31G basis set by Lathan, Hehre, Curtiss and Pople (75). There is some debate as to whether it is best to use the theoretically or experimentally determined geometry when calculating the spectroscopic properties of molecules. However, for some of the systems investigated here there are little or no experimental data available. As a result, in order to be consistent, the theoretical geometries (calculated at the SCF level with the 4-31G basis set) were used whenever possible. When this geometry was not available, other available information (either from other calculations at different levels or from experimental work) was used to formulate a "best guess" at a reasonable geometry. This was done rather than searching the potential surface for the absolute minimum (i.e., optimizing the geometry) because the main interest is in spectral changes of the interacting species, and not absolute numbers. Therefore, calculations for the isolated species (in this case water) and then for the interacting species were performed at the same level (*ab initio* level with the 4-31G basis set), and then the predicted differences were examined.

The principal cartesian coordinates for the theoretical geometry of the isolated water molecule (R = 0.951 A°, θ = 111.2°) are given in Table 3.1.

In order to do a full calculation of the frequencies and intensities, all the diagonal force constants, all the off-diagonal force constants, and all the dipole derivatives must be calculated according to equations 3, 4, and 5, respectively. Since the force constant matrix in $\overline{S}$ coordinates is block factored by symmetry, some of the off-diagonal force constants are equal to zero and do not have to be calculated. However, all the off-diagonal force constants within the same symmetry block must be calculated.

The water molecule has C_{2v} symmetry. The 9 degrees of freedom reduce to $3A_1 + A_3 + 2B_1 + 3B_2$, with the three vibrational coordinates reducing as $2A_1 + B_2$. According to equation 3, two displacements are needed for each calculation of the three diagonal force constants, one in the positive direction and one in the negative direction. This is a total of six displacements that are needed to calculate the three diagonal force constants. The B_2 symmetry block is 1 by 1, and contains no off-diagonal force constants. The A_1 block is a symmetric 2 by 2 block, and therefore there is one non-zero off-diagonal force constant. To calculate this off-diagonal force constant using equation 4, one additional displacement is needed, the simultaneous positive displacement of both coordinates. This makes a total of seven displacement geometry and one equilibrium geometry calculations that are necessary

Table 3.1 Principal cartesian coordinates for the isolated water monomer at the theoretical geometry (A°). Atom numbering is defined below.

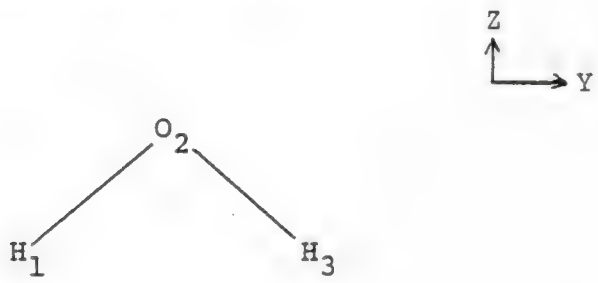

	X	Y	Z
H_1	0.0	-0.7847	-0.4772
O_2	0.0	0.0	0.0611
H_3	0.0	0.7847	-0.4772

for the full calculation of the frequencies and intensities for the isolated water molecule.

The calculated frequencies and intensities for the water monomer at its theoretical geometry are summarized in Table 3.2, where the experimental values (76,77) are also listed for comparison. As is usually the case with ab initio calculations, the predicted frequencies and intensities do not agree exactly with the experimental values (17,78). This is not too surprising considering the assumptions made and the errors inherent in these types of calculations. First, we have assumed that the molecule is a pure harmonic oscillator, and that the potentical curve can be well represented by a parabola. In reality, the potential curve is anharmonic, and the experimentally observed parameters reflect this anharmonicity. We have chosen to ignore this anharmonicity in our calculations. Strictly speaking this is not correct; therefore, the comparison between our calculated harmonic frequencies and the experimentally observed anharmonic frequencies cannot be expected to be in complete agreement. (The effect of anharmonicity can be quite significant, sometimes up to 200 cm^{-1}.) Secondly, the 4-31G basis set employed in these calculations is not large enough to correctly describe the electronic wavefunction. The inadequacies of this basis set (such as the improper behavior of the gaussian function at small distances, the absence of polarization functions and the inflexibility in the orbital exponents) are significant enough that the electronic wavefunction does not describe

Table 3.2 Predicted wavenumbers and intensities for isolated water compared to the experimental wavenumbers and intensities.

Mode	Wavenumbers ν (cm^{-1})			Intensity A (km/mole)	
	Calc.	Exp.[a]		Calc.	Exp.[b]
		Harmonic	Observed		
ν_1	3983	3832	3657	3.90	2.24
ν_2	1676	1648	1595	125	54
ν_3	4104	3942	3756	54	45

[a] Reference 58

[b] Reference 41

correctly the electronic behavior of this molecule, leading to additional errors in these calculations. Finally, the effect of neglecting electron correlation in these calculations is not entirely known. However, from some preliminary results by Bartlett (79), it appears that more sophisticated calculations may lead to much better agreement with experimental values. He has calculated the APTs for the isolated water molecule using "many body methods." The agreement between his calculated results and the elements of the experimental APTs given by Zilles (41) is within 0.05 e. This results suggests that the disagreement between the experimental frequencies and intensities and our calculated values is a result of the assumptions made and the methods used, and that this disagreement can be reduced by using more advanced theoretical methods. However, as a first approximation, the results one can obtain using ab initio methods with the 4-31G basis set are generally accurate enough to be useful in interpreting infrared spectra (17). For this particular type of calculation (SCF with 4-31G basis set), the frequencies are expected to be within 10-20% of the experimental ones (71), and the intensities are predicted to be within a factor of 2 of the experimental values (80). The wavenumbers and intensities listed in Table 3.2 predicted for the water molecule with the theoretical geometrical parameters do indeed reflect these limits.

Calculations of the frequencies and intensities were also done for the water monomer with varying bond angle and bond

lengths. Calculations were performed by varying the bond length while fixing the bond angle, by varying the bond angle while fixing the bond length, and by varying both the bond angle and bond length simultaneously. In addition, the frequencies and intensities were calculated for the experimentally determines geometry, where the bond length is 0.9572 A° and the bond angle is 104.5° (76,77). The calculated wavenumbers and intensities for these various geometries are summarized in Table 3.3.

The data in Table 3.3 indicates that the values of the calculated frequencies are fairly sensitive to the assumed geometry. The calculation at the experimental equilibrium geometry predicts wavenumbers in much better agreement with the observed values than does the calculation at the theoretical geometry. Changes as small as 0.006 A° in the assumed bond length for these calculations are responsible for changes of 100-150 cm^{-1} in the predicted frequencies for the bond stretches. The bending frequency is less sensitive to changes in the assumed molecular parameters, but is nevertheless still affected. Surprisingly, a change of slightly less than 7° in the assumed bond angle results in drastic changes of nearly 300 cm^{-1} for the two stretching modes. However, while the results on the frequencies indicate that close attention must be paid to the assumed geometry to predict reliable absolute numerical values, the predicted intensity values are much more independent of the assumed molecular structure. The intensities are predicted to be nearly the same for each of the normal modes for all the different assumed structures. The largest

Table 3.3 Predicted wavenumbers and intensities for different assumed geometries of the water molecule.

Mode	$R_1=R_2=0.951$ A° θ=111.2° (theoretical)	$R_1=R_2=.9572$ A° θ=111.2°	$R_1=R_2=.951$ A° θ=104.52°	$R_1=R_2=.9572$ A° θ=104.52° (Experimental)	$R_1=R_2=.9551$ A° θ=110.7°	$R_1=R_2=.950$ A° θ=112° (Electron Donor)	$R_1=0.950$ A° $R_2=0.958$ A° θ=111.3° (Electron Acceptor)
ν_1 (cm^{-1})	3983	3896	4328	3907	3928	3993	3896
A_1 (km/mole)	3.90	3.60	4.90	3.30	2.80	4.00	4.80
ν_2 (cm^{-1})	1676	1695	1692	1793	1694	1665	1751
A_2 (km/mole)	125	125	98	98	116	126	123
ν_3 (cm^{-1})	.4104	4017	4372	3985	4044	4121	4089
A_3 (km/mole)	54	52	25	27	46	58	50

difference is the change by a factor of 2 in the predicted intensity of the asymmetric stretching mode as the asummed bond angle is change by 7°. However, it is obvious that in general the predicted frequencies are very sensitive to changes in the assumed geometries, while the calculated intensities are very much less sensitive to these same changes in geometry.

At first glance, the strong dependence of the wavenumbers on the assumed geometry might seem very discouraging concerning the possibility of calculating absolute absorption frequencies because the final results are strongly dependent upon the initial assumed geometry. This problem has been examined in the past (12-16), but is not of interest here. In this thesis we shall be interested primarily in the changes that come about as a result of the interaction of the water molecule with its environment. Hence, the internal geometry of the water molecule can be chosen arbitrarily, and the intermolecular distance and orientation between the water molecule and the interacting species varied. In this way the resulting changes in the predicted spectrum can be attributed to the interaction and not a consequence of a geometry change. By fixing arbitrarily the internal geometries of the water molecules and varying only the intermolecular orientation or distances, we can then compare the predicted wavenumbers and intensities to observe their dependence only on the varying intermolecular parameters. Any dependence on the initial assumed geometry is eliminated because the internal geometry

Table 3.4 Predicted APTs and invariants for isolated water at the theoretical geometry, in e, where $1\,e = 1.602 \times 10^{-19}$ C. The coordinate system used is defined below.

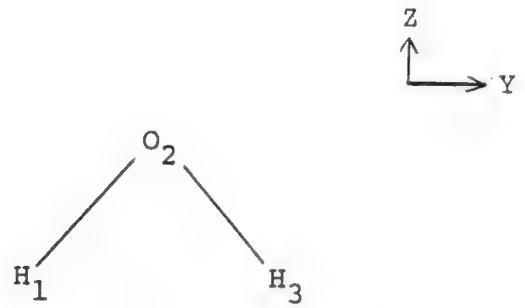

$$P_x^{H_1} = \begin{pmatrix} .482 & 0 & 0 \\ 0 & .274 & -.142 \\ 0 & -.095 & .226 \end{pmatrix} \qquad \begin{aligned} \chi^2 &= .1292\ e^2 \\ \bar{p}^2 &= .1071\ e^2 \\ \beta^2 &= .0995\ e^2 \end{aligned}$$

$$P_x^{O_2} = \begin{pmatrix} -.960 & 0 & 0 \\ 0 & -.548 & 0 \\ 0 & 0 & -.452 \end{pmatrix} \qquad \begin{aligned} \chi^2 &= .4754\ e^2 \\ \bar{p}^2 &= .4268\ e^2 \\ \beta^2 &= .2187\ e^2 \end{aligned}$$

$$P_x^{H_3} = \begin{pmatrix} .482 & 0 & 0 \\ 0 & .274 & +.142 \\ 0 & .095 & .226 \end{pmatrix} \qquad \begin{aligned} \chi^2 &= .1292\ e^2 \\ \bar{p}^2 &= .1071\ e^2 \\ \beta^2 &= .0995\ e^2 \end{aligned}$$

is eliminated because the internal geometries of all the water molecules are assumed to be the same.

The APTs (2) for the three atoms of the water molecule are presented in Table 3.4. The results presented here are for the principal cartesian coordinate system, but the coordinate system can be easily rotated to obtain APTs in any other coordinate system using equation 35. The invariants of the total APTs, χ_N, $\bar{P}^N$ and β_N, are presented also. The breakdown of the APTs into their three component CCFO tensors is given in Table 3.5. The overlap tensor is calculated by equation 70b as the difference between the total APT and the sum of the charge and charge flux tensors. All of the effective invariants for the constituent CCFO tensors are given in Table 3.5 also. These invariant properties will be discussed later.

The internal force constants for the water monomer with the theoretical geometry were calculated from the force constants in $\bar{S}$ coordinates using equations 18 and 33. The internal coordinates were defined as the two O-H bond stretching coordinates, and the H-O-H angle bending coordinate. The $\underline{B}$ matrix elements were calculated using the little $\underline{s}$ vectors as described by Califano (11). The resulting $\underline{B}$ matrix was then used to calculate the $\underline{A}$ matrix using equation 32. The resultant force constants calculated with this $\underline{A}$ matrix are given in Table 3.6, along with experimental values for comparison. The $\underline{B}$ matrix elements used in these calculations are not weighted. This means that the units of the stretching

Table 3.5 Predicted CCFO tensors and their effective invariants for the isolated water molecule at the theoretical geometry, in e (1 e = 1.602 x 10^{-19} C). The coordinate system is defined in Table 3.4.

$$P^{H_1}(C) = \begin{pmatrix} .4017 & 0 & 0 \\ 0 & .4017 & 0 \\ 0 & 0 & .4017 \end{pmatrix} \qquad P^{O_2}(C) = \begin{pmatrix} -.8034 & 0 & 0 \\ 0 & -.8034 & 0 \\ 0 & 0 & -.8034 \end{pmatrix}$$

$$P^{H_1}(CF) = \begin{pmatrix} 0 & 0 & 0 \\ 0 & .0550 & .0370 \\ 0 & .1040 & -.0450 \end{pmatrix} \qquad P^{O_2}(CF) = \begin{pmatrix} 0 & 0 & 0 \\ 0 & -.1090 & 0 \\ 0 & 0 & .0910 \end{pmatrix}$$

$$P^{H_1}(O) = \begin{pmatrix} .0803 & 0 & 0 \\ 0 & -.1827 & -.1790 \\ 0 & -.1990 & -.1307 \end{pmatrix} \qquad P^{O_2}(O) = \begin{pmatrix} -.1606 & 0 & 0 \\ 0 & .3644 & 0 \\ 0 & 0 & .2604 \end{pmatrix}$$

$$\chi_C^{H_1{}^2} = .1614\ e^2 \qquad \chi_C^{O_2{}^2} = .6455\ e^2$$

$$\chi_{CF}^{H_1{}^2} = .0017\ e^2 \qquad \chi_{CF}^{O_2{}^2} = .0067\ e^2$$

$$\chi_O^{H_1{}^2} = .0190\ e^2 \qquad \chi_O^{O_2{}^2} = .0755\ e^2$$

The invariants for H_2 are identical to those for H_1. The component tensors for H_2 are obtained simply by switching the signs on the off-diagonal terms for H_1.

Table 3.6 Predicted internal force constants for the water monomer at the theoretical geometry compared to the experimental values. Units are md/A° where the weighting factor d, where d = 1 A°, is used to weight the force constants involving bending coordinates (see text and also reference 11).

	Internal Force Constants (md/A°)	
	Calculated	Experimental[a]
$R_1 = R_2$	9.141	7.750
$d\theta 3$	0.714	0.668
R_1R_2	-0.065	-0.068
$R_1\theta_3$	0.300	0.270

[a] References 58; fit to observed frequencies.

coordinates are in A°, and the units of the bending coordinates are rad (11). As a result, the force constants calculated using the A matrix derived from this B matrix are also not weighted. If the energy is expressed in md-A°, then the units of the stretching force constants are md-A°, the bending force constants are given in md-A°/rad^2, and the stretch-bend interaction constants are given by md/rad. In order to compare these calculated force constants with other values in the literature, care must be taken that the same weighting scheme is used in both instances (48). In the remainder of this thesis the weighting factor (11) d, where d = 1 A° will be used to convert all force constants to units of md/A° without changing the numerical values of these constants. The normal coordinate transformation matrices obtained in these calculations, and all subsequent calculations, are summarized in Appendix B.

CHAPTER 4
THE LINEAR WATER DIMER

The geometry for the linear dimer was taken from Curtiss and Pople (30), and is the minimum energy structure for $(H_2O)_2$ obtained by optimizing all geometrical parameters with respect to the total energy of the complex using the 4-31G basis set. This geometry will now be referred to as the theoretical equilibrium geometry for the linear dimer. The principal cartesian coordinates are given in Table 4.1. This molecule has C_s symmetry, having only a single symmetry element, the plane of symmetry. The calculated heavy atom distance (O--O) is 2.832 A°, slightly shorter than the distance determined experimentally by Dyke, Mack and Muenter (81) of 2.98 A°. The discrepancies between the calculated value and the experimental value is due to the inadequacies of the basis set and the absence of electron correlation. Calculations performed with a larger basis set (including polarization functions) but without electron correlation predict a value for the O--O distance of 2.974 A°. This value is considerably closer to the experimental value than is the value calculated with the 4-31G basis set. This suggests that the 4-31G basis set overestimates the strength of the hydrogen bond, but if the deficiencies of the basis set are eliminated then more accurate results are predicted.

Table 4.1 Principal cartesian coordinates for the linear water dimer at the theoretical equilibrium geometry (A°). Atom numbering as in Figure 1.1.

	X	Y	Z
H_1	-.7876	.2207	1.8360
H_2	.7876	.2207	1.8360
O_3	0.0	-.0397	1.3729
H_4	0.0	.0271	-.4999
O_5	0.0	.0613	-1.4573
H_6	0.0	-.8109	-1.8337

The calculation performed by Curtiss and Pople (30) predict the hydrogen bond to be linear within 0.05°, with an optimized energy of -151.83038 hartrees. In addition, the O-H bond length involved in the hydrogen bond is predicted to be 0.958 A°. The remaining three O-H bonds are predicted to be all the same, and 0.950 A°. The H-O-H angles are calculated to be 111.3° in the electron acceptor, and 112.0° in the electron donor. A calculation by Lathan, Hehre, Curtiss and Pople (75) with the same basis set gives a bond length of 0.951 A° and a bond angle of 111.2° for the isolated water molecule, with a total energy of -75.90864 hartrees. Therefore, the binding energy of the dimer (the energy of the dimer minus twice the energy of the monomer) is calculated to be 8.2 kcal/mole. The internal geometries of the individual monomer units in the dimer are predicted to undergo slight changes upon complex formation. The bonded O-H bond length (H_4-O_5) is predicted to elongate by 0.007 A°, and the two internal bond angles increase slightly. While these changes appear to be very small, it is still surprising that the internal geometries of the individual monomer units are predicted to change. Most workers have assumed that the internal geometries of the two monomer units are unchanged from the values of the isolated molecule (81). Later in this chapter it will be shown that this geometry in the monomer units is very important towards understanding the spectral changes predicted for the dimer relative to the isolated monomer.

The irreducible representations of all 3N degrees of freedom for this molecule are 11A' + 7A". The 3N-6 or 12 vibrations

reduce as 8A' + 4A". For each of the 12 diagonal force constants two calculations at displaced geometries are necessary. This gives a total of 24 ab initio calculations that are needed to calculate all the diagonal force constants. For each non-zero off-diagonal force constant an additional ab initio calculation is necessary. In the A' symmetry block there are 7+6+5+4+3+2+1 or 28 additional calculations necessary to derive all non-zero off-diagonal force constants. In the A" block there are an addition 3+2+1 or 6 off-diagonal force constants that must be calculated. This bring the number of ab initio calculations necessary to calculate the complete vibrational force field to 24+28+6 or 58 displaced geometries plus one equilibrium calculation, or a total of 59 calculations.

4.1 The Predicted Spectrum for the Linear Dimer

The predicted frequencies and intensities for the theoretical equilibrium geometry for the linear configuration of the water dimer are summarized in Table 4.2. The corresponding frequencies and intensities for the isolated water molecule are listed for comparison adjacent to those for the corresponding vibration of the linear dimer. In addition, the frequencies and relative intensities observed experimentally by Tursi and Nixon (19) are also listed here for comparison. The pattern predicted by our ab initio calculation is in good agreement with the experimental spectrum assigned to the linear structure by Tursi and Nixon (19). Behrens and Luck (27) argue that the interpretation of the spectrum of $(H_2O)_2$ by Tursi and Nixon (19)

Table 4.2 Predicted wavenumbers and intensities for the theoretical equilibrium linear dimer compared to the predicted values for isolated water.

Mode	Description of Mode	CALCULATED				EXPERIMENTAL[a]			
		Linear Dimer[c]		Monomer[d]		Linear Dimer		Monomer	
		ν (cm^{-1})	A (km/mole)	ν (cm^{-1})	A (km/mole)	ν (cm^{-1})	Relative[b] Intensity	ν (cm^{-1})	Relative[b] Intensity
Intramolecular Mode									
1	Asymmetric stretch of Electron Donor (ED)	4127	111	4104	54	3713	3.99	3726	13.8
2	Asymmetric stretch of Electron acceptor (EA)	4076	110	4104	54	3097	1.88	3726	13.8
3	Symmetric stretch (ED)	3992	17.3	3983	3.90	3626	0.47	3633	3.71
4	Symmetric stretch (EA)	3873	279	3983	3.90	3548	3.08	3633	3.71
5	In phase EA bend with ED bend	1800	155	1676	125	1619	1.73	1598	7.85
6	Out of phase ED bend with EA bend	1715	137	1676	125	1600	2.20	1598	7.85
Intermolecular Modes									
7	O_3-H_4-O_5 out of plane bend with ED twist	835	310						
8	EA in plane twist with ED wagging in phase	479	334						
9	ED twist with EA out of plane bend	314	7.7						
10	EA out of plane twist with EA in plane twist	210	295						
11	EA in plane twist out of phase with ED wagging	209	340						
12	Hydrogen bond stretch	103	1.8						

[a] Reference 19

[b] Experimental relative intensities are obtained by fitting the absorbance, the half-width and the integrated area into the actual observed spectrum (19). These relative intensities represent the values which best reproduced the experimental spectrum (see reference 41, p. 67).

[c] For theoretical equilibrium geometry (see text).

[d] For theoretical equilibrium geometry (see text).

is not conclusive evidence for the linear structure. Their arguments are based on the fact that all six of the bands assigned to the linear structure do not follow the same concentration dependence, as they should if they all belonged to the same species. However, reliable assignments of these bands cannot be made solely on the basis of their concentration dependence because there are often overlapping and broad bands corresponding to higher aggregates which serve to hinder reliable measurements of relative intensities. The calculation of Curtiss and Pople (30) along with other work (19,26,81) points to the linear structure as the most energetically favorable one, and using this structure in our calculations we have been able to reproduce reasonably well the experimental spectrum of Tursi and Nixon (19) (see Table 4.2).

While it is probably true that these ab initio 4-31G calculations are still not accurate enough to give reliable absolute values, it is encouraging that the correct patterns are reproduced, including the spectral changes that occur upon complex formation. The nature of these spectral changes is of primary interest, and not the absolute values predicted for the frequencies and intensities. Since these ab initio calculations with the 4-31G basis set correctly reproduce the observed spectral changes, we believe that these calculations are valuable in understanding these changes. These changes in turn are important to understand because their nature might offer some valuable insights towards understanding intermolecular interactions.

The assignment of the vibrations as predominantly the electron donor symmetric stretch, or electron acceptor bending, for example, were made with the aid of a program which was written to picture a vibrating molecule. The program, VIBRATE, accepts the equilibrium cartesian coordinates for each atom in the molecule and then draws a ball and stick model of that molecule. This portion of the program has been adapted for our microcomputer from the PLUTO program of Motherwell (82). The cartesian coordinates corresponding to the displacements of an appropriate increment in both the positive and negative direction along the normal coordinates are also input from a disk data set into the program. Atoms (or circles) are then turned on and off at these displaced cartesian coordinates for any desired normal mode. These circles are turned on and off at both the positive and negative displacements, giving the illusion that the atoms in the molecule are actually vibrating along that particular normal coordinate. By observing the motions of all the atoms in the molecule for any particular normal vibration, the characteristic motions of that normal mode can be accurately described. These vibrations can be frozen on the graphics screen, then sent to the printer for hard copy. This program was written in BASIC and uses the Microangelo high resolution graphics screen for the display. The low frequency modes were also assigned using this program. This type of assignment has certain advantages over the Potential Energy Distribution (PED) (58) descriptions of normal vibrations because they allow one to actually visualize the

vibration. The PEDs can be misleading because they do not describe the actual normal vibration, but only the contributions from a given set of internal coordinates that make up that particular normal vibration.

At this point let us just briefly comment on the characteristics of the 12 vibrational modes for the theoretical linear configuration of two interacting water molecules. The highest frequency modes predicted at 4126 cm^{-1}, 4076 cm^{-1}, 3992 cm^{-1}, and 3872 cm^{-1} (Table 4.2) are all stretching modes and are isolated almost entirely in only one molecule. These vibrations are the asymmetric stretch of the electron donor, the asymmetric stretch of the electron acceptor, the symmetric stretch of the electron donor, and the symmetric stretch of the electron acceptor, respectively. The intermolecular interaction does not couple or perturb the form of these high frequency stretching modes at all, and in fact they remain localized in one molecule. These normal modes behave as if two separate molecules existed without any interaction. The two modes occuring at 1800 cm^{-1} and 1714 cm^{-1} correspond to bending vibration of the water units. However, these vibrations are no longer localized, but are coupled between both molecules. For instance, the vibration at 1800 cm^{-1} is predominantly the electron acceptor bending motion, coupled in phase (i.e., both molecules open their angles simultaneously) with some of the bending mode of the electron donating molecule. The vibration at 1714 cm^{-1} is mostly electron donor bending coupled out-of-phase with some electron acceptor bending.

In this lower wavenumber region the vibrations are no longer localized on the individualized water molecules, but rather become vibrations of the entire complex. While it is possible to classify the vibration at 1800 cm^{-1} and the one at 1714 cm^{-1} as electron acceptor and electron donor bending, respectively, strictly speaking this is not correct due to the presence of intermolecular coupling which perturbs and mixes these vibrations. These bending vibrations are not only coupled with each other, but they are also coupled to some of the low frequency intermolecular bending and twisting motions.

The low frequency (or intermolecular) modes are generally characterized by twisting and out-of-plane (where reference is made to the plane of the molecule) bending motions. The vibration predicted at 835 cm^{-2} is mainly the O_3-H_4-O_5 out-of-plane (of the electron acceptor) bend (hydrogen bond bend) along with some electron donor twisting motion. The mode at 749 cm^{-1} corresponds to in-plane electron acceptor twisting in phase with a little out-of-plane (of electron donor) electron donor wagging (electron acceptor twists upwards at the same time the hydrogen atoms of the electron donor wag upwards). The vibration at 208 cm^{-1} is the out-of-phase combination of these same electron acceptor twisting and electron donor wagging motions just described. The mode at 313 cm^{-1} can be characterized as predominately electron donor twisting motion mixed with electron acceptor hydrogen (free hydrogen) wagging motion. At 210 cm^{-1} the vibration corresponds to the out-of-plane (of electron acceptor) twisting of the electron acceptor mixed

with some in plane (of electron donor) electron donor bending. Finally, the vibration at 103 cm^{-1} is the hydrogen bond strech-ing mode.

The low frequency modes are presented here for completeness, but will not be discussed at any length. There is very little experimental evidence about them available from studies in this region of the spectrum. The uncertainties in the ab initio calculations are magnified in this region because the force constants are extremely small. These frequencies are therefore expected to be much more sensitive to the assumed geometry, and the confidence that one can place on the predicted values of these absolute frequencies is certainly limited. For some configurations some of the intermolecular modes were predicted to have imaginary frequencies. This result is a consequence of performing the calculations at displacements that are not about the absolute minimum of the potential surface. It is not expected that these imaginary frequencies affect greatly the frequencies of interest, namely the high frequencies intramolecular modes, due to the large energy separation. However, it is certainly interesting to note here that the predicted intensities for the low frequency modes are in general equal to or greater than those for the intermolecular vibrations. This might offer some hope to experimentalists interested in investigating the bands in this region. However, until now, the difficulties (such as the presence of internal rotation, and a low signal to noise ratio) in this region of the spectrum have made

the study of these bands extremely difficult. Even so, the intensities of these modes merit a few comments.

Four of the six low frequency modes are predicted to have a large intensity; greater in fact, than for the high frequency modes. As a result of comparing the motions involved in the high intensity low frequency modes, it was observed that these four vibrations all involved a considerable contribution from the atoms in the electron acceptor, while the remaining two low intensity modes were mainly motion of the electron donor. This suggests that perhaps most of the intensity for the complex originates in the electron acceptor.

In general, the data in Table 4.2 indicates that the intramolecular vibrations of the electron donor are essentially not affected by the interaction with another water molecule. However, the electron acceptor experiences considerable change, especially in the symmetric stretch [ν_1(EA)]. This band is predicted to shift 110 cm^{-1} to lower frequency and to increase in intensity by a factor of almost 72, from 3.90 km/mole to 279 km/mole. The remaining modes for this complex are not predicted to change very much from the corresponding vibrations in the isolated water molecule. Both asymmetric stretching vibrations are predicted to increase by slightly more than a factor of 2 in intensity, but this is certainly less than the factor of 72 predicted for the symmetric stretch of the electron acceptor.

4.2 Intensity Analysis for Linear Pair of Water Molecules

The change in intensity predicted for the symmetric stretch of the electron acceptor is extreme, from a relatively weak band in the monomer to a strong band in the dimer. A detailed *ab initio* calculation and analysis of the linear dimer has recently been published by Zilles and Person (39). However, our equilibrium calculation here utilizes a slightly different approach so that our results are slightly different from those reported previously (39). For instance, we have used an unscaled *ab initio* force field and unscaled *ab initio* polar tensors, while Zilles and Person (39) used the experimental force field of Tursi and Nixon (19) with scaled APTs. Secondly, while our equilibrium calculation was performed at the theoretical geometry, Zilles and Person (39) chose to use the experimental geometry. While the use of an experimental force field, scaled APTs and the experimental geometry usually gives better agreement with experimental results, our calculation is based on purely theoretical methods and therefore gives an indication of the quality of predictions that can be expected using these methods. Finally, we have extended the work of Zilles and Person (39) by actually quantifying the predicted changes in the polar tensors to changes in intensities. In addition, we have investigated the dependence of the predicted spectrum on both intermolecular orientation and distance by performing similar calculations at different geometries and intermolecular distances.

The results of our equilibrium calculation are very similar to the results reported by Zilles and Person (39). However, there are some slight differences in the two approaches so that caution must be used in making a different numerical comparison between the two results. Zilles and Person (39) found that the only significant change in the APTs of the dimer relative to the isolated monomer was in the P_{yy} term of the bonded hydrogen. Therefore they attributed the large predicted intensity increase (in the dimer relative to the monomer) in the symmetric stretching mode of the electron acceptor as due to this change in this term of this polar tensor. When the CCFO analysis was performed on the APTs by Zilles and Person (39), they found most of the increase in the APTs for the dimer was due to an increase in charge flux as the dimer was formed. Our results are similar, and are briefly summarized below.

In order to attempt to understand the large predicted intensity increase for the symmetric stretching mode of the electron acceptor, the intensity parameters were transformed to APTs. The APTs for the theoretical linear configuration in the coordinate system given in Figure 1.1, are given in Table 4.3, along with the properly rotated APTs for the theoretical water monomer. First, it must be remembered that the intensities are related to the normal coordinates via equation 24. Since the normal coordinates are mass weighted motions of all the atoms in a molecule, the heavier atoms will have smaller amplitudes and therefore contribute less to the normal coordinates.

Table 4.3 Calculated APTs for theoretical linear dimer along with corresponding APTs for monomer (e) ($1e = 1.602 \times 10^{-19}$ C). Atom numbering and coordinate system as given in Figure 1.1.

	Linear Dimer			Monomer[a]		
$P_x^{H_1}$ =	.3284	-.0777	.0596	.274	-.121	.074
	-.0406	.3231	.1079	-.081	.295	.113
	.0331	.0968	.4388	.040	.113	.412
$P_x^{H_2}$ =	.3284	+.0777	-.0596	.274	.121	0.074
	.0406	.3231	.1079	.081	.295	.113
	-.0331	.0968	.4388	-.040	.113	.412
$P_x^{O_3}$ =	-.6055	0	0	-.548	0	0
	0	-.7884	-.2154	0	-.591	-.228
	0	-.1633	-.8416	0	-.228	-.825
$P_x^{H_4}$ =	.4827	0	0	.482	0	0
	0	.5892	-.0688	0	.148	-.089
	0	-.0803	.3700	0	-.042	.351
$P_x^{O_5}$ =	-1.0010	0	0	-.964	0	0
	0	-.8115	-.0078	0	-.517	.047
	0	.0433	-.5055	0	.047	-.483
$P_x^{H_6}$ =	.4670	0	0	.482	0	0
	0	.3645	.0763	0	.369	.044
	0	.0066	.1000	0	-.003	.131

[a]The APTs for the atoms in the monomer are for coordinate systems rotated from Table 1 separately for each atom to correspond to the coordinate system of the dimer in Figure 1.1.

Therefore, when analyzing infrared intensities the lighter atoms are of greater importance than the heavier atoms. While bearing this fact in mind, the results in Table 4.3 show reasonably large changes in the APTs of both the oxygen and bonded hydrogen atoms of the electron acceptor. The P_{yy} terms for both of these atoms change by a substantial amount. The P_{yy} term for the oxygen atom decreases by 0.308 e, while the P_{yy} term for the bonded hydrogen increases by 0.441 e. Since the lighter atoms play a more important role in the calculation of infrared intensities, the following discussion will emphasize the bonded hydrogen atom when trying to explain the large predicted intensity increase in the symmetric stretching mode of the electron acceptor for the dimer.

The polar tensors were further analyzed to determine which, if any, of the three component tensors was mainly responsible for the change in the total APT. The charge, charge flux, overlap (CCFO) analysis was performed for all of the atoms in the linear pair of water molecules. The resultant charge, charge flux and overlap tensors are listed for the linear pair and the corresponding water monomer in Tables 4.4, 4.5, and 4.6, respectively.

The three tables, Tables 4.4, 4.5, and 4.6 indicate that the charge and overlap tensors for all of the atoms are relatively constant in going from the monomer to the linear pair. There are slight changes, but nothing significant. However, the charge flux tensors show most of the changes reflected in the total APTs. For the P_{yy} term of the bonded hydrogen, the

Table 4.4 Calculated charge tensors for the theoretical linear dimer compared to those of isolated water (e) (1 e = 1.602 x 10^{-19} C). Atom numbering and coordinate system as given in Figure 1.1.

	Linear Dimer			Monomer		
H_1 P(C) =	.4237	0	0	.4017	0	0
	0	.4237	0	0	.4017	0
	0	0	.4237	0	0	.4017
H_2 P(C) =	.4237	0	0	.4017	0	0
	0	.4237	0	0	.4107	0
	0	0	.4237	0	0	.4017
O_3 P(C) =	-.8184	0	0	-.8034	0	0
	0	-.8184	0	0	-.8034	0
	0	0	-.8184	0	0	-.8034
H_4 P(C) =	.4632	0	0			
	0	.4632	0			
	0	0	.4632			
O_5 P(C) =	-.8734	0	0			
	0	-.8734	0			
	0	0	-.8734			
H_6 P(C) =	.3812	0	0			
	0	.3812	0			
	0	0	.3812			

Table 4.5 Calculated charge flux tensors for the theoretical linear dimer compared to the corresponding tensors for isolated water monomers (e) (1 e = 1.602 x 10^{-19} C). Atom numbering and coordinate system as given in Figure 1.1.

	Linear Dimer			Monomer		
H_1 $P(CF)$ =	.0957	.0661	-.0370	.053	+.034	-.012
	.1293	-.0470	.0151	-.089	-.033	.020
	-.0663	.0087	-.0132	-.054	.020	-.012
H_2 $P(CF)$ =	.0957	-.0661	.0370	.053	-.034	.021
	-.1293	-.0470	.0151	-.089	-.033	.020
	.0663	.0087	-.0132	.054	.020	-.012
O_3 $P(CF)$ =	-.1769	0	0	-.105	0	0
	0	-.0760	-.0320	0	.066	-.040
	0	.0218	.0337	0	-.040	.025
H_4 $P(CF)$ =	-.0268	0	0	0	0	0
	0	+.4495	-.0276	0	.089	-.051
	0	=.0352	-.0905	0	.012	-.081
O_5 $P(CF)$ =	.0184	0	0	0	0	0
	0	-.2354	.0436	0	-.043	.091
	0	.0919	.0499	0	.091	.029
H_6 $P(CF)$ =	-.0061	0	0	0	0	0
	0	-.0442	-.0141	0	-.046	-.040
	0	-.0960	.0334	0	-.104	.054

Table 4.6 Calculated overlap tensors for the theoretical linear dimer compared to the corresponding tensors for isolated water monomers (e) (1 e = 1.602 x 10^{-19} C). Atom numbering and coordinate system are given in Figure 1.1.

$$\overset{H_1}{P(O)} = \begin{pmatrix} -.1910 & -.1438 & .0966 \\ -.1699 & -.0536 & .0928 \\ .0994 & .0881 & .0283 \end{pmatrix} \quad \begin{pmatrix} -.181 & -.155 & .095 \\ -.170 & -.074 & .093 \\ +.094 & .093 & .022 \end{pmatrix}$$

$$\overset{H_2}{P(O)} = \begin{pmatrix} -.1910 & .1438 & -.0966 \\ .1699 & -.0536 & .0928 \\ .0994 & .0881 & .0283 \end{pmatrix} \quad \begin{pmatrix} -.181 & +.155 & -.095 \\ .170 & -.074 & .093 \\ -.094 & .093 & .022 \end{pmatrix}$$

$$\overset{O_3}{P(O)} = \begin{pmatrix} .3898 & 0 & 0 \\ 0 & .1060 & -.1834 \\ 0 & -.1851 & -.0569 \end{pmatrix} \quad \begin{pmatrix} .360 & 0 & 0 \\ 0 & .146 & -.188 \\ 0 & -.188 & -.047 \end{pmatrix}$$

$$\overset{H_4}{P(O)} = \begin{pmatrix} .0463 & 0 & 0 \\ 0 & -.3236 & -.0412 \\ 0 & -.0451 & -.0031 \end{pmatrix} \quad \begin{pmatrix} .065 & 0 & 0 \\ 0 & -.343 & -.038 \\ 0 & -.054 & .030 \end{pmatrix}$$

$$\overset{O_5}{P(O)} = \begin{pmatrix} -.1461 & 0 & 0 \\ 0 & .2972 & -.0486 \\ 0 & -.0541 & .3180 \end{pmatrix} \quad \begin{pmatrix} -.161 & 0 & 0 \\ 0 & .329 & -.044 \\ 0 & -.044 & .291 \end{pmatrix}$$

$$\overset{H_6}{P(O)} = \begin{pmatrix} .0919 & 0 & 0 \\ 0 & .0275 & .1026 \\ 0 & .0904 & -.3144 \end{pmatrix} \quad \begin{pmatrix} .065 & 0 & 0 \\ 0 & .013 & .084 \\ 0 & .101 & -.325 \end{pmatrix}$$

increase in the total APT is predominately due to the increase in the charge flux tensor, and not a result of a change in the charge or overlap tensor. Quantitatively, the increase in the charge flux tensor is responsible for 0.360 e, or 82% of the change in the P_{yy} term of the total APT for this atom.

A program was written, PXPQ (see Appendix A), to determine exactly what percentage of the total intensity increase from monomer to dimer was due to the difference in the normal coordinates (or due to the mechanical effect), and what amount was a result of the change in charge, charge flux and overlap in the bonded hydrogen. This program uses a normal coordinate transformation matrix and a set of polar tensors as input. It allows the operator to adjust any of the elements in any of the polar tensors for any of the atoms as he wishes. The intensities using the input normal coordinate transformation matrix and these adjusted polar tensors are then recalculated. If we use the rotated monomer polar tensors as the initial input APTs, and the calculated normal coordinate transformation for the linear dimer, the calculated intensities will show the effects due to the changing normal coordinates (mechanical effect), but not the electronic effects from the interaction. If we then add only the increase in charge flux for the P_{yy} term of bonded hydrogen and recalculate the intensities, these intensities will reflect only the normal coordinate effect and the effect of the increase in charge flux for the bonded hydrogen atom. The results of both of these calculations are given in columns four and five of Table 4.7. The

Table 4.7 Calculated contributions to the predicted intensities for the six intramolecular vibrations of the theoretical linear dimer (km/mole).

Mode	DIMER $\nu(cm^{-1})$	MONOMER A(km/mole)	A(km/mole) Using Monomer APTs	A(km/mole) H_4 add P(CF)	A(km/mole) H_4 add P(C)	A(km/mole) H_4 add P(O)	A(km/mole) add $P^{H_1}_{xx}$	A(km/mole) Dimer
1	4127	54	55	55	55	55	83	111
2	4076	54	47	123	132	138	116	110
3	3992	3.90	4.57	3.5	3.3	3.3	3.5	17.3
4	3873	3.90	11.6 (3%)	235 (82%)	250 (6%)	268 (7%)	268	279
5	1800	125	130	140	141	141	141	155
6	1715	125	119	118	117	117	117	137

normal coordinate effect is minimal, as evidenced by only a slight increase in the intensities of the symmetric stretching modes, from 3.90 km/mole to 4.57 km/mole for the electron donor and to 11.6 km/mole for the electron acceptor. This is to be expected based on the fact that the stretching vibrations of the dimer were already seen not to couple or become perturbed much by the interaction. When the charge flux increase for the P_{yy} term of the bonded hydrogen is added to the monomer APTs, the predicted intensities for the electron acceptor exhibit considerable changes. The asymmetric stretch increases from 47 km/mole to 123 km/mole, and the symmetric stretch increases from 11.6 km/mole to 235 km/mole. The predicted intensities for this pair of vibrations in the complex are 110 km/mole and 279 km/mole respectively. By adding only the increase in charge flux for the P_{yy} term of the bonded hydrogen of the electron acceptor (H_4) all of the predicted intensity increase for the asymmetric stretch of the electron acceptor for the linear pair can be reproduced. By comparing columns five and nine of Table 4.7, it is obvious that practically all of the predicted intensity increase for the linear dimer is a direct consequence of the increase in charge flux in the P_{yy} term of the bonded hydrogen. The effect of both the change in charge and overlap tensors on this intensity increase can be seen by successively adding the differences from dimer to monomer in the P_{yy} term of the charge

and overlap tensors to those APTs used for column five. It is seen in columns six and seven that these contributions are indeed minimal; containing only 6% and 7% of the total predicted intensity increase respectively.

The only band of the linear dimer which is not adequately reproduced in column seven is the asymmetric stretch of the electron donor. It is still a factor of 2 too low compared to the predicted intensities in column nine. If we refer back to Table 4.3 and look again at the hydrogen atoms for the electron donor, there is an increase of 0.054 e in the P_{xx} term of both hydrogen atoms in the dimer relative to the monomer. This change is relatively small, but is still large enough to be responsible for the increase in intensity for the asymmetric stretch of the electron donor. From Table 4.5, 0.0427 e or 78% of this change is due to an increase in charge flux. The terms for both hydrogens were increased by this amount, and the resulting predicted intensities are given in column eight of Table 4.7. By adding the difference in charge flux from dimer to monomer to the P_{xx} term, the predicted intensity for the asymmetric stretching mode of the electron donor rises from 55 km/mole to 83 km/mole. The value of 83 km/mole is in closer agreement with the predicted value for the dimer of 110 km/mole. Therefore, by considering only the increase in charge flux in the dimer relative to the monomer, almost 76% of the intensity of the symmetric stretch for the electron donor can be accounted for. Therefore, we conclude that the

intensities for the six intramolecular vibrations of the dimer are well reproduced by adjusting only the three terms in the polar tensors--the $P^{H_4}_{yy}$ term, the $P^{H_1}_{xx}$ and the $P^{H_2}_{xx}$ term--and that most of the change in these terms as the dimer is formed is due to a change in charge flux and not to changes in charge or overlap.

4.3 Frequency Analysis for the Linear Pair of Water Molecules

The predicted frequencies for the six intramolecular vibrations of the linear dimer (see Table 4.2) are in good agreement with the predicted values for the corresponding vibration in the isolated monomer, differing by only 20-30 cm^{-1}. However, three of these vibrations are predicted to occur at wavenumbers considerably different from the corresponding vibration in the monomer. The symmetric stretching vibration of the electron acceptor is predicted to decrease 110 cm^{-1} in the dimer relative to the monomer. The two bending vibrations in the dimer are predicted to increase by 124 cm^{-1} and 39 cm^{-1}. In order to understand these changes the calculated frequency parameters or force constants were analyzed.

The frequency parameters in $\bar{S}$ coordinates were transformed to internal force constants using equations 18 and 33. The internal coordinate definitions are given in Table 4.8, and the resultant $\underline{B}$ and $\underline{A}$ matrices were calculated with the programs BMAT and AMATRIX respectively (see Appendix A). The weighting factor d, where d = 1 A° has been applied to all the calculated force constants and therefore the units of

Table 4.8 Internal coordinate definitions used for the linear dimer. Atom numbering as given in Figure 1.1. (d is a weighting factor where d = 1 A°.)

Coordinate No.	Definition
R_1	R $(H_1\text{-}O_3)$
R_2	R $(H_2\text{-}O_3)$
R_3	R $(H_4\text{-}O_5)$
R_4	R $(H_6\text{-}O_5)$
R_5	dθ $(H_1\text{-}O_3\text{-}H_2)$
R_6	dθ $(H_4\text{-}O_5\text{-}H_6)$
R_7	R $(H_4\text{-}O_3)$
R_8	dθ $(H_1\text{-}O_3\text{-}H_4)$
R_9	dθ $(H_2\text{-}O_3\text{-}H_4)$
R_{10}	dτ $(H_1\text{-}O_3\text{-}O_5\text{-}H_6)$ + $\tau(H_2\text{-}O_3\text{-}O_5\text{-}H_6)$
R_{11}	dθ $(O_3\text{-}H_4\text{-}O_5)$ (in plane)
R_{12}	dθ $(O_3\text{-}H_4\text{-}O_5)$ (out of plane)

all these force constants are md/A° (48). The weighted internal force constants for the theoretical linear dimer are given in Table 4.9.

The calculated force constants for the intermolecular vibrations are all very small, generally having a magnitude about 0.05 md/A°. Therefore, the effect of these force constants on the high frequency vibrations is expected to be minimal, so only the force constants corresponding to the intramolecular vibrations will be discussed here. These force constants can be found in the upper left 6 by 6 corner of the matrix given in Table 4.9. The values for the first six diagonal force constants in the table represent either O-H stretching force constants or H-O-H bending force constants. These values can be directly compared to force constants calculated for isolated water because there exists a corresponding stretching or bending coordinate in the monomer. The calculated values for the theoretical geometry of isolated water can be found in Table 3.6. The most obvious and most significant difference is in the bonded O-H stretching constant, which changes from 9.14 md/A° in the monomer to 8.54 md/A° in the linear dimer. The exact nature of the effect of this change on the frequencies was investigated using the program PERTURB (see Appendix A).

PERTURB accepts a set of internal force constants from an 8-inch floppy disk and calculates the corresponding wavenumbers using this set of force constants. It then gives the operator the choice of adjusting any of the force

Table 4.9 Predicted internal force constants for the theoretical linear dimer (md/A°). Internal coordinate definitions as given in Table 4.8. Weighting is done by d, where d = 1 A° (see text).

	R_1	R_2	R_3	R_4	R_5	R_6	R_7	R_8	R_9	R_{10}	R_{11}	R_{12}
R_1	9.213	-.0913	-.0391	-.0049	.293	-.0024	-.0243	.0213	-.001	.002	-.002	-.007
R_2		9.213	-.0391	-.0049	.293	-.0024	-.0243	-.001	.0213	-.002	.002	-.007
R_3			8.540	-.173	.024	.309	.054	.022	.022	0	0	-.006
R_4				9.145	-.009	.345	-.057	-.024	-.024	0	0	-.003
R_5					.726	.035	.047	.026	.026	0	0	-.031
R_6						.753	.047	.035	.035	0	0	.031
R_7							.087	.033	.033	0	0	-.034
R_8								.120	.055	.003	.016	-.030
R_9									.120	-.003	-.016	-.030
R_{10}										.004	-.001	0
R_{11}											.118	0
R_{12}												.054

constants, and recalculates the wavenumbers using these adjusted force constants. In this way we are able to investigate how changes in individual force constants affect the predicted wavenumbers.

The calculated internal force constants for the dimer were used as the initial input to the program PERTURB. The bonded O-H stretching force constant of the electron acceptor was then increased from 8.54 md/A° to 9.14 md/A°, or to the same value for the O-H stretch in the isolated water molecule. The frequencies were then recalculated with this force constant changes and the remaining force constants at their original calculated values. The results are listed in column three of Table 4.10. The frequency of the symmetric stretch for the electron acceptor increases from 3873 cm^{-1} to 3968 cm^{-1}, and this can be compared to a frequency of 3983 cm^{-1} for the isolated water molecule. Almost 86% of the total predicted frequency shift in the dimer (relative to the monomer) of 110 cm^{-1} can be accounted for with the bonded O-H stretching force constant. As the electron donor perturbs the electron acceptor, the strength of the bond between the bonded hydrogen and the oxygen atom in the electron acceptor decreases, and therefore the force constant for this O-H stretch decreases. This decrease in turn is almost entirely responsible for the predicted decrease in the symmetric stretching mode of the electron acceptor in the dimer relative to the same stretching mode in the monomer.

Table 4.10 Calculated wavenumbers for the theoretical linear dimer obtained by adjusting certain force constants (see text) (cm^{-1}).

Mode	WAVENUMBERS (cm^{-1})						
	Calculated Dimer	Adjust F_{33}	Adjust F_{55} and F_{66}	Using Only Intramolecular Force Constants	Isolated[a] Electron Donor	Isolated[a] Electron Acceptor	Calculated Monomer
1	4126	4126	4126	4127	4121		4104
2	4076	4115	4115	4085		4089	4104
3	3992	3992	3992	3992	3993		3983
4	3873	3969	3968	3867		3896	3983
5	1800	1801	1758	1743		1751	1676
6	1715	1715	1699	1659	1665		1676

[a]Taken from Table 3.3.

However, it must be remembered that the individual monomer units in the theoretical geometry for the linear dimer do not retain the theoretical monomer geometry. The calculation of the optimized geometry for the linear dimer (30) predicts that the geometry of both the electron donor and acceptor are perturbed (relative to the optimized geometry for an isolated water molecule) by the presence of the second molecule. The calculated frequencies and intensities for isolated water molecules at the geometry of the electron acceptor and electron donor are given in Table 3.3. For the electron acceptor the calculated wavenumbers in the dimer are in good agreement with the same values calculated for an isolated water molecule with the same geometry as the electron acceptor. The largest difference is in the bend-ind mode, where the frequency is predicted to be 1800 cm^{-1} in the dimer, and is calculated to be 1751 cm^{-1} in the isolated electron acceptor. The asymmetric and symmetric stretching modes agree within 13 cm^{-1} and 23 cm^{-1} respectively. This suggests that the predicted change in the vibrational frequency of the symmetric stretch of the electron acceptor of the dimer, relative to the isolated monomer frequency, is due to the change in geometry of the acceptor water molecule in the complex relative to the geometry in the isolated water molecule. Since we have already shown that the predicted frequency shift for the symmetric stretching mode of the electron acceptor was due to the decrease in the stretching force constant of the bonded O-H, we conclude that this decrease in the force constant is due to the change in the geometry of the

acceptor molecule in the dimer relative to the isolated monomer. For the electron donor, the calculated wavenumbers in the complex are in fair agreement with the calculated values for the isolated water molecule at the theoretical geometry. However, when the frequencies for an isolated water molecule with the geometry of the electron donor are calculated, the frequencies of the stretching modes are in almost exact agreement with those predicted for the donor molecule in the dimer. The bending frequency for the electron donor is in somewhat worse agreement, still being 50 cm^{-1} too high in the complex.

While we have been able to account for the predicted shifts in the stretching frequencies of the dimer (relative to the monomer) by the changes in geometry of the individual monomer units, the same cannot be said for the predicted shifts in the bending frequencies. Even after correcting for the geometry changes, the bending frequencies predicted in the dimer are still about 50 cm^{-1} higher than expected. This is due to the coupling of these vibrations between the two molecules. If we recall the descriptions of the bending vibrations of the dimer given earlier, they were no longer isolated in one molecule but were instead mixed between both molecules. However, these bending vibrations are not only coupled to the bending vibration of the second molecule, but they are also coupled to the low frequency intermolecular vibrations. Column five of Table 4.10 gives the calculated frequencies using only the complete vibrational force field corresponding to the six intramolecular vibrations (i.e., the upper left 6 by 6 block

of Table 4.9). In this way, the interaction constants between the high frequency modes and the low frequency modes are assumed to be zero, and therefore no coupling between these modes can occur. The bending frequencies calculated in this way agree almost exactly with the values that one would expect based only on the geometry change. Therefore, we conclude that the difference in the bending frequencies in the dimer relative to the isolated theoretical monomer is a result of two effects. The first effect is the predicted geometry change of the two interacting molecules in the dimer relative to the monomer, and the second effect is the coupling between the bending vibrations and the low frequency intermolecular vibrations.

4.4 Further Calculations on Weaker and Stronger Interacting Linear Pairs of Water Molecules

There exists a great deal of evidence for the relationship between the energies of OH---O hydrogen bonds, as manifested by the bonded O-H stretching wavenumber, and the OH--O hydrogen bond length, or the intermolecular separation between the bonded species (43,83). The question of the effect on the wavenumbers and intensities of the vibrations of a hydrogen bonded dimer as the distance of separation of the monomer units is changed may be addressed by performing calculations at a series of O------O interatomic distances R, distributed about the theoretical equilibrium value of 2.832 A°.

Hence, calculations were done for the linear structure as the interaction distance between the two molecules was varied over a region -0.30 A° to +0.30 A° relative to the theoretical

equilibrium interatomic distance. The intramolecular parameters were left constant and equal to the parameters in the theoretical equilibrium geometry for the dimer. The only parameter that was allowed to vary was the distance between the two molecules. The entire calculation was repeated at each new interaction distance, encompassing changes of -0.30 A°, -0.15 A°, + 0.15 A°, and +0.30° relative to the theoretical equilibrium value of R(O---O) = 2.832 A°. The predicted frequencies and intensities for the linear dimer at these varying intermolecular distances are reported in Table 4.11. The low frequency modes are reported here also, but will not be discussed. Just let us say that upon inspection of the predicted frequencies and intensities for these modes it becomes apparent that these parameters are strongly dependent upon the assumed intermolecular distance.

The high frequency intramolecular vibrations are easily assigned using the program VIBRATE (see Appendix A). The changes in both intensity and frequency as the interatomic distance is varied seem to follow logical trends. All three frequencies for the electron donor are relatively constant, being within 10 cm^{-1} of each other across the entire series. In addition, it appears that as the intermolecular distance increases, these frequencies approach the values calculated for the isolated electron donor given in column six of Table 4.10. The intensities vary a little bit more, with a variation of 40 km/mole from the highest value (at the shortest intermolecular distance) to the lowest value (at the longest

Table 4.11 Predicted wavenumbers and intensities for the linear dimer as the interatomic distance R(O---O), is varied.

	R=2.532 A°		R=2.682 A°		R=2.832 A°		R=2.982 A°		R=3.132 A°	
Mode	cm^{-1}	km/mole	cm^{-1}	km/mole	cm^{-1}	km/mole	cm^{-1}	km/mole	cm^{-1}	km/mole
1	4117	131	4124	119	4127	111	4124	102	4134	96
2	4057	138	4071	138	4076	110	4080	102	4089	97
3	3983	17	3990	15	3992	17	3987	9.7	4001	15
4	3843	657	3865	413	3873	279	3880	195	3889	127
5	1767	180	1792	172	1800	155	1801	153	1802	148
6	1723	138	1737	144	1715	137	1719	135	1712	140
7	895	355	855	304	835	310	720	299	731	193
8	463	243	493	318	479	334	499	354	568	398
9	392	149	356	89	314	7.7	385	132	443	44
10	230	217	348	3.4	210	295	302	300	376	199
11	a	--	263	342	209	1.8	249	194	228	388
12	a	--	236	212	103	340	182	14	151	66

[a] Imaginary frequency

intermolecular distance) for the asymmetric stretch. However, the changes predicted in the intensities as the intermolecular distance is increased are towards the values calculated for the isolated electron donor. This indicates that as the intermolecular distance is lengthened, the electron donor behaves more like an isolated electron donor molecule, and takes on the properties of the isolated molecule. This is what should be expected based on the fact that as the distance between the two molecules is lengthened, the effect of the intermolecular interaction on the spectral properties of the molecule should be reduced. In summary, the predicted frequencies and intensities for the electron donor of the linear dimer do not change much at interaction distances shorter than equilibrium. At longer interaction distances, the predicted frequencies and intensities approach the isolated electron donor values.

However, as the intermolecular distance is varied, the frequencies and intensities for the electron acceptor show considerable changes (see Table 4.11). These changes are primarily isolated in the symmetric stretching mode, and therefore we will limit our discussion to this vibration. The frequency and intensity for this mode were plotted against the interaction distance and this plot is shown in Figure 4.1. Both parameters exhibited some dependence on the interaction distance, but the nature of the dependence of the frequency and nature of the dependence of the intensity were quite different. The frequency exhibited a linear dependence, while the intensity fit equally well to an exponential and

Figure 4.1 Dependence of wavenumber and intensity on the assumed intermolecular distance for the symmetric stretching vibration of the electron acceptor molecule in the linear dimer. [(wavenumber (—), intensity (---)].

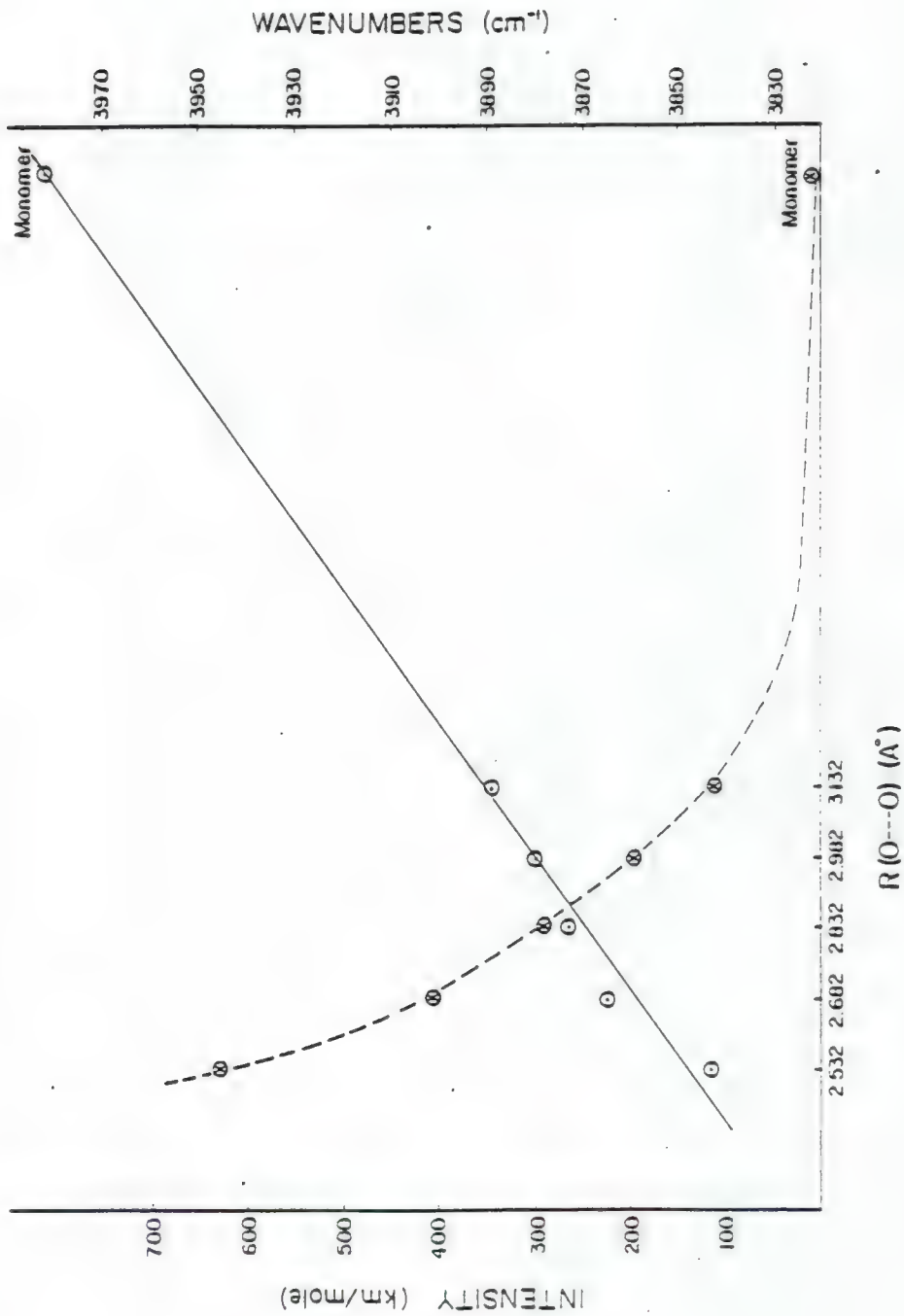
WAVENUMBERS (cm⁻¹)
3970
3950
3930
3910
3890
3870
3850
3830
Monomer
Monomer
INTENSITY (km/mole)
700
600
500
400
300
200
100
2.532
2.682
2.832
2.982
3.132
R (O---O) (Å)

quadratic function. The exponential fit was chosen over the quadratic fit because the quadratic function does not correctly describe the dependence of the intensity at very long intermolecular distances. As the two molecules are infinitely separated, it is expected that the intensities of their vibrations would approach a limiting value, namely the value for the isolated molecules. The quadratic function would predict that at long intermolecular distances the intensities of the isolated molecules would begin to rise again, and eventually, at distances long enough, would reapproach the values calculated at short intermolecular distances. On the other hand, the exponential function predicts that the intensities would approach a limiting value at extremely long intermolecular distances, and is therefore preferred over the quadratic fit. The plot in Figure 4.1 indicates that both absorption parameters for the symmetric stretch of the electron acceptor are dependent upon the intermolecular interaction distance, but that the intensity is much more sensitive to the interaction distance than the frequency. The intensity exhibits larger and more drastic changes than the frequency for the same change in interaction distance. This suggests that the intensity changes and the frequency shifts as the interaction distance is varied have different origins. This was analyzed by interpreting both the intensity and frequency parameters as a function of R.

The intensity parameters were transformed to APTs for each case. Using the arguments given above, our attention

was focused on the APT of the bonded hydrogen. It was found that this atom contained the only significant change in its APT elements relative to the same terms in the isolated monomer. This change was isolated in the P_{yy} term in all cases, similar to the theoretical geometry described above. By using the CCFO analysis most of the predicted change for the P_{yy} term, in each case, can be attributed to an increase in charge flux relative to the isolated monomer, and not to change in either atomic charge or overlap. The total APT and the constituent tensors for the bonded hydrogen are listed for all the interaction distances calculated, along with the corresponding invariants, in Table 4.12.

The effective invariants, described in Chapter 2, for the constituent CCFO tensors are useful in analyzing the various contributions to the effective invariant of the total APT (effective charge). According to the sum rule (see equation 54), the square of the effective charge is directly proportional to the intensity sum for a molecule. If we recall the data presented earlier, the APTs for all of the atoms in the linear dimer with the exception of the bonded hydrogen were essentially unchanged from the isolated monomer tensors. Therefore, we believe that the changes in intensity predicted for the linear dimer relative to the isolated monomer, as the interaction distance is varied, can be monitored by observing the changes in the effective charge for the bonded hydrogen atom. In turn, the relative contributions from the CCFO tensors to the effective charge can be visualized by using the effective invariants for the CCFO tensors.

Table 4.12 Predicted polar tensors and CCFO tensors, along with their calculated effective invariants, for the linear dimer as the intermolecular distance, R(O---O), is varied (e) (1 e = 1.602 x 10^{-19} C). Atom numbering and coordinate system as in Figure 1.1.

	R = 2.532 A°	R = 2.682 A°	R = 2.832 A°	R = 2.982 A°	R = 3.132 A°
$P_x^{H_4}$	$\begin{pmatrix} .470 & 0 & 0 \\ 0 & .858 & -.059 \\ 0 & -.119 & .376 \end{pmatrix}$	$\begin{pmatrix} .478 & 0 & 0 \\ 0 & .706 & -.065 \\ 0 & -.093 & .373 \end{pmatrix}$	$\begin{pmatrix} .478 & 0 & 0 \\ 0 & .589 & -.080 \\ 0 & -.069 & .370 \end{pmatrix}$	$\begin{pmatrix} .484 & 0 & 0 \\ 0 & .499 & -.071 \\ 0 & -.070 & .366 \end{pmatrix}$	$\begin{pmatrix} .482 & 0 & 0 \\ 0 & .431 & -.073 \\ 0 & -.063 & .362 \end{pmatrix}$
$\left(\chi_{H_4}\right)^2$ (e^2)	.3661	.2887	.2390	.2057	.1830
$P(C)^{H_4}$	.489 E	.477 E	.463 E	.451 E	.440 E
$\left(\chi_C^{H_4}\right)^2$ (e^2)	.239	.228	.214	.203	.194
$P(CF)^{H_4}$	$\begin{pmatrix} -.039 & 0 & 0 \\ 0 & .649 & -.009 \\ 0 & -.077 & -.094 \end{pmatrix}$	$\begin{pmatrix} -.032 & 0 & 0 \\ 0 & .536 & -.002 \\ 0 & -.049 & -.092 \end{pmatrix}$	$\begin{pmatrix} -.027 & 0 & 0 \\ 0 & .450 & -.035 \\ 0 & -.028 & -.091 \end{pmatrix}$	$\begin{pmatrix} -.023 & 0 & 0 \\ 0 & .383 & -.033 \\ 0 & -.025 & -.089 \end{pmatrix}$	$\begin{pmatrix} .019 & 0 & 0 \\ 0 & .332 & -.037 \\ 0 & -.017 & -.087 \end{pmatrix}$
$\left(\chi_{CF}^{H_4}\right)^2$ (e^2)	.1459	.0997	.0712	.0523	.0399
$P(O)^{H_4}$	$\begin{pmatrix} .020 & 0 & 0 \\ 0 & -.284 & -.050 \\ 0 & -.042 & -.019 \end{pmatrix}$	$\begin{pmatrix} .034 & 0 & 0 \\ 0 & -.307 & -.053 \\ 0 & -.044 & -.011 \end{pmatrix}$	$\begin{pmatrix} .046 & 0 & 0 \\ 0 & -.324 & -.045 \\ 0 & -.041 & -.003 \end{pmatrix}$	$\begin{pmatrix} .056 & 0 & 0 \\ 0 & -.334 & -.038 \\ 0 & -.046 & -.004 \end{pmatrix}$	$\begin{pmatrix} .045 & 0 & 0 \\ 0 & -.340 & -.036 \\ 0 & -.046 & .009 \end{pmatrix}$
$\left(\chi_O^{H_4}\right)^2$ (e^2)	.0286	.0333	.0369	.0394	.0404

The effective charge, the effective atomic charge, the effective charge flux, and the effective overlap were calculated for the bonded hydrogen atom at each interaction distance. The values of these invariants for all of the component tensors as well as the total APT for the bonded hydrogen atom at all of the interaction distances calculated are listed in Table 4.12. These values were then plotted as a function of interatomic distance in Figure 4.2. The effective charge exhibited an exponential dependence on the interaction distance, similar in form to the dependence that the calculated integrated intensity for the symmetric stretch of the electron acceptor exhibited with these same changes in intermolecular distance (see Figure 4.1). While the effective charge flux also showed an exponential dependence on the interaction distance, the effective atomic charge and the effective overlap both exhibited a linear dependence. In addition, the slopes of these lines were very small, indicating that the effective atomic charge and the effective overlap changed very little as the interaction distance was varied. This further indicates that the contributions from the effective atomic charge and the effective overlap to the change in effective charge as the intermolecular distance is varied are also minimal. However, the fact that the effective charge flux followed an exponential dependence on this distance indicates that it is primarily responsible for the predicted increase in effective charge for the bonded hydrogen. Therefore, we conclude that the charge flux tensor is mainly responsible

Figure 4.2 Plot of the effective invariants $(\chi)^2$ for the polar tensor (T), and the charge (C), charge flux (CF), and overlap (O) tensors versus the intermolecular O---O distance (effective invariants are plotted for only the bonded hydrogen atom of the linear dimer, see text).

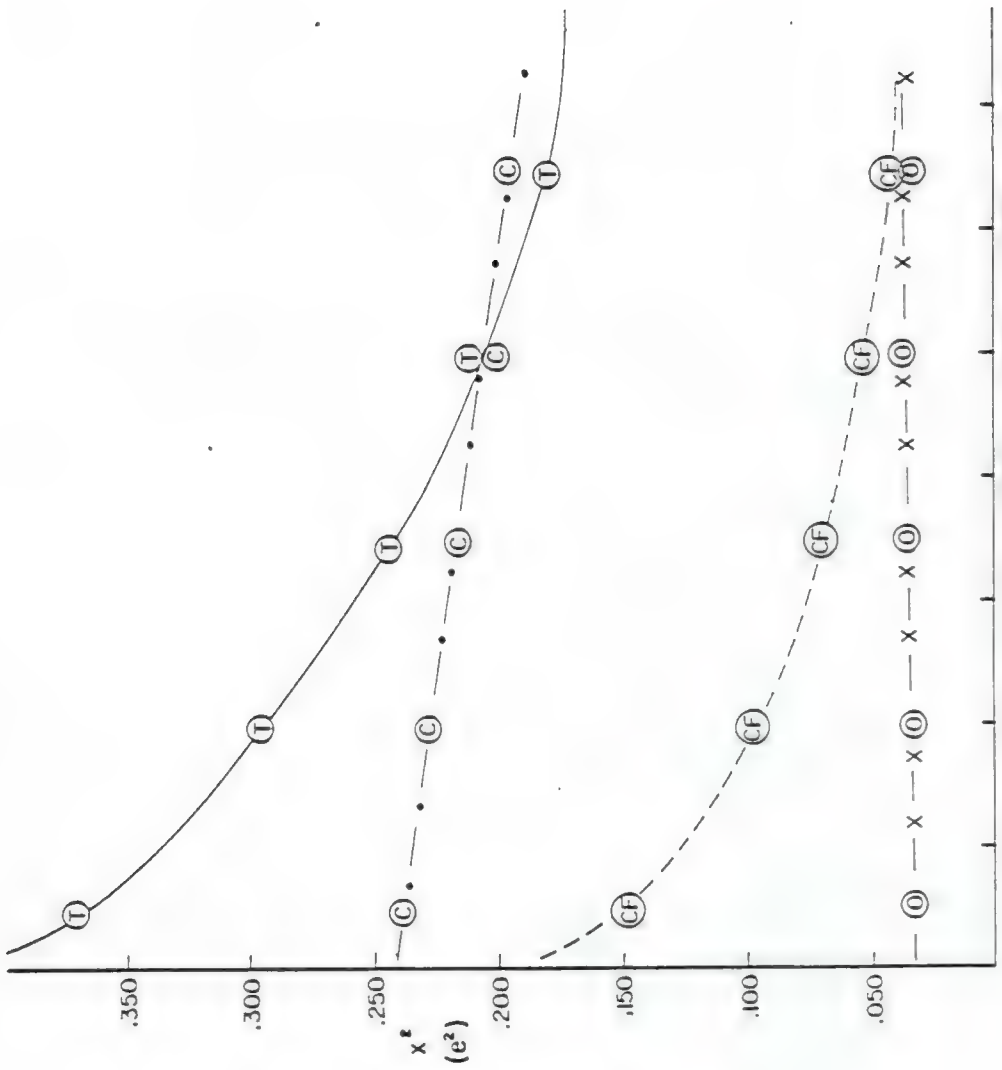
.350
.300
.250
.200
.150
.100
.050
x^2 (e^2)
2.583
2.683
2.783
2.883
2.983
3.083
3.183
R (O---O) (Å)
T
C
CF
O — X — X O — X — X O — X — X O — X

for the predicted intensity increase in the linear dimer, at distances both shorter and longer than the equilibrium distance.

As shown in Figure 4.1, the frequency of the symmetric stretching mode of the electron acceptor exhibited a linear dependence on the interaction distance. The frequency parameters were transformed to internal force constants via equation 33 in order to analyze exactly the origin of this linear dependence. The force constants in md/A° for the four intramolecular stretching coordinates, the two intramolecular bending coordinates and the hydrogen bond stretching coordinate are given, for all the interaction distances calculated, in Table 4.13. There appears to be no obvious dependence on a single force constant on the interatomic distance. In fact, while some of the expected trends in the force constants are found, others are not. For example, it would be expected that the hydrogen bond stretching constant $F(R_7R_7)$ would decrease as the interaction distance increased. This is not the case as indicated by Table 4.13. However, we see in Table 4.13 that this force constant does increase as the intermolecular distance decreases from the equilibrium value. Hence, the expected trend in the hydrogen bond force constant is observed for shorter intermolecular distances but not for longer distances. However, the predicted changes in the hydrogen bond stretching constant are certainly not of the same order of magnitude at shorter distances compared with those at longer distances. At shorter distances there is a definite increase in this force constant; in fact it is

Table 4.13 Selected diagonal internal force constants (md/A°) for the linear dimer as the intermolecular distance, R(O---O), is varied. Internal coordinate definitions as given in Table 4.8.

Internal Coordinate	R = 2.532 A°	R = 2.682 A°	R = 2.832 A°	R = 2.982 A°	R = 3.132 A°
R_1	9.171	9.205	9.213	9.193	9.251
R_2	9.171	9.205	9.213	9.193	9.251
R_3	8.747	8.885	8.540	8.737	8.811
R_4	9.084	9.119	9.145	9.158	9.159
R_5	.746	.775	.726	.793	.793
R_6	.696	.740	.753	.772	.757
R_7	.848	.647	.087	.186	.253

almost eight times greater (or an increase of almost 0.600 md/A°) for an increment in R(O---O) of only -0.15 A°. At longer intermolecular distances this increase is not as pronounced, being less than 0.100 md/A° for an increment of 0.15 A° in R(O---O). We believe that the predicted increase in the hydrogen bond force constant as the interaction distance becomes longer is actually within the limits of error for these types of calculations, and that if this distance were lengthened even further, then this force constant would indeed actually decrease from the theoretical equilibrium value.

It is interesting that even though the errors inherent in the force constant calculations create somewhat unexpected trends in the predicted force constants, the calculated frequencies (for the symmetric stretch of the electron acceptor) do seem to follow the expected trends. This suggests that there is another effect present which is of greater importance than the limits of error in the force constant calculations. This effect is the intermolecular coupling that is present between the two molecules as they are allowed to interact. Using the program VIBRATE (see Appendix A), the symmetric stretching vibration for the electron acceptor at three different intermolecular distances R were frozen and dumped to the printer. These vibrations are pictured in Figures 4.3, 4.4, and 4.5 for distances of R = 2.532 A°, 2.832 A°, and 3.132 A° respectively. At R = 2.832 A°, or the theoretical equilibrium, the symmetric stretching vibration for the

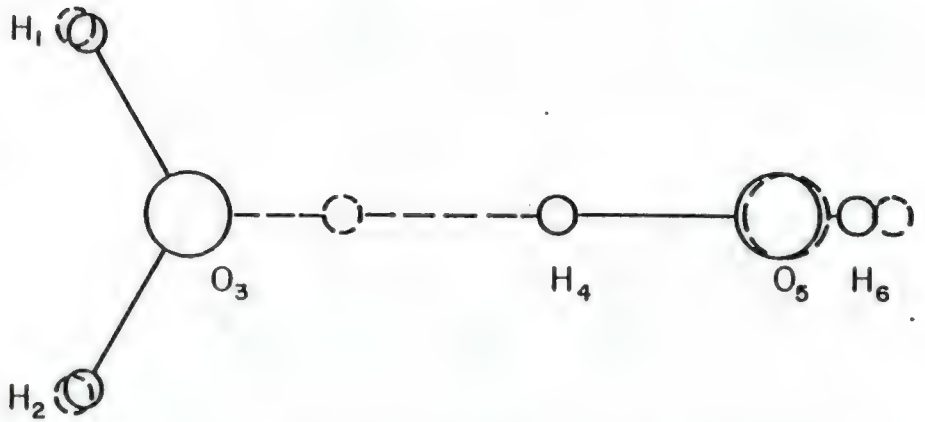

Figure 4.3 Pictorial representation of the symmetric stretching vibration for the electron acceptor molecule of the linear dimer at an assumed intermolecular distance of 2.532 A°. The solid circles represent the equilibrium structure for the dimer. The dotted circles represent the positions of the corresponding atoms during one phase of the symmetric stretching vibration.

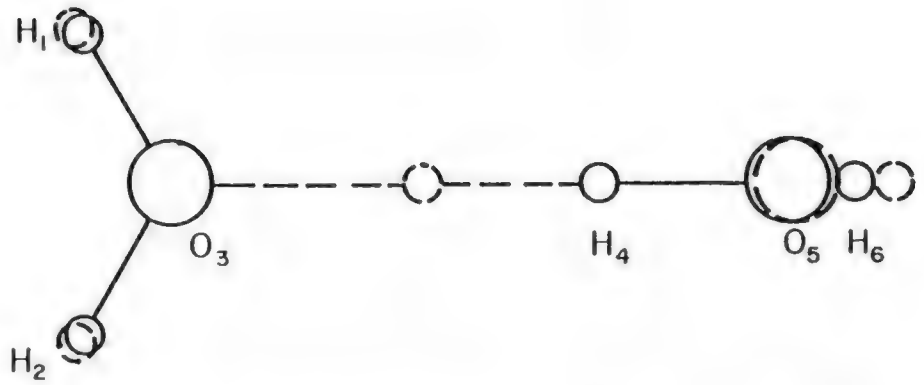

Figure 4.4 Pictorial representation of the symmetric stretching vibration for the electron acceptor molecule of the linear dimer at an assumed intermolecular distance of 2.832 A°. The solid circles represent the equilibrium structure for the dimer. The dotted circles represent the positions of the corresponding atoms during one phase of the symmetric stretching vibration.

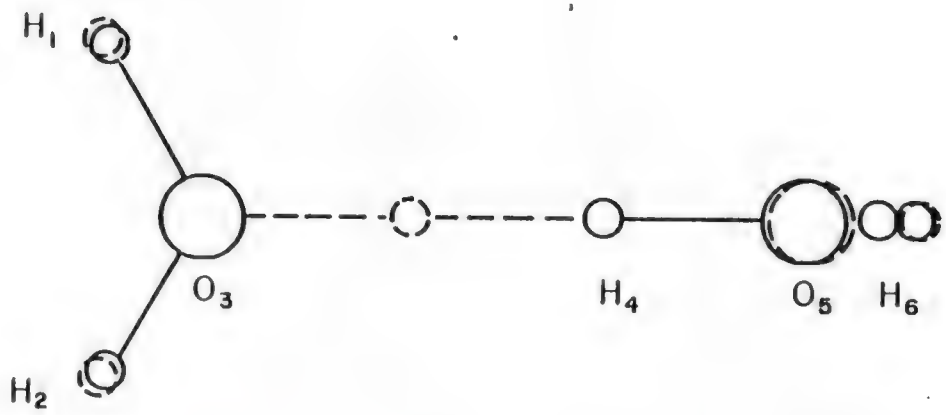

Figure 4.5 Pictorial representation of the symmetric stretching vibration for the electron acceptor molecule of the linear dimer at an assumed intermolecular distance of 3.132 A°.

electron acceptor is predominately of electron acceptor character, with only a small amount of mixing with the motion of the two hydrogen atoms of the electron donor. Essentially this vibration is localized on the electron acceptor, and there is very little coupling between the two molecules. For R = 3.132 A°, the symmetric stretching vibrations of the electron acceptor and the electron donor are still essentially uncoupled. The slight increase in the frequency of this vibration relative to the frequency of this same vibration at R = 2.832 A° is due instead to the slight increase in the O-H stretching force constant as seen in Table 4.13. This increase in both the force constant and the frequency would be expected based on the argument that as the molecules are separated further, they should behave more like independent monomers, and the corresponding properties of these molecules should approach those of the isolated molecules. Therefore the bonded O-H stretching force constant increases, and is tending towards the monomer value of 9.14 md/A°. Finally, at R = 2.532 A°, the frequency of the symmetric stretching vibration of the electron acceptor is slightly less than the frequency of the corresponding vibration at R = 2.832 A°. The vibration for R = 2.532 A° is pictured in Figure 4.3. Here, as evidenced by the slight increase in the amplitudes of motion for the hydrogen atoms in the electron donor relative to these same amplitudes of motion for this same vibration pictured in Figure 4.4 for R = 2.832 A°, we can see that the intermolecular coupling becomes more important as the distance is shortened.

This increase in coupling results in a further decrease in frequency (relative to R = 2.832 A°) due to the decrease in local O-H oscillator stretching character of this vibration.

Physically, these results appear to make much sense. As the two molecules are separated, they would be expected to begin to regain the properties of the totally separated and isolated molecules. This fact is evidenced by the increase in the frequency of the symmetric stretching vibration of the electron acceptor and the increase in the O-H stretching force constant, both towards the monomer values. At shorter distances we would expect that the coupling between the two molecules would become more important. This is supported by the increased coupling present between the electron acceptor and the electron donor in the symmetric stretching mode of the electron acceptor, as depicted in Figure 4.3.

CHAPTER 5
THE CYCLIC WATER-WATER COMPLEX

The cyclic configuration of a pair of interacting water molecules was believed by some workers (20,27) to be the correct interpretation of the experimental spectrum for the water dimer. Behrens and Luck (27) argue that the available experimental and theoretical data do not exclude the presence of cyclic dimers in matrices, and that there may be both linear and cyclic structures present.

In an ab initio SCF calculation using a 4-31G basis set, Kerns and Allen (40) have determined the stabilization energy of the cyclic complex to be 7.22 kcal/mole. This value can be compared with the value of 8.2 kcal/mole calculated by Curtiss and Pople (30), which is in exact agreement with the value calculated by Kerns and Allen (40) for the linear dimer. While the calculations of the binding energy for the cyclic complex by Kerns and Allen (40) was carried out using only a restricted geometry optimization (intermolecular parameters R and θ in Figure 1.2), the predicted order of stability (linear is more stable than cyclic) is in agreement with other theoretical predictions (31,35-37). However, this increased stabilization predicted for the linear form over the cyclic form is not more than 1.0 kcal/mole. Therefore, is it of interest to calculate the infrared spectrum

expected for the cyclic structure to compare these results with those predicted for the linear form in case both forms might be present in the matrix.

The assumed equilibrium geometry of the pair of water molecules in a cyclic configuration is given in Figure 1.2. The internal geometries of the two water molecules were chosen to be the same as for the monomer at its calculated geometry, and the intermolecular parameters were taken from the SCF calculation by Morokuma and Pedersen (36). In their calculation Morokuma and Pedersen (36) have used a smaller basis set than the 4-31G basis set (3 s-type orbitals on H, 5 s-type with 3 p-type orbitals on O) and chose to optimize the cyclic structure with respect to only three intermolecular parameters R, θ and ϕ (see Figure 1.2). Therefore, our assumed structure does not have the totally optimize geometry for this configuration that we might calculate using the 4-31G basis set, but it is believed that the optimized geometry would not differ by much. The calculation of Morokuma and Pedersen (36) on the linear structure gave a distance of R = 2.68 A°. This distance can be compared to the value calculated by Curtiss and Pople (30) for the linear structure using the 4-31G basis set of R = 2.832 A°. The agreement between these two results is fair, and suggests that the parameters calculated by Morokuma and Pedersen (36) for the cyclic configuration are a good estimate of the geometry that we might calculate with the 4-31G basis set. However, it should be emphasized here that the intermolecular distance (R(O---O) = 2.74 A°) calculated by Morokuma and Pedersen (36) for the cyclic complex appears

to be shorter than the value that we might predict using the 4-31G basis set.

The cyclic configuration pictured in Figure 1.2 has C_i symmetry, with the center of inversion marked by the asterisk. Both molecules are involved in electron donor-acceptor action, and therefore neither one can be classified strictly as one or the other. For this discussion, we will examine the calculations done at the optimized intermolecular distance of Morokuma and Pedersen (36) of R = 2.74 A°, where R is defined as the distance between heavy atoms (in this case O atoms). This distance is probably shorter than the value that would be predicted using the 4-31G basis set and we would expect that this will overemphasize the importance of any interaction which may be indicated by the calculation. The principal cartesian coordinates for the cyclic configuration at this intermolecular distance are given in Table 5.1. The 3N = 18 degrees of freedom for this complex are $9A_g + 9A_u$, and the 3N-6 or 12 vibrational degrees of freedom are $6A_g + 6A_u$. The 6 symmetric A_g vibrations are not infrared active, but only Raman active, while the 6 asymmetric A_u vibrations are infrared active, but not Raman active. The net result is that three high frequency modes and three low frequency modes are infrared active, while corresponding numbers of modes are Raman active.

The frequencies and intensities predicted using the procedure described earlier for the cyclic pair of water molecules at an intermolecular distance of 2.74 A° are listed in Table 5.2. The corresponding assignments were made with the aid of

Table 5.1 Principal cartesian coordinates for the assumed equilibrium geometry of the cyclic complex (A°). Atom numbering as given in Figure 1.2.

	X	Y	Z
O_1	.0204	-.0606	-1.3692
H_2	.4294	.4603	-.6855
O_3	-.0204	.0606	1.3692
H_4	-.4294	-.4603	.6855
H_5	-.3590	.4902	-2.0438
H_6	.3590	-.4902	2.0438

the graphics program VIBRATE (see Appendix A). The negative eigenvalues arise due to the fact that the assumed geometry was not the optimized equilibrium positions. From our earlier calculations on the linear dimer we would not expect the low frequency modes to exert much influence (certainly almost no influence on the stretching modes, with only a slight influence expected on the bending modes) on the high frequency modes due to the large difference in energy. In addition, it has been our experience from earlier calculations on isolated water monomers that the intensities are almost independent of the assumed geometry.

The essential characteristics of the high frequency vibrational modes are such that the individual modes of the two molecules are coupled either in phase (A_g) or out-of-phase (A_u) to form the normal mode for the complex. One of these vibrations, the infrared active symmetric stretching mode, is pictured in Figure 5.1. This figure depicts the magnitude and phase of the coupling present in this vibration, both of which are a direct consequence of the symmetry of the molecule. From this figure it is seen that the vibrational displacements contain equal contributions from both molecules, and that the phase of the coupling between the molecules determines the activity of the vibration in the infrared spectrum. In this case, the two symmetric stretching vibrations are coupled out-of-phase, and therefore this vibration is infrared active. Similar descriptions of the remaining vibrations are given in Table 5.2.

Table 5.2 Predicted wavenumbers and intensities for the assumed equilibrium geometry of the cyclic complex at R(O---O) = 2.74 A°, compared to the corresponding predicted wavenumbers and intensities for the monomer.

		Complex		Monomer	
Mode	Description	$\nu(cm^{-1})$	A(km/mole)	$\nu(cm^{-1})$	A(km/mole)
1	Out of phase asymmetric stretch	4115	260	4104	54
2	In phase asymmetric stretch	4115	0[a]	4104	54
3	Out of phase stretch	3957	46	3983	3.9
4	In phase symmetric stretch	3929	0[a]	3983	3.9
5	In phase bending	1771	0[a]	1676	125
6	Out of phase bending	1740	270	1676	125
7	Out of phase twisting of both molecules	776	756		
8	In phase O_1H_5 and O_3H_5 wagging	339	0[a]		
9	Ring breathing	208	0[a]		
10		b			
11		b			
12		b			

[a]Zero by symmetry.

[b]Imaginary frequency.

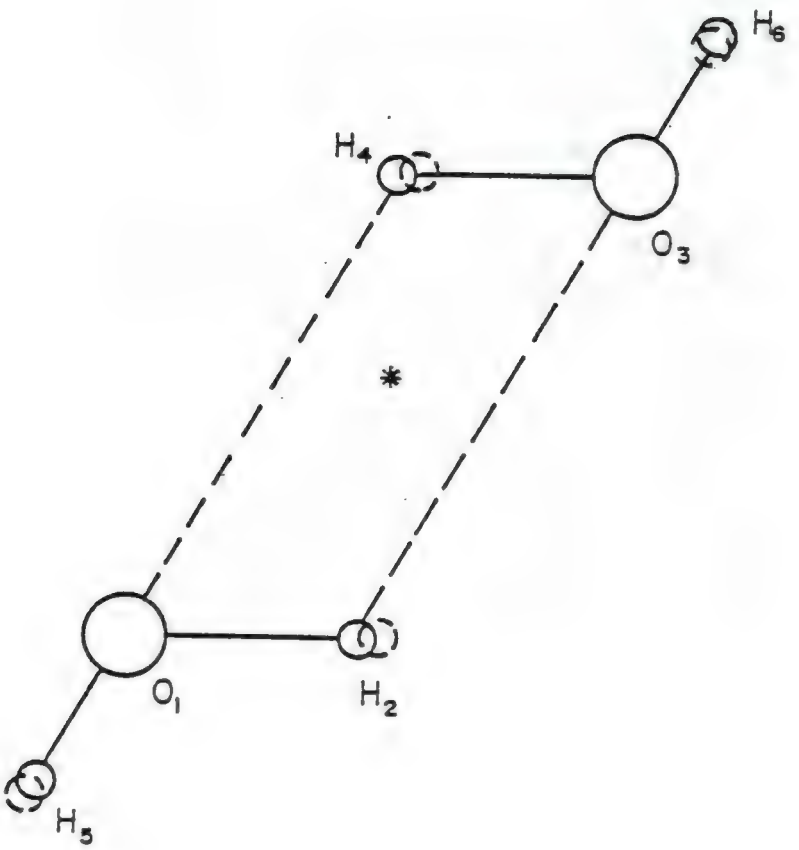

Figure 5.1 Pictorial representation for the infrared active symmetric stretching vibration of the cyclic configuration of a pair of water molecules with an assumed intermolecular distance of 2.74 A°. The solid circles represent the equilibrium positions of the atoms while the dotted circles are the positions of the atom during one phase of the vibration.

The frequencies for these high frequency modes are predicted not to be shifted very much from their corresponding monomer values even at this very close interaction distance. The vibrations corresponding to A_g and A_u asymmetric stretching remain almost constant, while the symmetric stretching modes shift 26 cm^{-1} and 54 cm^{-1} towards lower energy for the infrared and Raman active modes respectively. These predicted shifts are considerably less than the value predicted for the shift of the symmetric stretch of the electron acceptor in the linear case. The bending modes are predicted to shift upwards 64 cm^{-1} for the infrared active mode and 95 cm^{-1} For the Raman active band, again less than the prediction for the corresponding modes of the dimer in the linear configuration. The predicted intensity pattern is very interesting, since each of the three infrared active bands are predicted to be more intense than the corresponding bands in the monomer. The asymmetric stretch increases by almost a factor of four from 54 km/mole to 260 km/mole, the symmetric stretch by a factor of 11, from 3.9 km/mole to 46 km/mole, and the bending mode by a factor of two from 125 km/mole to 270 km/mole. The predicted changes for these individual bands are rather large, but nevertheless still much smaller than the predicted changes for the same bands in the linear configuration. Let us just point out here that the intensity sum for these three infrared active bands is 576 km/mole, and this sum is comparable to twice the intensity sum for an isolated water molecule (366 km/mole).

5.1 Intensity Analysis for the Cyclic Complex

Before beginning, it is necessary to determine exactly which effects are responsible for the predicted intensity changes; is it the change of the normal coordinates (mechanical effect) or the electronic effects of the interaction which would be reflected in the APTs? In the linear case we saw that the mechanical effect was very small, while the electronic effects were mainly responsible for the predicted intensity changes. In order to determine if the same situation is true for the cyclic configuration, the program PXPQ (see Appendix A) was used. The intensities calculated with the normal coordinate transformation for the cyclic configuration and the corresponding calculated monomer APTs are given in column three of Table 5.3. These intensities reflect the values that would be expected from two water molecules that were not allowed to interact electronically, but were only allowed to mix their vibrations to form new normal vibrations. It can be seen that the changes in the normal coordinates upon complex formation are responsible for almost 93% of the total increase in the bending intensity, 42% of the total increase in the asymmetric stretching intensity, and 18% of the total increase in the symmetric stretching intensity. These results indicate that some of the predicted changes in the band intensities in the cyclic configuration (relative to the isolated monomer) are due to a mechanical effect. This result was not found to be true in the linear case. However, this can be

Table 5.3 Calculated contributions to the predicted intensities of the six intramolecular vibrations for the assumed equilibrium geometry of the cyclic complex.

	Intensities (km/mole)				
$\nu(cm^{-1})$	Calculated Cyclic	Calculated Using Monomer APTs	Add H_2 P(CF)	Add H_2 P(C) + H_2 P(O)	Monomer
4115	260	110	184	222	54
4115	0[a]	-	-		
3957	46	8.3	24	35	3.9
3929	0[a]	-	-		
1771	0[a]				
1740	270	250	253	255	125

[a]Zero by symmetry.

partially explained by remembering that the normal coordinates for the cyclic configuration are simply the in phase and out-of-phase coupled vibrations of the individual monomer units. Based only on these normal coordinates, this would lead us to believe that the intensity for each of the three infrared active bands would be approximately twice that of the corresponding monomer value. The intensities calculated taking only this effect into account are almost in exact agreement with twice the intensity for the corresponding band in the monomer (see columns three and six of Table 5.3). The remainder of the predicted intensity increase must be due to some electronic effects of the interaction between the two molecules, and its origin must lie in the polar tensors.

The predicted intensities for the cyclic configuration were then analyzed by transforming the intensity parameters to APTs using equations 20 and 22. The APTs for three of the atoms of the cyclic configuration are listed in Table 5.4 in the coordinate system shown in Figure 1.2, along with the corresponding monomer APTs rotated to the same coordinate system for comparison. Only three of the six atoms are reported here because the center of inversion of the molecule requires that each atom have an equivalent partner, and therefore the APTs for each pair of atoms must be exactly the same (i.e., O_1, O_3; H_2, H_4; H_5, H_6).

Since the normal coordinates are mass weighted motions of all the atoms in the molecule, the hydrogen atoms are the most important atoms to consider in analyzing the intensities. The

Table 5.4 Calculated APTs for the assumed equilibrium geometry of the cyclic complex compared to the corresponding APTs for the mononer (e) (1 e = 1.602 x 10^{-19} C). Atom numbering and coordinate system as in Figure 1.2.

		Cyclic			Monomer		
$P_X^{O_1}$ =		-.7464	-.0642	.2257	-.686	-.034	.238
		+.0177	-.6635	-.1188	-.034	-.517	-.029
		.2006	-.1022	-.8411	.238	-.029	-.760
$P_X^{H_2}$ =		.4094	.0406	-.0495	.407	.032	-.064
		.0470	.2926	.1361	.068	.148	.058
		-.0705	.0760	.5137	-.064	.027	.427
$P_X^{H_5}$ =		.3370	.0236	-.1762	.280	.002	-.173
		-.0647	.3710	-.174	-.034	.369	-.029
		-.1301	.0227	.3274	-.173	.002	.333

hydrogen atoms H_2 and H_4 exibit the most significant changes in their APT elements. Some changes are predicted in the APTs for these atoms; the largest change occurs in the P_{yy} term, where there is a predicted increase of 0.1446 e or almost a 98% increase. The predicted changes are relatively small compared to the changes predicted for the linear configuration. The APTs of the remaining hydrogen atoms are not predicted to change much from the corresponding polar tensors in the monomer.

The CCFO analysis was performed on the APTs for the cyclic configuration, as described earlier. The atomic charge, charge flux and overlap tensors for the three non-equivalent atoms of this geometry are given in Tables 5.5, 5.6, and 5.7 respectively. The CCFO analysis is helpful in determining which effects are primarily responsible for the increase in the APT element, and hence in the intensity. For the atomic charge tensor and the overlap tensor, the P_{yy} term of H_2 is almost constant on going from the monomer to the cyclic pair. However, the charge flux term for this atom increases by 0.1018 e or 70% of the total change in the APT element. It becomes clear then that the main contribution to the increase in the APT element is due to an increase in the charge flux term, and not due to a change in either the atomic charge or overlap terms.

Column four of Table 5.3 gives the calculated intensities for the cyclic configuration using the calculated normal coordinates for this complex and the calculated monomer APTS, except now we have adjusted the P_{yy} term of the monomer APTs to reflect the predicted increase in charge flux in this term

Table 5.5 Calculated charge tensors for the assumed equilibrium geometry of the cyclic complex compared to the corresponding tensors in isolated water (e) (1 e = 1.602 x 10^{-19} C). Atom numbering and coordinate system as in Figure 1.2.

	Cyclic			Monomer		
$P(C)^{O_1}$ =	-.8381	0	0	-.8034	0	0
	0	-.8381	0	0	-.8034	0
	0	0	-.8381	0	0	-.8034
$P(C)^{H_2}$ =	.4312	0	0	.4017	0	0
	0	.4312	0	0	.4017	0
	0	0	.4312	0	0	.4017
$P(C)^{H_5}$ =	.4069	0	0	.4017	0	0
	0	.4069	0	0	.4017	0
	0	0	.4069	0	0	.4017

Table 5.6 Calculated charge flux tensors for the assumed equilibrium geometry of the cyclic complex compared to the corresponding tensors in the monomer (e) (1e = 1.602 x 10^{-19} C). Atom numbering and coordinate system as given in Figure 1.2.

	Cyclic			Monomer		
O_1 P(CF)=	.0102	-.0902	-.0265	.016	-.070	.013
	-.0634	-.1583	-.1648	-.070	-.046	-.060
	-.0132	-.1381	-.0622	.014	-.060	.011
H_2 P(CF)=	-.0551	.0050	-.0173	-.046	-.009	-.039
	.0223	.1908	.1442	.041	.089	.035
	-.0428	.0577	.0458	-.039	-.008	-.034
H_3 P(CF)=	.0449	.0852	.0437	.030	.080	.026
	.0411	-.0325	.0206	.030	-.043	.025
	.0559	.0803	.0164	.026	.069	.022

Table 5.7 Calculated overlap tensors for the assumed equilibrium geometry of the cyclic complex compared to the corresponding tensors in the monomer (e) (1e = 1.602 x 10^{-19} C). Atom numbering and coordinate system as given in Figure 1.2.

		Cyclic			Monomer		
O_1 P(O)	=	.082	.026	.253	.101	.035	.224
		.081	.332	.046	.035	.329	.030
		.214	.036	.059	.224	.030	.031
H_2 P(O)	=	.033	.036	-.033	.052	.041	-.024
		.0258	-.329	-.008	.027	-.343	.023
		-.027	.021	.036	-.024	.035	.060
H_5 P(O)	=	-.115	-.062	-.220	-.153	-.077	-.200
		-.106	-.003	-.038	-.065	.013	-.055
		-.186	-.057	-.096	-.200	-.065	-.092

upon complex formation. These calculated intensities indicate that the increase in charge flux in the P_{yy} term of atom H_2 is responsible for 50% and 42% of the intensity increase above the mechanical effect, for the asymmetric and symmetric stretching modes respectively. In addition, these two effects combined also account for 71% and 52% of the total intensity increase for these two modes. Column five of Table 5.3 gives the intensities calculated for the cyclic configuration by adding the differences from the complex to the monomer in both charge and overlap. The differences in the charge and overlap tensors are small, and it is seen that their influence on the intensities is also smal. In fact, these intensities are not much different from those in column four, where we have only included the change in charge flux and the mechanical effect. The intensities in column five are not quite equal to the predicted intensities for the cyclic configuration (column two) because of some minor contributions from other APT elements besides the P_{yy} term.

To summarize, the results in Table 5.3 indicate that the predicted intensity increase for the cyclic pair of water molecules has two contributions. Without any changes in electrical properties due to the interaction, the mechanical coupling of the vibrations of the two individual molecules to form the normal coordinates of the complex is responsible for almost half of the predicted intensity changes. However, the change in electrical properties from the charge flux contributions

the P_{yy} terms in the APT of H_2 are also responsible for approximately an equal amount for the stretching modes. The contributions from charge and overlap are minor.

5.2 Frequency Analysis for the Cyclic Complex

The predicted frequencies for the cyclic configuration are in general not perturbed much from the corresponding frequencies in the isolated monomer. The frequencies corresponding to the stretching vibrations of the complex are all within 65 wavenumbers of the corresponding monomer values. However, the bending frequencies are in a bit worse agreement with the monomer values, being predicted about 100 cm^{-1} higher in the cyclic complex. These differences can be analyzed by calculating the frequency parameters in internal coordinates.

The transformation from force constants in $\overline{S}$ coordinates to internal force constants is given by equations 18 and 33. This transformation requires the $\underline{A}$ matrix, or the "inverse" of the $\underline{B}$ matrix, derived using equation 32. This requires that the $\underline{G}$ matrix, defined in equation 29, be non-singular. The $\underline{G}$ matrix is non-singular only when a complete non-redundant set of internal coordinates have been defined. For cyclic molecules it is necessary to define 3N "typical" internal coordinates to completely define the kinetic energy of the molecule (10,11). This introduces six cyclic redundancies, which must first be removed before the $\underline{A}$ matrix can be calculated. Various workers have discussed this problem in the past (84-90), and have proposed different solutions,

any one of which can be used. In essence, the solution to this problem involves choosing the proper combinations of internal coordinates such that these combinations are exactly the redundant coordinate. These redundant coordinates can then be ignored, provided the remaining vibrational coordinates are described by taking symmetrized linear combinations of these internal coordinates such that these combinations are orthogonal to the redundant coordinates. In this way we can reduce the number of original internal coordinates (by the number of redundancies) to the appropriate number of symmetry coordinates (usually 3N-6). More detailed discussions concerning the actual procedures involved can be found elsewhere (84-90).

After reducing the number of internal coordinates (by the number of redundancies) in order to form the symmetry coordinates, the potential energy in terms of these symmetry coordinates can be uniquely determined. However, it can be shown that the transformation of the potential from the set of non redundancy symmetry coordinates to the original redundant set of internal coordinates is not unique (see Appendix C, equation 114). Instead, the force constants in the original set of redundant internal coordinates can only be determined by making some assumption concerning the form of the potential in these internal coordinates. In these calculations we have assumed that the force constants corresponding to the interaction between the intramolecular and the intermolecular vibrations are all equal to zero. We have seen

from previous results that this approximation is almost true, but not entirely correct. The vibrations corresponding to the bending motions were shown to mix with the low frequency intermolecular vibrations. Therefore, using this assumed potential, the internal bending force constants are determined as "effective" bending constants ("effective" with respect to the fact that they now include the interactions with the low frequency vibrations and are no longer pure bending force constants), and are not strictly comparable to the bending constants calculated in other isolated molecules. We would expect that the stretching constants calculated in this way are almost pure stretching constants though because these vibrations do not mix with the low frequency intermolecular modes.

The set of intramolecular internal coordinates used in these calculations are defined in Table 5.8, and the corresponding calculated force constants using the approximation previously discussed are given in Table 5.9. The frequencies calculated with these force constants are given in Table 5.10, column three. These frequencies agree very well with the ones given in Table 5.10, column two, which were calculated without any assumptions about the form of the potential.

The intramolecular frequencies given in Table 5.10 can now be analyzed in terms of these calculated force constants. The diagonal force constants are not much different from the corresponding monomer values (see Table 3.6), which is to be expected since the individual monomer geometries in the cyclic configuration were not changed from the isolated monomer

Table 5.8 Intramolecular internal coordinate definitions used in the cyclic complex. Atom numbering as in Figure 1.2.

Coordinate No.	Definition
R_1	R (O_1-H_2)
R_2	R (O_1-H_5)
R_3	R (O_3-H_4)
R_4	R (O_3-H_6)
R_5	d θ $(H_5-O_1-H_2)$
R_6	d θ $(H_6-O_3-H_4)$

Table 5.9 Calculated internal "effective" force constants (see text) for the six intramolecular internal coordinates (md/A°) of the cyclic complex. Internal coordinate definitions as given in Table 5.8 (weighting is done by d, where d = 1 A°).

	R_1	R_2	R_3	R_4	R_5	R_6
R_1	9.029	-.1646	-.1264	-.0203	.2289	-.0143
R_2		9.123	-.0203	.0602	.3459	-.002
R_3			9.029	-.1646	-.0145	.2289
R_4				9.123	-.002	.3459
R_5					.7743	.0081
R_6						.7743

Table 5.10 Calculated wavenumbers for the intramolecular vibrations of the cyclic complex at the assumed equilibrium geometry as several internal force constants are adjusted. Internal coordinates as defined in Table 5.8, force constants as defined in Table 5.9.

Mode	Calculated Cyclic	Calculated Approximate Potential	Change F_{55} and F_{66}	Change F_{11} and F_{33}	Change F_{12} F_{34}	Change F_{13} F_{24}	Calculated Monomer
1	4115	4115	4115	4126	4103	4121	4118
2	4115	4115	4115	4123	4098	4107	4118
3	3957	3957	3957	3965	3990	3950	3997
4	3929	3928	3928	3943	3967	3940	3997
5	1771	1759	1689	1689	1689	1760	1673
6	1740	1739	1668	1668	1668	1739	1673

geometry. The bending constant is the only one which is predicted to change, increasing slightly by 0.06 md/A° from 0.714 md/A° in the monomer to 0.774 md/A° in the cyclic complex. However, this bending force constant is an "effective" bending constant and cannot be strictly compared to the bending constant calculated in the isolated monomer. However, if we assume that this "effective" bending constant is the same in the cyclic complex as for the monomer (0.714 md/A°) the resulting predicted frequencies are given in Table 5.10, column four. Both bending frequencies are then predicted to shift down from 1759 cm^{-1} and 1739 cm^{-1} to 1689 cm^{-1} and 1668 cm^{-1}, close to the expected monomer value of 1673 cm^{-1}. This suggests that the origin of the predicted increases in the bending frequencies is due to coupling between these bending motions and the low frequency intermolecular vibrations. The predicted stretching force constants for all four O-H bonds of the cyclic complex (Table 5.9) are not very different from the monomer values. The differences are small, predicted to be less than 0.5%. These changes do not affect the predicted frequencies very much. The differences between columns four and five of Table 5.10 indicate the effect of these changes, which are less than 0.25%. The change in the stretching frequencies upon complex formation can be explained by the predicted change in the interaction constant between the two stretching coordinates of one molecule. This force constant (F_{12} and F_{34}) is predicted to be -.1646 md/A° in the cyclic complex, and only -0.065 md/A° in the monomer. The frequencies calculated after adjusting this force constant

to its monomer value are listed in Table 5.10, column six. These frequencies are now in good agreement with the monomer values, the average of the two frequencies being less than 0.5% different from the monomer value of 3997 cm^{-1}. This interaction constant determines the amount of splitting between the asymmetric and symmetric stretching modes within an individual molecule. The large negative value (-0.1646 md/A°) in the cyclic complex indicates that in the formation of the complex these two modes are split further than they are in the isolated monomer. The splitting of these modes in the isolated monomer is 121 cm^{-1}, while these same splittings are 158 cm^{-1} and 187 cm^{-1} in the cyclic complex. If the value of this interaction constant is changed from its predicted value of -0.164 md/A° to the predicted monomer value of -0.065 md/A°, then the splittings predicted for the cyclic complex are reduced to 110 cm^{-1} and 138 cm^{-1} (see Table 5.10, column six). In addition the stretching frequencies predicted with this interaction constant are now in better agreement with the predicted monomer values.

The predicted increases in the splitting between the stretching modes in the cyclic complex can best be explained by referring back to the structure of the cyclic configuration given in Figure 1.2. The symmetry is reduced from C_{2v} symmetry in the monomer to C_i symmetry in the complex. With this reduction in symmetry the two O-H bonds within each molecule are no longer equivalent, and the coupling between these two bonds changes. As a result, the predicted stretching frequencies

are split further in the complex than in the isolated monomer. This seems to point to the origins of the predicted frequency shifts in the cyclic complex relative to the isolated monomer as being related to symmetry arguments. We have shown that the predicted shifts in bending frequencies are due to the increase in the "effective" bending constant, which in turn is probably due to the presence of intermolecular coupling between the bending vibrations and the low frequency vibrations. In addition, the predicted shifts in the stretching frequencies have been shown to be due to the presence of increased intramolecular coupling, reflected in the interaction force constants R_1R_2 and R_3R_4. These results are completely different from the results predicted for the linear dimer, where we saw that the frequency shift of the symmetric stretching mode for the electron acceptor was almost entirely a result of the weakening of the bonded O-H bond upon dimer formation. Finally, it is also interesting to note that the intermolecular coupling does not seem to play an important role in determining the frequencies of the six intramolecular vibrations. The intermolecular coupling constants between the stretching coordinates of the two different molecules (F_{13}) is -0.12644 md/A°, a reasonably large amount. However, the effect of changing this constant to -0.05 md/A° is minimal. The frequencies calculated using this value are listed in column six of Table 5.10. The changes from the predicted intramolecular frequencies of the cyclic complex are insignificant.

5.3 Further Calculations on the Cyclic Complex at Different Interaction Distances

In the linear dimer it was shown that the predicted spectral changes upon complex formation were strongly dependent upon the assumed geometrical orientation of the two molecules. In the cyclic configuration the spectral changes are predicted to be much less significant than those predicted for the linear dimer. This suggests that for less energetically stable complexes the dependence of the spectral properties of the intermolecular distance might be expected not to be as strong as in more energetically favorable complexes. Therefore, additional calculations were performed on the cyclic configurations with varying intermolecular distances. The infrared spectrum of the cyclic pair was calculated at a shorter intermolecular distance (2.65 A°), a longer distance (2.99 A°), and also with one molecule rotated 180 degrees so that the center of inversion was destroyed. The predicted frequencies and intensities for these different configurations of the cyclic pair of water molecules are given in Table 5.11. The predicted frequencies for an intermolecular distance of 2.65 A° are strongly perturbed from the expected monomer values. This is not what would be expected for such a weak energetically stabilized system. A calculation at a distance of 2.51 A° predicted even more highly perturbed results. The large predicted changes in frequencies at these shorter intermolecular distances are not due to the interaction of the two molecules, but are believed to result instead from the presence of extremely strong mechanical effects. The effect of forcing two molecules together

Table 5.11 Predicted wavenumbers and intensities for the intramolecular vibrations of the cyclic complex as the intermolecular distance, R(O---O), is varied.

Mode	R = 2.65 A°		R = 2.74 A°[c]		R = 2.74 A°[a,c]		R = 2.99 A°	
	cm^{-1}	km/mole	cm^{-1}	km/mole	cm^{-1}	km/mole	cm^{-1}	km/mole
1	3978	0[b]	4115	0[b]	4146	190	4121	0[b]
2	4176	332	4115	260	4124	32	4117	207
3	3747	24	3957	46	4011	50	3962	26
4	3656	0[b]	3929	0[b]	3989	10	3938	0[b]
5	1946	0[b]	1771	0[b]	1876	89	1759	0[b]
6	1340	282	1740	270	1810	183	1738	281

[a] Without the center of inversion. The center of inversion has been destroyed by rotating the water molecule (H_4-O_3-H_6) (see Figure 1.2) 180 around the H_4-O_3 bond. In this orientation, H_5 and H_6 both lie in the same plane, below the plane of the ring, and the center of inversion is destroyed.

[b] Zero by symmetry.

[c] This is the calculated heavy atom distance R(O_3--O_1) as given in reference 36.

is that we no longer have two interacting molecules, but rather one unrecognizable entity which retains none of the properties of the individual molecules. For example, the predicted high frequency normal vibrations for the cyclic configuration at an intermolecular distance of 2.51 A° do not even begin to resemble the corresponding vibrations in isolated water. This is shown in Figure 5.2, where we have pictured the normal mode for the vibration which should correspond to the out-of-phase combination of the asymmetric stretching modes of the two molecules. While the bonded O-H bonds are indeed stretching, the non-bonded O-H bonds are wagging. Clearly, the combinations of the molecular vibrations that one would expect (for example see Figure 5.1 and the descriptions of these vibrations in Table 5.2) to form the normal vibrations are not present at this intermolecular distance. Instead, the predicted vibrations are unrecognizable and uninterpretable. For this reason the frequencies predicted for the intermolecular distance of 2.51 A° are not believed to carry much significance and are not listed in Table 5.11.

Therefore, disregarding the configuration without the center of symmetry for now, we are left with only two additional distances to consider. The predicted frequencies for the molecular separation of 2.74 A° and 2.99 A° are listed in Table 5.11. The predicted wavenumbers for the cyclic complex at both of these distances are almost identical, with the largest difference being only 12 cm^{-1} for the Raman active bending mode. Because of the near equivalence of the two sets of

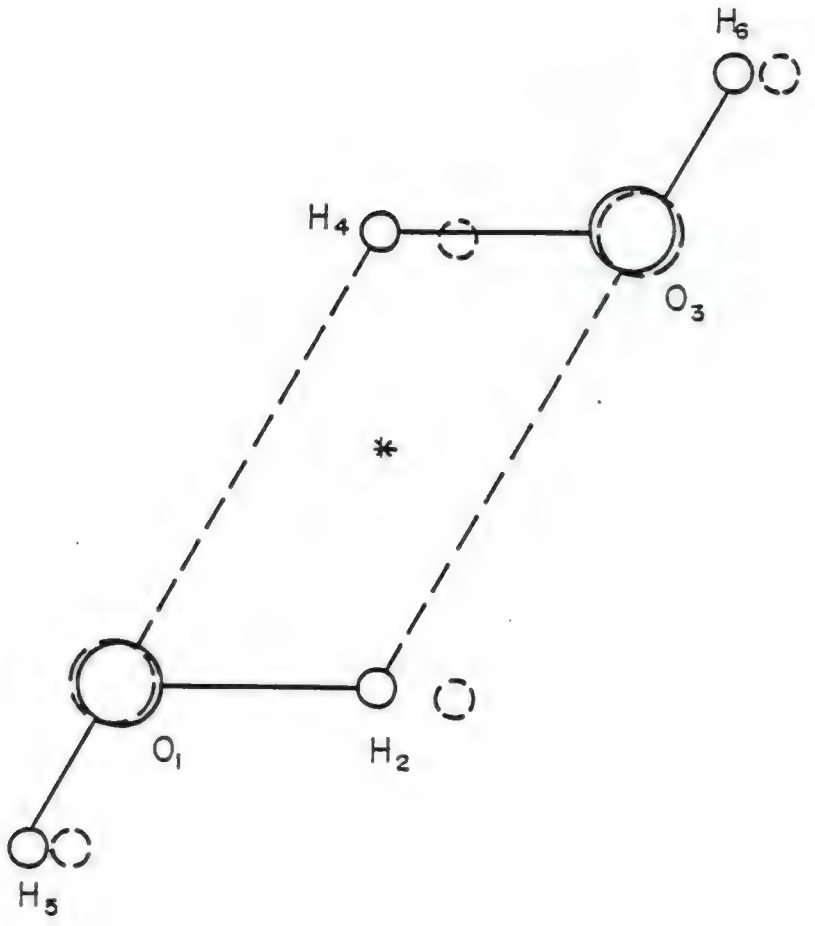

Figure 5.2 Pictorial representation for the infrared active asymmetric stretching vibration of the cyclic configuration of a pair of water molecules with an assumed intermolecular distance of 2.51 A°. The solid circles represent the equilibrium positions of the atoms while the dotted circles are the positions of the atoms during one phase of the vibration.

predicted frequencies, it is not worthwhile to try to analyze these differences based on changes in force constants as the distance is changed. It suffices to say here that the absorption frequencies for weak energetically stabilized complexes are almost independent of the interaction distance (at reasonable values for this distance). This statement is further supported by a series of calculations performed on the weak van der Waals complex H_2O--CO at different interaction distances (91).

On the other hand, the predicted intensities for these complexes discussed above show more significant changes. In general, the predicted intensities for the cyclic configuration exhibit a slight increase as the interaction distance is decreased. These results are similar to those that were found earlier for the linear dimer. Even at the interaction distance of 2.65 A°, where the predicted frequencies are physically unreasonable, the intensities follow the expected trend, in that they are predicted to show a slight increase over those predicted at longer distances (2.74 A° and 2.99 A°). In addition, these predicted values seem to be reasonable quantities based on the predicted intensities at an intermolecular distance of 2.74 A°. It appears from these results that the prediction of infrared intensities is not as sensitive to the assumed geometry as the prediction of infrared absorption frequencies. This may be due in part to the fact that the frequencies are directly dependent upon the geometry due to the contributions from the kinetic energy ($\underline{G}$ matrix) (see equation 6), while the intensities are not directly dependent on the geometry in any way.

The predicted changes in intensities in the cyclic complex, which are due to electronic effects as the interaction distance is changed, can be analyzed by interpreting the predicted APTs for this complex at varying interaction distances. We have previously shown that the bonded hydrogen atom is the most important atom to consider when trying to explain the predicted electronic intensity changes in the cyclic complex relative to isolated water. Therefore, the APTs for the bonded hydrogen atoms at various intermolecular distances were calculated and are listed in Table 5.12. The calculation at R = 2.65 A° was also included in this table because while the predicted frequencies seem unreasonable, the predicted intensities are reasonable values for what we might expect. The CCFO analysis for these predicted APTs is also given in this table. These tensors are all reported in the coordinate system given in Figure 1.2. Upon inspection of the APTs, it becomes obvious that there are changes as the interaction distance is varied, but that these changes are not very drastic. In addition, when the CCFO tensors are analyzed, it appears that the majority of these changes in the APTs are due to differences in charge flux. The validity of this statement can be tested by analyzing the effective invariants of the APT and its constituent tensors, the CCFO tensors.

The effective invariants for the APT and its constituent tensors have been previously defined in Chapter 2. These four effective invariants are plotted versus the interaction distance in Figure 5.3. From this figure it becomes obvious that

Table 5.12 Calculated APTs and CCFO tensors for the bonded hydrogen atom of the cyclic complex as the intermolecular distance, R(O---O), is varied (e) (1 e = 16.02 x 10^{-19} C). The calculated effective invariants for these tensors are also listed. Atomic number and coordinates as given in Figure 1.2.

	R = 2.65 A°	R = 2.74 A°	R = 2.74 A° [a]	R = 2.99 A°
$P_x^{H_2}$	$\begin{pmatrix} .4118 & .0999 & .0698 \\ .1369 & .3008 & .0682 \\ .0452 & .0313 & .5218 \end{pmatrix}$	$\begin{pmatrix} .4010 & .0848 & .0620 \\ .1294 & .2930 & .0629 \\ .0420 & .0269 & .5210 \end{pmatrix}$	$\begin{pmatrix} .3783 & .0749 & .0449 \\ .1353 & .2923 & .0568 \\ .0566 & .0390 & .5424 \end{pmatrix}$	$\begin{pmatrix} .3891 & .0684 & .0501 \\ .1170 & .2479 & .0449 \\ .0356 & .0139 & .5155 \end{pmatrix}$
$(\chi_{H_2})^2$ (e^2)	.1912	.1841	.1856	.1675
$P(C)^{H_2}$	.4350	.4312	.4311	.4226
$(\chi_C^{H_2})^2$	.1892	.1859	.1859	.1786
$P(C)^{H_2}$	$\begin{pmatrix} -.0250 & .0575 & .0707 \\ .1207 & .1933 & .0927 \\ .0373 & -.0431 & .0245 \end{pmatrix}$	$\begin{pmatrix} -.0347 & .0443 & -.0632 \\ .1177 & .1908 & .0862 \\ .0377 & .0373 & .0254 \end{pmatrix}$	$\begin{pmatrix} -.0656 & .0383 & .0511 \\ .1188 & .1923 & .0840 \\ .0463 & .0503 & .0550 \end{pmatrix}$	$\begin{pmatrix} -.0435 & .0209 & .0543 \\ .1018 & .1613 & .0653 \\ .0329 & .0214 & .0243 \end{pmatrix}$
$(\chi_{CF}^{H_2})^2$ (e^2)	.0244	.0228	.0247	.0160
$P(CF)^{H_2}$	$\begin{pmatrix} .0018 & .0424 & -.0009 \\ .0162 & -.3275 & -.0245 \\ .0079 & -.0118 & .0623 \end{pmatrix}$	$\begin{pmatrix} .0045 & .0405 & -.0012 \\ .0117 & -.0390 & -.0233 \\ .0043 & -.0104 & .0644 \end{pmatrix}$	$\begin{pmatrix} .0128 & .0376 & -.0062 \\ .0615 & -.3311 & -.0272 \\ .0103 & -.0113 & .0563 \end{pmatrix}$	$\begin{pmatrix} .0100 & .0439 & -.0042 \\ .0152 & -.3360 & -.0204 \\ .0028 & -.0075 & .0686 \end{pmatrix}$
$(\chi_O^{H_2})^2$ (e^2)	.0380	.0383	.0386	.0401

[a] Without a center of inversion, see Table 5.11.

Figure 5.3 Plot of the effective invariants (χ) for the polar tensor (T), and the charge (C), charge flux (CF) and overlap (O) tensors versus the assumed intermolecular distance for the bonded hydrogen atom in the cyclic configuration. Note scale change from Figure 4.2.

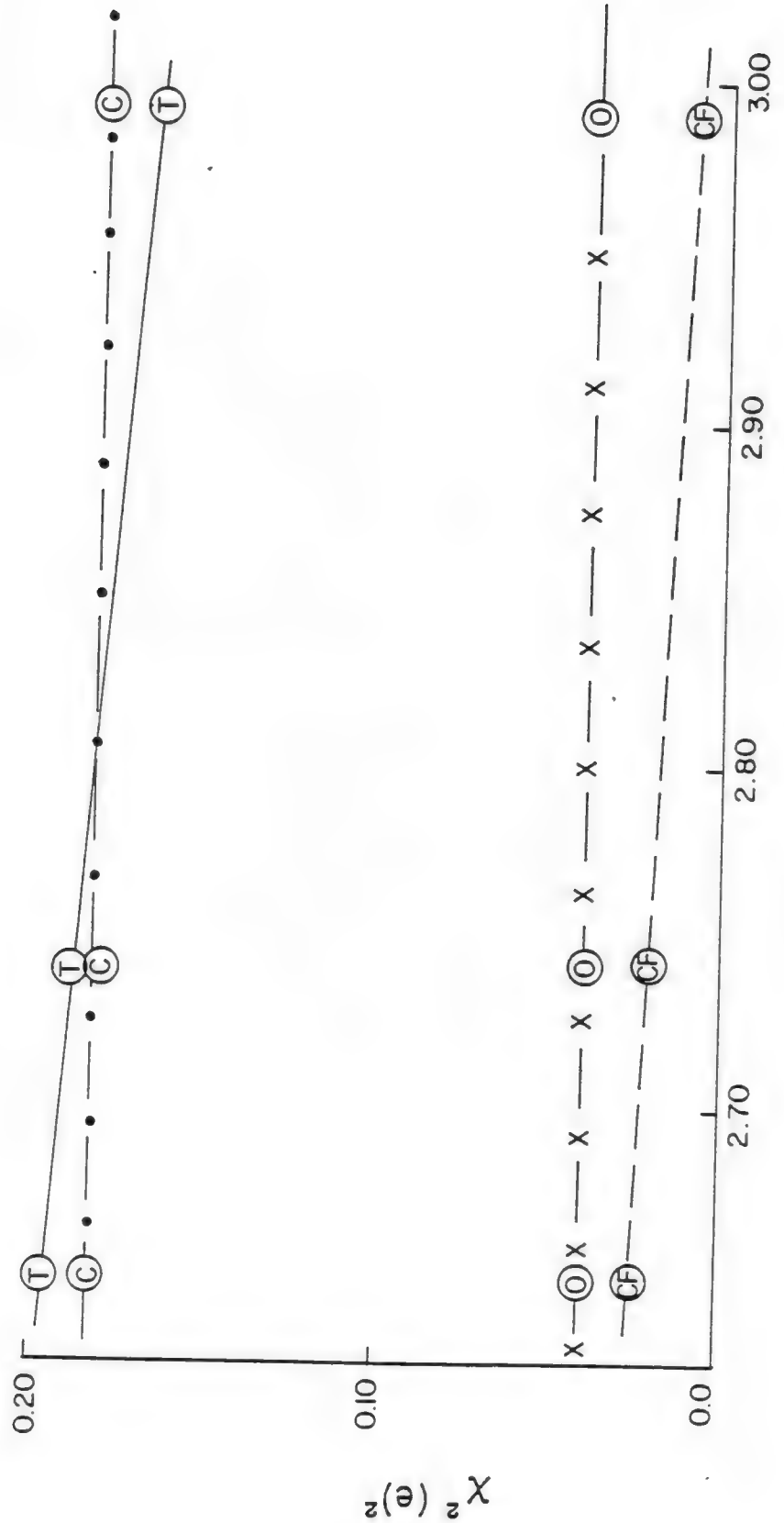
0.20
0.10
0.0
χ^2 (e)^2
2.70
2.80
2.90
3.00
R (O---O) (A°)
T
C
O
CF

the total effective charge exhibits a small rise as the interaction distance is decreased, thereby reflecting the predicted slight increase in intensity as the interaction distance is shortened (see Table 5.11). Also, the effective atomic charge and the effective overlap remain almost constant with the change in interaction distance; in fact, the two linear least squares lines drawn through these two sets of points are both almost exactly horizontal. The effective charge flux exhibits a slight rise with decreasing interaction distance indicating that it is the tensor that is responsible for the changed predicted in the behavior of the total APT.

The predicted frequencies and intensities for the cyclic configuration without a center of inversion, and with an intermolecular distance of 2.74 A° are listed in Table 5.11. The frequencies are similar, but significantly different, from those predicted for the configuration with the same intermolecular distance but with the center of inversion. Of course, the predicted intensities for the individual bands in these two complexes are somewhat different because of the different symmetries in these two complexes. In the complex with the center of inversion only three intramolecular vibrations are infrared active. However, in the complex without the center of inversion all six intramolecular vibrations are infrared active. Therefore we would expect that the form of the normal vibrations would be different in these two complexes, and that this would have an effect on the intensity distribution among the normal modes (i.e., the mechanical effect previously

discussed). If the intensity sums for the two configurations are compared they are found to be almost equal (576 km/mole with the center of inversion compared to 554 km/mole without the center of inversion). This indicates that the predict intensities for this complex are indeed distributed differently as the orientation of the two molecules is changed, but that there is no predicted change in total intensity. This emphasizes the importance of the mechanical effect (form of the normal coordinates) in determining infrared intensities. Finally, this calculation also reinforces the notion that the predicted frequencies are very sensitive to the assumed geometry, while the total predicted intensities are less sensitive to these parameters.

5.4 Comparisons Between Linear and Cyclic Complexes

The cyclic configuration of a pair of interacting water molecules is energetically less favorable than the linear configuration (40). In addition, the predicted spectra for these two different configurations are quite different from each other, and also from the predicted spectrum of isolated water.

The predicted frequency shifts in the cyclic complex are considerably smaller than those predicted in the linear dimer. In addition, the origin of these shifts is different in the two complexes. In the linear dimer we have shown that the large predicted shift in the symmetric stretching mode of the electron acceptor was due primarily to the predicted weakening

of the bonded O-H bond. In the cyclic configuration, the predicted shifts in the stretching modes are due to increased intermolecular coupling. Additionally, while the predicted shift in the symmetric stretching mode of the electron acceptor in the linear dimer was dependent upon the assumed intermolecular distance, the frequencies of the stretching modes in the cyclic complex were almost independent of this distance.

In the case of the predicted intensities, the linear dimer was predicted to have a large intensity increase, relative to the monomer, in the symmetric stretching mode of the electron acceptor. This increase was shown to be due almost entirely to electronic effects present in the polar tensor of the bonded hydrogen atom, specifically isolated to the charge flux tensor. In the cyclic complex the predicted intensities exhibited less significant differences from the predicted intensities for isolated water. The origin of these differences were also found to be a bit different from the linear dimer. In the cyclic configuration the predicted intensity increases were due to two effects in almost equal contributions. The first effect was responsible for almost half of the predicted intensity increases and is called the mechanical effect, or the changing of the form of the normal coordinates in the complex relative to the monomer. This effect was not found to be of any significance in the linear dimer. The second effect was the electronic effect reflected in the polar tensor of the bonded hydrogen, specifically in the charge flux tensor. This effect is similar to the electronic effect in the linear dimer, but

its magnitude and importance were considerably reduced for the cyclic configuration. Finally, the electronic effect was shown to be rather strongly dependent upon the assumed interaction distance in the linear dimer. In the cyclic complex the electronic effect exhibited only a very subtle dependence on the interaction distance.

CHAPTER 6
THE IN-PLANE BIFURCATED WATER-WATER COMPLEX

The third orientation for the water-water complex which has received some attention by past experimental (26) and theoretical (34,36,40) work is the in-plane bifurcated structure pictured in Figure 1.3. This structure is predicted theoretically (40) to be the least energetically favorable (predicted binding energy of 5.96 kcal/mole, compared to 7.22 kcal/mole and 8.2 kcal/mole in the cyclic and linear forms respectively), and has all but been eliminated as a possible structure for the water dimer in an inert gas matrix (26). However, the experimental conditions in a carbon monoxide matrix can be considerably different from the conditions in an inert gas matrix. Hagen and Tielens (26) have suggested that in a CO matrix the bifurcated structure for the water-water complex may be the most stable form. Therefore, from the experimental point of view it becomes of interest to predict the spectrum for the bifurcated structure. Additionally, it is of interest to this study because it offers the opportunity to investgate the effect on the predicted spectrum of yet another orientation for the water-water complex.

The intermolecular distance used in these calculations was taken from the SCF calculation of Morokuma and Pedersen (36), where the same calculational procedure was followed

as was the case of cyclic complex. The geometries of the individual monomer units were fixed at the predicted theoretical values (R = 0.941 A°, and θ = 111.2°). The complex was assumed to have C_{2v} symmetry, and both molecules were constrained to lie in the same plane. The calculated O--O distance of Morokuma and Pedersen (36) was 2.89 A°. The calculated principal cartesian coordinates for this interaction distance are listed in Table 6.1.

The irreducible representations for the 3N = 18 degrees of freedom for this molecule are $6A_1 + 2A_1 + 6B_1 + 4B_2$ and the 3N-6 = 12 vibrational degrees of freedom are $5A_1 + A_2 + 4B_1 + 2B_2$.

In this particular orientation, both hydrogens of the electron acceptor molecule (H_4 and H_6 in Figure 1.3) are able to interact with the electron donating oxygen (O_2 in Figure 1.3) of the second molecule. These two interaction vectors are not orientated along the same direction, but are at an angle of 39 degrees to each other for R(O---O) = 2.89 A°.

6.1 The Predicted Spectrum for the Bifurcated Water-Water Complex (R = 2.89 A°)

The calculated wavenumbers and intensities for the bifurcated complex at this interaction distance are given in Table 6.2, along with the corresponding predicted monomer values. The vibrational characteristics of the calculated normal modes listed in this table were assigned with the aid of the program VIBRATE (see Appendix A). The predicted frequencies for this

Table 6.1 Principal cartesian coordinates for the in-plane bifurcated water-water complex using an assumed intermolecular distance R(O---O) = 2.89 A°. Atom numbering as given in Figure 1.3. (A°)

	X	Y	Z
H_1	-1.9272	0	0.7847
O_2	-1.3899	0	0
H_3	-1.9272	0	-0.7847
H_4	0.9728	0	0.7847
O_5	1.5101	0	0
H_6	0.9728	0	-0.7847

Table 6.2 Predicted wavenumbers and intensities for the bifurcated complex (R(O---O) = 2.89 A°) compared to those predicted for isolated water monomers.

Mode	Description	Bifurcated Complex		Monomer	
		$\nu(cm^{-1})$	A(km/mole)	$\nu(cm^{-1})$	A(km/mole)
1	Asymmetric stretch of Electron Acceptor (EA)	4119	79	4104	54
2	Asymmetric stretch of Electron Donor (ED)	4102	79	4104	54
3	EA symmetric stretch in phase with ED symmetric stretch	3960	6.5	3983	3.90
4	ED symmetric stretch out of phase with EA symmetric stretch	3949	14	3983	3.90
5	ED bend in phase with EA bend	1777	234	1676	125
6	EA bend out of phase with ED bend	1757	117	1676	125
7	EA H_4 and H_6 wagging in phase with ED H_1, H_3 wagging	460	700		

Table 6.2 continued

Mode	Description	Bifurcated Complex		Monomer	
		$\nu(cm^{-1})$	A(km/mole)	$\nu(cm^{-1})$	A(km/mole)
8	ED H_1, H_3 wagging out of phase with EA H_4, H_6 wagging	262	346		
9	EA and ED twisting	257	0[b]		
10	Ring stretching	236	46		
11	ED twist out of phase with EA twist	157	0.30		
12	EA twist in phase with ED twist	a			

[a] Imaginary frequency.

[b] Zero by symmetry.

bifurcated configuration exhibit only minute changes from the predicted frequencies for the isolated monomer. The largest predicted frequency shift occurs for the bending modes, where these modes for both molecules in the complex are predicted to increase about 90 cm^{-1} in frequency from the isolated monomer.

This predicted increase in the frequencies of the bending modes appears to be typical of these types of calculations. Approximately the same increase was predicted in the linear and cyclic configurations. Since there is a marked difference between these three interactions, there does not appear to be any direct correlation between the predicted increase in the bending frequencies and the nature of the interaction. Instead, these shifts are predicted to occur because of the coupling between these bending vibrations and the intermolecular vibrations of the complex. This effect is present in all three configurations, and therefore appears to be mechanical in nature. It was reflected in the linear dimer by the calculated coupling constants between the low frequency vibrations and the bending vibrations and was seen in the cyclic complex by the predicted increase in the effective bending constant. In the bifurcated complex we have used an approximate potential similar to the one used in the cyclic configuration to describe the intermolecular vibrations. This potential contains only the six intramolecular coordinates defined in Table 6.3, and does not include any coupling constants between the intramolecular high frequency and intermolecular low frequency vibrations. The force constants calculated in this way are listed in Table 6.4. This table predicts an increase in the effective bending constant from a

Table 6.3 Internal coordinate definitions used for the assumed equilibrium geometry of the bifurcated complex (R(O---O) = 2.89 A°). Atom numbering as given in Figure 1.3 (d is a weighting factor where d = 1 A°).

Coordinate No.	Definition
R_1	R (H_4-O_5)
R_2	R (H_6-O_5)
R_3	R (H_1-O_2)
R_4	R (H_3-O_2)
R_5	d_0 θ $(H_4-O_5-H_6)$
R_6	d_0 θ $(H_1-O_2-H_3)$

Table 6.4 Calculated "effective" internal force constants (see text Chapter 5)(md/A°) for the assumed equilibrium geometry of the bifurcated complex (R(O---O) = 289 A°). Internal coordinate definitions as given in Table 6.3. (Weighting is done by d, where d = 1 A°).

	R_1	R_2	R_3	R_4	R_5	R_6
R_1	9.062	-.1373	-.0029	-.0051	.3157	.0084
R_2		9.062	-.0051	-.0029	.3157	.0084
R_3			9.1208	-.1525	.0123	.3043
R_4				9.1208	.0123	.3043
R_5					.8022	.0064
R_6						.7850

value of 0.714 md/A° in the monomer to the predicted value of 0.802 md/A° in the bifurcated complex. When both effective bending constants are lowered to the predicted monomer value, the calculated bending frequencies in the bifurcated complex are 1667 cm^{-1} and 1679 cm^{-1}, almost in exact agreement with the predicted value of 1676 cm^{-1} for the isolated monomer. This suggests that the predicted increase in the bending frequencies of the bifurcated complex are a result of the predicted increases in the effective bending constants. These effective force constants are predicted to increase as a result of the mechanical intermolecular coupling present in the complex.

In summary, the predicted wavenumbers for the bifurcated complex agree very well with the predicted monomer value. The small differences are not believed to be significant, or can be explained on the basis of mechanical coupling between the bending vibrations and the low frequency intermolecular vibrations.

The predicted integrated intensities for the bifurcated configuration are also given in Table 6.2, along with the corresponding monomer values. Here again, the intensities for the four stretching modes are predicted to be practically the same as the corresponding values for the isolated monomer, while the bending modes are predicted to be slightly more intense than in the monomer. The small differences for the stretching modes are not considered to be significant.

However, the predicted increase of almost a factor of two in the intensity for the bending mode of the electron donor does need to be explained.

The APTs, and the charge, charge flux and overlap tensors for the bifurcated complex are listed in Tables 6.5, 6.6, 6.7, and 6.8 respectively. The coordinate system used is defined in Figure 1.3. The predicted values for the monomer in the same coordinate system are also listed for comparison. There does not appear to be any significant difference between the APTs of the complex and those of the monomer, perhaps indicating that the predicted changes in the intensity of the bending vibrations are not an electronic effect, but rather a mechanical effect. The charge, charge flux and overlap tensors are also very similar in the two systems. The CCFO analysis appears not to offer any reason for the apparent increase in intensity for the bending mode of the electron donor. This leaves the explanation with the second contributing factor in the calculation of infrared intensities, namely changes predicted in the form of the normal coordinates as the complex is formed, or the mechanical effect.

The increase in the frequency of the bending vibration of the electron donor was explained on the basis of the presence of intermolecular coupling between this vibration and the low frequency vibrations of the complex. It is expected that this coupling affects not only the predicted vibrational frequency, but also the form of the normal vibration. Any change in the form of the normal vibration

Table 6.5 Calculated APTs for the assumed equilibrium geometry of the bifurcated complex (R(O---O) = 2.89 A°) (e) ($1e = 1.602 \times 10^{-19}$ C). Atom numbering and coordinate system as given in Figure 1.3.

	Bifurcated			Monomer		
$P_x^{H_1}$ =	.4969	0	0	.4820	0	0
	0	.1995	-.0638	0	.1482	-.0887
	0	-.0411	.3434	0	-.0147	.3518
$P_x^{O_1}$ =	-.9856	0	0	-.9640	0	0
	0	-.535	+.0010	0	-.5714	.0448
	0	+.0010	-.5348	0	.0448	-.4826
$P_x^{H_3}$ =	.4969	0	0	.4820	0	0
	0	.3599	+.0211	0	.3692	.0440
	0	-.0016	.1830	0	-.0030	.1308
$P_x^{H_4}$ =	.4900	0	0			
	0	.1867	-.0232			
	0	-.0330	.3971			
$P_x^{O_5}$ =	-.9882	0	0			
	0	-.5992	+.0195			
	0	+.0195	-.5841			
$P_x^{H_6}$ =	.4900	0	0			
	0	.3886	+.0453			
	0	+.0551	.1953			

Table 6.6 Calculated charge tensors[a] for the assumed equilibrium geometry of the bifurcated complex (R(O---O) = 2.89 A°) (e) (1 e = 1.602 x 10^{-19} C). Atom numbering and coordinate system as given in Figure 1.3.

	Bifurcated	Monomer
H_1	.4129	.4017
O_2	-.8180	-.8034
H_3	.4129	.4017
H_4	.4097	.4017
O_5	-.8272	-.8034
H_6	.4097	.4017

[a]The quantities listed here are the calculated Mulliken charges, Q_A, where the charge tensor is simply $P^A(C) = Q_A \underline{E}$.

Table 6.7 Calculated charge flux tensors for the assumed equilibrium geometry of the bifurcated complex (R(O---O) = 2.89 A°) (e) (1e = 1.602 x 10^{-19} C). Atom numbering and coordinate system as given in Figure 1.3.

	Bifurcated			Monomer		
H_1 P(CF)=	0	0	0	0	0	0
	0	.1279	-.0353	0	.0888	-.0546
	0	.0063	-.1025	0	.0124	-.0788
O_2 P(CF)=	0	0	0	0	0	0
	0	-.0392	.0699	0	-.0451	.0932
	0	.0699	.0151	0	.0932	.0272
H_3 P(CF)=	0	0	0	0	0	0
	0	-.0626	-.0675	0	-.0426	-.0386
	0	-.1091	.0880	0	-.1056	.0526
H_4 P(CF)=	0	0	0			
	0	.1089	.0263			
	0	.0143	-.0418			
O_5 P(CF)=	0	0	0			
	0	-.0991	.0484			
	0	.0484	-.0616			
H_6 P(CF)=	0	0	0			
	0	.0358	-.0418			
	0	-.0298	.1028			

Table 6.8 Calculated overlap tensors for the assumed equilibrium geometry of the bifurcated complex (R(O---O) = 2.89 A°) (e) (1e = 1.602×10^{-19} C). Atom numbering and coordinate system as given in Figure 1.3.

	Bifurcated			Monomer		
H_1 P(O) =	.0840	0	0	.0803	0	0
	0	-.3413	-.0285	0	-.3423	-.0341
	0	-.0474	.0330	0	-.0541	.0289
O_2 P(O) =	-.1676	0	0	-.1606	0	0
	0	.3127	-.0689	0	.331	-.0484
	0	-.0689	.2681	0	-.0484	.2936
H_3 P(O) =	.0840	0	0	.0803	0	0
	0	.0096	.0886	0	.0101	.0826
	0	.1075	-.3179	0	.1026	-.3235
H_4 P(O) =	.0803	0	0			
	0	-.3319	-.0495			
	0	-.0473	.2092			
O_5 P(O) =	-.1610	0	0			
	0	.3271	-.0289			
	0	-.0289	.3047			
H_6 P(O) =	.0803	0	0			
	0	.0147	.0871			
	0	.0849	-.3172			

upon complex formation should reflect a corresponding change in the predicted intensity for that mode due to the dependence of the predicted intensity on the normal coordinates (see equation 24). The intensities calculated with the monomer APTs and the predicted normal coordinate transformation for the bifurcated complex are listed in Table 6.9, along with the intensities predicted for the bifurcated pair. The predicted intensities using the monomer APTs are in good agreement with the values predicted for the bifurcated complex. This indicates that the change in the form of the normal coordinate is responsible for almost all of the predicted intensity increase in the bifurcated complex compared to the isolated monomer. Finally, it also indicates that in a complex that is only slightly energetically stabilized (40) the predicted frequencies and intensities should be very similar to the isolated monomer values. Any difference between the two sets of values are probably not due to an electronic interaction, but rather a mechanical effect.

6.2 Additional Calculations on the Bifurcated Water-Water Complex

The calculated wavenumbers and intensities for the bifurcated pair of water molecules at different interaction distances and with the two molecular planes perpendicular instead of parallel are listed in Table 6.10. The predicted values listed here for all three cases are not much different from each other or from the isolated monomer numbers. The

Table 6.9 Calculated mechanical effect (see text) on the predicted intensities for the six intramolecular vibrations of the assumed equilibrium geometry of the bifurcated complex (km/mole).

Mode	Intensity (km/mole) Calculated Monomer	Calculated bifurcated using monomer APTs	Calculated bifurcated
1	54	57	79
2	54	51	79
3	3.9	2.6	6.5
4	3.9	4.7	14
5	125	192	234
6	125	58	117

Table 6.10 Predicted wavenumbers and intensities for the six intramolecular vibrations of the bifurcated complex as the interaction distance, R(O---O), is varied.

Mode	R = 2.89 A°		R = 2.89 A°[a]		R = 3.05 A°	
	$\nu(cm^{-1})$	A(km/mole)	$\nu(cm^{-1})$	A(km/mole)	$\nu(cm^{-1})$	A(km/mole)
1	4119	79	4112	88	4113	72
2	4102	79	4102	85	4101	81
3	3960	6.5	3954	6.5	3955	6.1
4	3949	14	3948	18	3948	14
5	1777	234	1776	306	1779	216
6	1757	117	1748	51	1756	123

[a]The electron donor molecule is rotated 90° so that the two molecules no longer lie in the same plane, but have their molecular planes now pendicular to each other.

intensities of the bending modes are the only vibrations that are predicted to differ from the monomer intensities. However, the sum of the intensities for the two bending modes remains almost constant for the three different cases. Therefore, the distribution of the total intensity changes in each case, but the sum is constant. This indicates that the predicted differences in intensity between the bifurcated complex and the isolated monomer are due to a mechanical effect and not an electronic interaction. This mechanical effect is the coupling present between the bending modes and the low frequency vibrations, and is responsible for changing the character of the normal vibrations, and hence the distribution of the total intensity. The small differences predicted in the frequencies of the stretching modes relative to the monomer in all three cases are not considered significant. Finally, the predicted shifts in the bending vibrations for the bifurcated complex are independent of the interaction distance assumed, or of the orientation of the two molecules. This is additional evidence that the predicted frequency shifts in the bifurcated complex are due to mechanical coupling and not due to an intermolecular interaction between the two molecules. If these predicted shifts were due to some type of intermolecular interaction then we would expect that they would change as some of the intermolecular parameters were varied.

CHAPTER 7
THE $O^M.H_2O.O^M$ COMPLEX, M=0, -1, -2

Until now, we have been concerned with the calculation and interpretation of the infrared spectra of one water molecule interacting with another water molecule in various configurations and at different interaction distances. The predicted spectra for these species have varied considerably, and depend rather strongly on both the assumed geometry and the interaction distance. Analysis of these predicted spectra has provided considerable insight into the mechanical and electrical contributions to the predicted changes in intensity upon complex formation, and also into the influence of factors such as geometry, intramolecular coupling and intermolecular coupling on the predicted frequencies. Naturally, it follows that it would be of interest to study the effect of changing the strength of the electron donor in these types of calculations, and to determine if the effects predicted in the water-water complex are dependent upon the physical presence of the second water molecule or if they might be a general characteristic of intermolecular interactions.

One way to do this is to investigate the interaction of water with two single oxygen atoms of varying charge. It would be expected that as the charge on the oxygen atom increased (i.e., became more negative), then that atom would

became a better electron donor. Therefore, we have made calculations of the spectra of water in three such complexes, with M, the charge on the O atom varying from 0 to -1 to -2. The oxygen atoms with M = 0 are expected to be the weakest electron donors, and those oxygen atoms with M = -2 are expected to be the strongest electron donors.

7.1 Intensity Theory for Charged Species

Before beginning a discussion of the predicted spectra for these complexes it is first necessary to present some additional theory pertaining to the prediction of infrared intensities of charged species. The main points will be reviewed briefly here; more details have been given elsewhere (55,56).

The problem of calculating and interpreting APTs is slightly complicated for a charged species. First, the value of the dipole moment is determined by the choice of the origin, due to the charge on the molecule (92). We have adopted for these calculations the same unique coordinate system as for the normal coordinate calculations, namely the space fixed (not molecule fixed) principal cartesian coordinate system (with the origin fixed at the center of the mass by the Eckart conditions). The value of the dipole moment calculated for the charged species at the equilibrium geometry is arbitrary because of its dependence on this arbitrary choice of origin. However, we are interested in calculating dipole derivatives using the method of finite differences; hence the arbitrary choice of origin affects each of the

calculated dipole moments for each displacement in the same manner; therefore the calculated change in the dipole is meaningful. For example, the dipole derivative is approximated using the method of finite differences with equation 5, rewritten here for convenience:

$$\frac{\partial P_\alpha}{\partial X} \quad \frac{\partial P_\alpha}{\partial X} = \frac{P_\alpha(X_o+\Delta X) - P_\alpha(X_o-\Delta X)}{2\Delta X} \qquad (5)$$

where all the terms have been previously defined (Chapter 2). The values calculated for $P_\alpha(X_o+\Delta X)$ and $P_\alpha(X_o-\Delta X)$ are arbitrary due to the choice of the origin. However, the displacements are constrained by the Eckart conditions to keep the center of mass fixed. The calculated values of $P_\alpha(X_o+\Delta X)$ and $P_\alpha(X_o-\Delta X)$ are consistent with this constraint so that the dipole derivative $\partial P_\alpha/\partial X$ is meaningful.

The second complication in calculating APTs for charged species arises because there is a contribution to the dipole derivative as a result of the charge on the molecule. We have already seen that the dipole moment for a charged species is dependent on the choice of origin. Therefore, as a charged molecule is translated through space, its position relative to the origin changes and the calculated value of its dipole moment changes. The subsequent change in the dipole moment as the molecule is translated through space represents the translational correction to the dipole derivative. The translational contribution to the dipole derivative is automatically included in the value of the atomic polar tensors that we have calculated.

However, it is separate from the vibrational contribution to the dipole derivatives and makes no contribution to the intensities, so that the translational contribution should be explicitly separated if one is interested in analyzing dipole derivatives in order to explain vibrational intensities. It will be seen that the translational correction to the atomic polar tensors is, in most cases, not small. The APTs calculated for a molecular ion with this correction included cannot be compared with the APTs of the corresponding neutral molecule. Therefore, the translational contribution for the ion must be removed from the calculated APTs before comparing them with the APTs for the corresponding neutral molecule.

The translational contribution to the APT of atom A in the ion is a diagonal tensor, given by

$$\text{Translational Correction} = \left[\left(\frac{M_A}{M_o}\right) q_e\right] \underline{E} \qquad (87)$$

Here q_e is the total charge on the molecular species in question (either positive or negative), M_A is the mass of atom A, and M_o is the mass of the molecule. Before these corrections are applied to the predicted polar tensors, the null condition (see equation 47) is

$$\sum_N P_{\underline{x}}^N = q_e \underline{E} \qquad (88)$$

where the sum runs over all the atoms in the molecule and the other terms are as previously defined. After subtracting the translational corrections to the APTs (given in equation 87), the null condition again returns to its original form (55)

because we have now corrected the dipole derivatives for the presence of the charge on the molecule

$$\sum_{N} P^{N}_{\underline{X,C}} = 0\,\underline{E} \qquad (89)$$

where $P^{N}_{\underline{X,C}}$ represents the "corrected APTs."

7.2 The $O^{M}\cdot H_2O\cdot O^{M}$ Complex

The geometry for the $O^{M}\cdot H_2O\cdot O^{M}$ complex is given in Figure 1.4. The principal cartesian coordinates for the assumed geometry for this molecule are given in Table 7.1. The same principal cartesian coordinates were used in the three different calculations. The charge on the oxygen atoms was varied from 0 to -1 to -2, but the geometry assumed for the complex was the same (Figure 1.4) for each calculation. The symmetry of the molecule is C_{2v}, with the 3N-6 = 9 vibrations corresponding to the irreducible representations $4A_1 + A_2 + B_1 + 3B_2$ and the three translations and three rotations belonging to $A_1 + A_2 + 2B_1 + 2B_2$. In this orientation of atoms in the complex, both of the free oxygen atoms are electron donating in nature, and both hydrogen atoms in the water molecule are electron accepting in nature.

The predicted wavenumbers and intensities for the neutral, -2 and -4 charged species are given in Table 7.2 along with the corresponding monomer values. For all three cases the predicted wavenumbers and intensities of the vibrations of the complexed water are considerably different from the predicted values for the isolated monomer. The large discrepancies in the predicted

Table 7.1 Principal cartesian coordinates for the $O^M \cdot H_2O \cdot O^M$ complex (M = 0, -1, -2) (A°). Atom numbering as in Figure 1.4.

	X	Y	Z
O_1	0	-.3010	2.4645
H_2	0	.0549	.8320
O_4	0	.5952	0
H_4	0	.0549	-.8320
O_5	0	-.3010	-2.4645

Table 7.2 Predicted wavenumbers and intensities for the three intramolecular vibrations of the $O^{M}\cdot H_2O\cdot O^{M}$ complex (M = 0, -1, -2). Geometry in Figure 1.4.

Mode	Calculated Monomer		$O\cdot H_2O\cdot O$		$O^{-1}\cdot H_2O\cdot O^{-1}$		$O^{-2}\cdot H_2O\cdot O^{-2}$		Experimental[a]	
	$\nu(cm^{-1})$	A(km/mole)	$\nu(cm^{-1})$	A(km/mole)	$\nu(cm^{-1})$	A(km/mole)	$\nu(cm^{-1})$	A(km/mole)	$\nu(cm^{-1})$	A(km/mole)
1	3983	3.9	3402	4.9	3248	226	3035	367	3165	429
2	1676	125	1779	106	1873	107	1741	62	1514	60
3	4104	54	3570	143	3297	1498	2991	2696	3144	1437

[a] Reference 44.

frequencies of the complexed water versus those of isolated water caused us some concern about whether or not our assignment was correct. However, we could easily investigate this question using the graphics program VIBRATE to display the normal modes.

The general pattern for the frequencies is that the two stretching modes of the complexed water are shifted to considerably lower energy relative to the isolated monomer, while the bending mode is predicted to be unchanged from the monomer value. The corresponding predicted intensities for complexed water range from values approximately equal to the monomer values (for the neutral species), to values increasingly more intense (in the -2 and then the -4 charged species).

7.3 Intensity Analysis for the $O^M \cdot H_2O \cdot O^M$ Complex

The intensities calculated for these water complexes have been summarized previously in Table 7.2. The "corrected APTs" corresponding to these calculated intensities are given in Table 7.3.

The "corrected APTs" reported in Table 7.3 are corrected for the translational contribution to the dipole derivative as described previously. However, these corrections have been applied in a manner unique to these complexes. We are calculating the infrared spectra for neutral water complexed with charged oxygen atoms. Therefore, the charge present in the complex is almost entirely localized in these oxygen atoms.

Table 7.3 Corrected APTs for the $O^{M}\cdot H_2O\cdot O^{M}$ complexes, M = 0, -1, -2 (e) (1e = 1.602 x 10^{-19} C). The translational correction to these APTs has been removed (see text). Atom numbering and coordinate system as given in Fig. 1.4.

	$O\cdot H_2O\cdot O$			$O^{-1}\cdot H_2O\cdot O^{-1}$			$O^{-2}\cdot H_2O\cdot O^{-2}$			Monomer		
$P^{H_2}_{X,C}$ =	.4754	0	0	.4738	0	0	.3703	0	0	.4820	0	0
	0	.2382	-.1020	0	.8902	-.1876	0	1.1968	-.1755	0	.1482	-.0887
	0	-.0777	.3240	0	-.1948	.3692	0	-.3151	.3048	0	-.0417	.3518
$P^{O_3}_{X,C}$ =	-.9499	0	0	-1.5028	0	0	-1.206	0	0	-.9640	0	0
	0	-.5989	.0842	0	-1.322	.2654	0	-1.818	.4219	0	-.5174	.0448
	0	.0842	-.5239	0	.2654	-1.0856	0	.4219	-1.442	0	.0448	-.4826
$P^{H_4}_{X,C}$ =	.4754	0	0	.4738	0	0	.3703	0	0	.4820	0	0
	0	.3766	-.0161	0	.5975	-.3251	0	.6346	-.5654	0	.3692	.0440
	0	-.040	.1856	0	-.3180	.6619	0	-.4258	.8669	0	-.003	.1308
$P^{O_1}_{X,C}$ =	-.0004	0	0	.2777	0	0	.2328	0	0			
	0	-.0107	.0143	0	-.1694	.0629	0	-.0646	.1208			
	0	.0170	.0099	0	.1070	.1141	0	.1464	.1932			
$P^{O_5}_{X,C}$ =	-.0004	0	0	.2777	0	0	.2328	0	0			
	0	-.0051	.0195	0	.0041	.1843	0	.0513	.1979			
	0	.0168	.0044	0	.1401	-.0594	0	.1724	.0773			

Hence the translational corrections are applied by assuming that the water molecule in the complex is neutral, and that the charge present in the complex results entirely from the charge on these oxygen atoms. The APTs for the charged oxygen atoms are "corrected" using this assumption while the APTs for the neutral water molecule are not "corrected." The resulting APTs are those listed in Table 7.3.

Upon careful inspection of Table 7.3, the similarites and differences between the APTs of the atoms in the complexes and in the isolated water molecule can be seen. For the neutral complex, the predicted polar tensors for the atoms in the complex are very similar to the values predicted for the monomer. This is to be expected since the predicted intensities for this complex are very similar to those values predicted for the monomer (see Table 7.2). Based on these results one would expect that this interaction is relatively weak.

The situation for H_2O in the -2 and -4 charged complexes is entirely different. For the stretching mode of the charged complex we predict a rather drastic increase in intensity (almost a factor of 60 and 30 in the symmetric and asymmetric modes, respectively). For the -4 charged complex these factors are even greater, being close to 94 and 50 respectively.

The CCFO analysis of these APTs for these species offers some insight into the nature of these drastic predicted intensity increases. The predicted charge, charge flux, and overlap tensors for the three complexes, and also for isolated water, are given in Tables 7.4, 7.5, and 7.6 respectively.

Table 7.4 Calculated charge tensors[a] for the $O^{M}\cdot H_2O\cdot O^{M}$ complexes, M = 0, -1, -2, with and without the translational corrections applied (see text) (e) (1 e = 1.602×10^{-19} C). Atom numbering and coordinate system as given in Figure 1.4.

	$O\cdot H_2O\cdot O$	$O^{-1}\cdot H_2O\cdot^{-1}$	$O^{-2}\cdot H_2O\cdot O^{-2}$	Monomer
With translational contribution				
O_1	-.0062	-.8873	-1.7340	
H_2	.4292	.4257	.3310	.4017
O_3	-.8460	-1.0767	-1.1930	-.8034
H_4	.4292	.4257	.3310	.4017
O_5	-.0062	-.8873	-1.7340	
With translational contribution removed				
O_1	-.0062	.1127	.2660	
H_2	.4292	.4257	.3310	.4017
O_3	.8460	-1.0767	-1.1930	-.8034
H_4	.4292	.4257	.3310	.4017
O_5	-.0062	.1127	.2660	

[a]The charge tensor is obtained by multiplying these Mulliken charges by the (3x3) identity matrix $\underline{E}$; $\underline{P}^{A}(C) = Q_A\underline{E}$.

Table 7.5 Calculated charge flux tensors (e) for the water molecule in the $O^{M} \cdot H_2O \cdot O^{M}$ complexes, M = 0, -1, -2 (1 e = 1.602 c 10^{-19} C). Atom numbering and coordinate system as given in Figure 1.4.

	$O \cdot H_2O \cdot O$			$O^{-1} \cdot H_2O \cdot O^{-1}$			$O^{-2} \cdot H_2O \cdot O^{-2}$			Monomer		
$P(CF)_{H_2}$ =	0	0	0	0	0	0	0	0	0	0	0	0
	0	.0017	-.0286	0	.6949	-.1457	0	1.808	-.1816	0	.0888	-.0546
	0	.0107	-.0936	0	-.1554	-.0464	0	.2891	-.0237	0	.0124	-.0788
$P(CF)_{O_3}$ =	0	0	0	0	0	0	0	0	0	0	0	0
	0	.0083	.0864	0	-.5135	.2820	0	-.9282	.4536	0	-.0451	.0932
	0	.0865	.0854	0	.2820	-.2624	0	.4536	-.5243	0	.0934	.0272
$P(CF)_{H_4}$ =	0	0	0	0	0	0	0	0	0	0	0	0
	0	-.0711	-.0217	0	.1881	-.3811	0	.3339	-.6217	0	-.0426	-.0386
	0	-.0611	-.0207	0	-.3714	.4604	0	-.5141	.7232	0	-.1056	.0526

Table 7.6 Calculated overlap tensors (e) for the water molecule in the $O^{M}.H_2O.O^{M}$ complexes, M = 0, -1, -2 (1 e = 1.602 x 10^{-19} C). Atom numbering and coordinate system as given in Figure 1.4.

	$O \cdot H_2O \cdot O$			$O^{-1} \cdot H_2O \cdot O^{-1}$			$O^{-2} \cdot H_2O \cdot O^{-2}$			Monomer		
H_2 P(O) =	.0462	0	0	.0481	0	0	.0393	0	0	.0803	0	0
	0	-.1927	-.0734	0	-.2304	-.0149	0	-.2150	.0061	0	-.3423	-.0341
	0	-.0884	-.0116	0	-.0394	-.0101	0	-.0260	-.0025	0	-.0541	.0289
O_3 P(O) =	-.1039	0	0	-.4261	0	0	-.0130	0	0	-.1606	0	0
	0	.2388	-.0023	0	.2682	-.0166	0	.3035	-.0317	0	.3311	-.0484
	0	-.0023	.6763	0	-.0166	.2535	0	-.0317	.2753	0	-.0484	.2936
H_4 P(O) =	.0462	0	0	.0481	0	0	.0393	0	0	.0803	0	0
	0	.1157	.0056	0	-.0163	.0560	0	-.0303	.0563	0	.0101	.0826
	0	.0207	-.2229	0	.0534	-.2242	0	.0883	-.1873	0	.1026	-.3235

The predicted APTs for the neutral complex will not be discussed further because they are essentially unchanged from those of the corresponding monomer. Upon careful inspection of Tables 7.4, 7.5 and 7.6, it becomes obvious that the largest single contribution to the difference between the predicted APTs for the complexed H_2O and the predicted APTs of the monomer is from the charge flux terms. However, there are also some significant differences predicted in the charge and overlap tensors. It is impossible to determine the exact contributions from each of these three tensors to the total predicted intensity increase of the complexed water by simply examining the APTs and the CCFO tensors alone. Therefore Table 7.7 becomes much more useful.

Table 7.7 lists the calculated contributions to the total predicted intensity increase from each of the charge, charge flux, and overlap changes from monomer to complex. The second column gives the calculated intensities for the vibrations of the complexed water using the unchanged predicted monomer APTs and the normal coordinate transformation calculated for H_2O in the complex (the APTs for the charged (or free) oxygen atoms are included as the null tensor). This column therefore gives the relative contribution to the total intensities that occurs from the perturbed normal coordinates of the H_2O in the complex (as opposed to the monomer), or what has been termed the "mechanical effect" on the intensities. We see here that the mechanical effect on the predicted intensities is very small. For the case of

Table 7.7 Calculated contributions to the predicted intensities in km mole^{-1} of the three intramolecular vibrations of the $O^{M}\cdot H_2O\cdot O^{M}$ complex, M = 0, -1, -2.

Mode	Monomer APTs	Add APTs for O_1 and O_5	Add $P(\overset{H_2}{\overset{|}{C}}F)$ and $P(\overset{H_4}{\overset{|}{C}}F)$	Add $P(\overset{H_2}{\overset{|}{C}})$ and $P(\overset{H_4}{\overset{|}{C}})$	Add $P(\overset{H_2}{\overset{|}{C}})$ and $P(\overset{H_4}{\overset{|}{C}})$	Complex
$O^{-1}\cdot H_2O\cdot O^{-1}$						
1	5.5	5.5	302	317	420	226
2	123	123	141	135	135	107
3	55	55	911	982	1257	1498
$O^{-2}\cdot H_2O\cdot O^{-2}$						
1	11	11	764	672	838	367
2	116	112	81	83	78	62
3	47	46	1982	1759	2170	2696

the -2 charged species this effect is almost nonexistent. For the -4 charged species this effect is a bit larger, but nevertheless still not large enough to be significant. Column three gives the calculated intensities obtained by including the contributions from the calculated APTs of the free oxygen atoms. This column indicates that the APTs for these atoms have very little effect on the total predicted intensities of the H_2O vibrations in the complex, and therefore that these normal vibrations must not involve much motion of these oxygen atoms. This further indicates that the normal vibrations of the complexed water molecule are perturbed very little from the corresponding vibrations in isolated water. The next three successive columns show the relative contributions to the predicted intensity increase from the differences in charge flux, charge, and overlap between the complex and the monomer in the P_{yy} term of the APT for H_2, and will be described below. Finally, the last column lists the total calculated intensities for the complex. The discrepancies between column six and seven occur because there are other minor contributions to the total intensity increase due to changes in other APT elements besides the P_{yy} term of H_2.

Columns four, five and six of Table 7.7 were obtained in the following manner. The predicted APTs and the charge, charge flux, and overlap tensors are given for the complexes and for the monomer in the coordinate system shown in Figure 1.4. The light hydrogen atoms are considerably more important

than the heavy oxygen atoms and therefore we focus our attention on these two atoms. Using this "bond" coordinate system (Figure 1.4) it is easy to see the predicted changes in the APTs of complexed water relative to isolated water (see Table 7.3). By examining Table 7.3 it is obvious that the P_{yy} term of H_2 is drastically different from the monomer value, while the remaining terms in the APT for this atom are similar to those in the monomer. Similarly, there are differences in the APT of H_4, but not isolated to one term as in H_2. This result arises because if we place H_2 in the "bond" coordinate system H_4 is now oriented differently from H_2 with respect to this coordinate system. However, by symmetry, the two atoms are identical. In other words, the APT for one hydrogen atom is exactly the same as the APT for the second atom as long as the proper rotations are performed.

Columns four, five and six in Table 7.7 are obtained by adding the differences between the complex and the monomer in charge flux, charge, and overlap in the P_{yy} term of H_2 to the corresponding APT of the monomer. The APT for H_4 is then obtained by properly rotating the adjusted APT for H_2. The APT for O_3 is then obtained by insuring that the combined changes in both hydrogen atoms are cancelled by the changes in the oxygen atom (i.e., the null condition still holds). As each separate contribution (CCFO tensors) is added to the monomer APTs the intensities are recalculated using these APTs and the normal coordinate transformation for the complex.)

In this fashion each contribution (CCFO contributions) to the total predicted intensity is investigated separately.

The predicted intensity for the vibrations of the complexed water molecule are considerably greater than those predicted for isolated water (see Table 7.2). We have already seen that the mechanical effect and the contributions from the "free" oxygen atoms are both negligible. The drastic predicted increase in intensity must therefore be a result of electronic effects reflected in the APTs.

The -2 charged complex will be discussed first. The majority of the differences between the APTs of the complexed water molecule and isolated water are in the charge flux tensors. The P_{yy} term of H_2 (and the corresponding terms for H_4) are responsible for most of the predicted intensity increase in complexed water relative to monomer value (59% of the total increase in the asymmetric stretching mode). There is also a smaller but significant contribution from overlap (19%), and a relatively insignificant contribution from the change in charge (5%).

For the -4 charged complex the results are similar. Both the mechanical effect and the effect of the "free" oxygen atoms are very small. The primary source of the intensity increase comes from the large increase in the charge flux as the complex is formed. This large increase is responsible for 73% of the total predicted intensity increase in the asymmetric stretching mode. The change in overlap offers a smaller contribution (16%), with the change in charge actually decreasing the predicted intensities (-8%).

Qualitatively, the results for the -2 and -4 charged species are exactly the same. Namely that most of the intensity increase in the complex with respect to the monomer is due to a large increase in charge flux of the P_{yy} term of the two hydrogen atoms. In addition, there is a smaller but nevertheless significant contribution from overlap in both cases. Finally, there is essentially no contribution (as the complex is formed) from the perturbation of the normal coordinates, from the "free" oxygen atoms, or from the change in charge.

Quantitatively, there are some differences between the results for the two species. The predicted intensity changes in the -4 charged species are definitely greater than the changes predicted for the -2 charged species. When the numerical results for the two species are compared, it becomes immediately apparent that the intensity increase in the complex with the stronger electron donor is considerably greater than in the complex with the weaker electron donor (by almost a factor of two). This suggests that a stronger electron donor would result in larger predicted changes in intensities than a weaker electron donor. In addition, while the relative contributions from the change in overlap remain almost constant (16% vs. 19%), there is a rather substantial increase in the contribution from charge flux (59% vs. 73%) as the donor strength is varied. This would indicate that as the strength of the electron donor increases, the importance of charge flux in the predicted intensities increases also.

7.4 Frequency Analysis for the $O^M \cdot H_2O \cdot O^M$ Complexes

The predicted absorption frequencies for the vibrations of the water molecule in these complexes have been summarized in Table 7.2, and compared to the predicted monomer values. In general, the frequencies for the stretching vibrations are considerably lower than those of the isolated molecule. In order to analyze these changes, the frequency parameters were transformed to force constants in internal coordinates. A potential function was assumed which does not include any interaction between the intramolecular vibrations of the water molecule and the intermolecular vibrations of the complex. This seems reasonable because it appears from the intensity data that the normal vibrations of the neutral complexed water molecule are not much different from the corresponding vibrations in isolated water. Therefore, the coupling predicted between the intramolecular vibrations of complexed H_2O and the intermolecular vibrations of the complex must be small. With this assumption a potential function which included only the intramolecular internal coordinates of the complexed H_2O molecule was used. The calculated force constants corresponding to these intramolecular internal coordinates are given in Table 7.8. The frequencies calculated using this approximation are listed in column one of Table 7.9. A comparison to the frequencies from the "total" (i.e., including all possible interactions among vibrations; see Table 7.2) calculation shows that the agreement between the two calculations is very good.

Table 7.8 Calculated "effective" (see text) internal force constants (md/A°) for the internal coordinates of the water molecule in the $O^{M}\cdot H_2O\cdot O^{M}$ complexes, M = 0, -1, -2. Internal coordinates are defined the same as for isolated water (see Table 3.6). Atom number and coordinate system as given in Figure 1.4.

	Force constants (md/A°)			
	Monomer	$O\cdot H_2O\cdot O$	$O^{-1}\cdot H_2O\cdot O^{-1}$	$O^{-2}\cdot H_2O\cdot O^{-2}$
$F_{11}=F_{22}$	9.141	6.778	5.984	5.028
F_{33}	.714	.874	.9437	.815
F_{12}	-.065	-.162	.064	.195
F_{13}	.300	.340	.090	-.083

Table 7.9 Predicted wavenumbers for the intramolecular vibrations in the $O^{M}\cdot H_2O\cdot O^{M}$ complexes, M = 0, -1, -2, as several internal force constants are adjusted (see text). Force constants as defined in Table 7.8.

Mode	Wavenumbers (cm^{-1}) Calculated Complex	Adjust F_{11} and F_{22}	Adjust F_{12}	Adjust F_{33}	Monomer
$O\cdot H_2O\cdot O$					
1	3402	3957	3978	3978	3983
2	1766	1778	1778	1601	1676
3	3568	4130	4109	4109	4104
					$O\cdot H_2O\cdot O$
$O^{-1}\cdot H_2O\cdot O^{-1}$					
1	3248	3454	3397	3397	3402
2	1873	1872	1872	1802	1779
3	3297	3509	3568	3568	3570
$O^{-2}\cdot H_2O\cdot O^{-2}$					
1	3035	3475	3410	3411	3402
2	1730	1734	1733	1795	1779
3	2997	3500	3568	3568	3570

The discrepancies between the two sets of wavenumbers differ at most by 13 cm^{-1} with most values within 5 cm^{-1} of each other.

We will begin our discussion of the predicted changes in absorption frequencies with the neutral complex. The predicted intensities for the neutral complex exhibited only slight changes from the monomer values, but the predicted stretching frequencies are considerably different from the corresponding monomer values. The stretching frequencies are predicted to be approximately 500 cm^{-1} lower in the complexed water than in the monomer, while the bending frequency is almost constant. Therefore, it is important to understand why such large changes are predicted in the stretching frequencies. First, it must be remembered that the assumed geometry for the water molecule in the complex ($R_1 = R_2 = 0.991$ A°, and $\theta = 114.0°$) is considerably different from the calculated geometry of isolated water ($R_1 = R_2 = 0.951$ A°, and $\theta = 111.2°$). Therefore, before a direct comparison can be made of the calculated frequencies of the neutral complex and the isolated monomer, we must first determine what one might expect for the predicted spectral parameters (including both frequencies and intensities) of an isolated water molecule with the assumed geometry of the water molecule in the complex.

If we recall the data presented in Table 3.3, the effect of the assumed geometry on the predicted spectral parameters can be seen. While the predicted intensities remain relatively insensitive to the assumed geometry, the predicted frequencies are very sensitive to the assumed geometry. The plot given in

Figure 7.1 of the O-H stretching force constant versus the O-H bond length shows that there is an inverse linear relationship between the two quantities (i.e., as the bond is lengthened, the force constants decreases). If this plot is extrapolated to 0.991 A° for the O-H bond length, the predicted stretching force constant is 6.634 md/A°. The frequencies calculated using this value in place of the value calculated for monomer water at the theoretical geometry (o.141 md/A°) are 3392 cm^{-1}, 1665 cm^{-1} and 350 cm^{-1} for ν_1, ν_2, ν_3 respectively. These frequencies are close to the values that one might expect for an isolated water molecule with the assumed geometry of the water molecule in the $O \cdot H_2O \cdot O$ species. The agreement between the values predicted for the vibrations of H_2O in the neutral complex (see Table 7.2) with these values calculated for an isolated water molecule with this same assumed geometry indicates that the predicted spectrum for the neutral complex is what one might expect from an isolated water molecule with the same assumed geometry of the water molecule in the neutral complex. This suggests that in this complex the interaction between the water molecule and the neutral oxygen atom is weak, with little effect on the vibrational properties.

The -2 charged complex exhibits a further decrease of the stretching frequencies relative to the neutral complex of about 200 cm^{-1} for both stretching vibrations. Since the assumed geometry of the water molecule in this complex is exactly the same as in the neutral complex, this decrease can be attributed to the presence of an intermolecular interaction between the

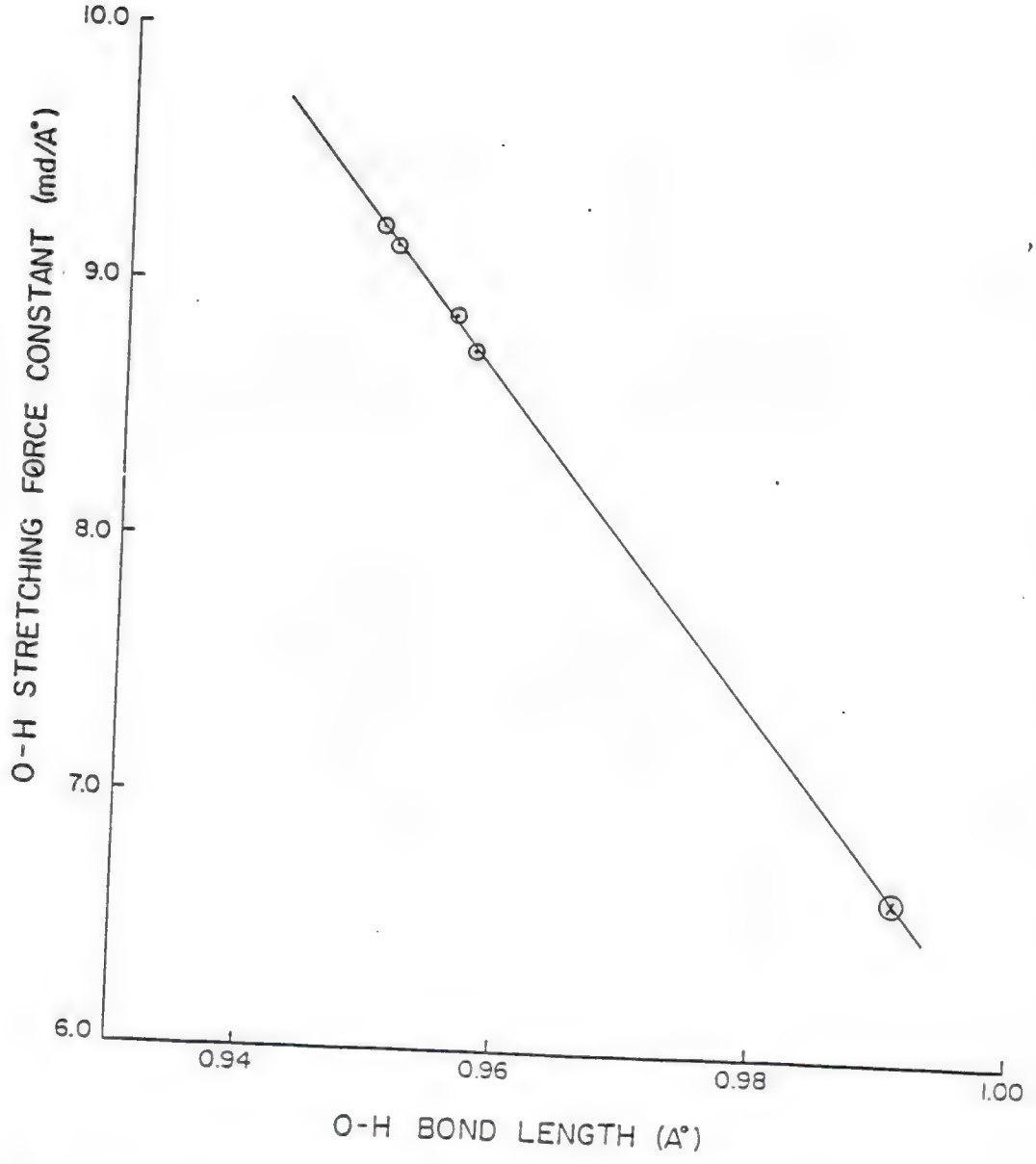

Figure 7.1 Plot of O-H stretching force constant versus the assumed O-H bond length for H_2O.

water molecule and the two "free" oxygen atoms. The calculated internal force constants for monomeric water, and for water complexed in the neutral, -2, and -4 charged species are listed in Table 7.8. From this data, the predicted decrease in the stretching frequencies can be attributed primarily to a decrease in the O-H stretching force constant from 6.778 md/A° in the neutral complex, to 5.985 md/A° in the -2 charge complex. This change alone is responsible for 134% and 78% of the frequency shifts in the symmetric and asymmetric stretching modes respectively. The slight increase in intramolecular coupling between the two stretching coordinates (reflected in F_{12} in Table 7.8) is responsible for the remaining shifts in stretching frequencies, -37% and 21% respectively. The increase in the bending constant from 0.8744 md/A° in the neutral complex to 0.9437 md/A° in the -2 charged species is responsible for 75% of the increase in the bending frequency (see Table 7.9).

In the -4 charged complex, the results are qualitatively similar. The predicted decrease in the stretching freqencies are greater than for the -2 charged complex, as would be expected in the case of a stronger electron donor. These predicted shifts from the neutral complex are 367 cm^{-1} and 573 cm^{-1} for the symmetric and asymmetric stretching modes respectively. The predicted decrease in the stretching force constant from the neutral complex) from 6.778 md/A° to 5.028 md/A° is responsible for 120% and 88% of these predicted shifts, respectively. The predicted increase in the intramolecular coupling between the two O-H stretching coordinates

reflected in F_{12} of Table 7.8) is responsible for the remaining -81% and 12%, respectively (see Table 7.9).

Quantitatively, the frequency shifts predicted in the -2 and -4 charged complex are considerably different, with the shifts of the symmetric and asymmetric stretching modes greater in the latter complex by 213 cm^{-1} and 300 cm^{-1}, respectively (relative to the noninteracting neutral complex). Qualitatively, the results of the frequency analyses for both complexes are similar. The asymmetric stretching mode is predicted to undergo a larger shift than the symmetric stretching mode in both cases (273 cm^{-1} and 154 cm^{-1} in the -2 charged complex, versus 573 cm^{-1} and 367 cm^{-1} in the -4 charged complex). (It is worthwhile to note here that the predicted shift of the asymmetric stretching mode in the -4 charged complex is such that this vibration is now of lower frequency than the symmetric stretching mode.) Most of these predicted frequency shifts are due to the large decrease predicted in the O-H stretching force constant in both cases (over and above the decrease expected as a result only of the geometry change.) This data suggests that while the natures of the predicted frequency shifts are similar, a stronger electron donor is responsible for larger predicted shifts in the stretching frequencies than a weaker electron donor.

7.5 Model for the Infrared Spectra of Beta-Alumina

Water, as an impurity in the structure of beta-alumina, is important in the mechanical strength and electrical conductivity properties of the beta-alumina. This in turn is important in the use of beta-alumina as a solid electrolyte in batteries. Some of the kinetic and thermodynamic properties of the hydration reaction of water in a crystal of beta-alumina might best be studied by using the infrared spectrum as a probe (44,45). Hence, the crystal structure and infrared spectrum of water isolated in beta-alumina has been investigated recently by Bates and coworkers (44). Figure 7.2 gives the orientation of the water molecules in the crystal. The orientation is such that the nearest neighbors of the water molecule are two oxygen atoms belonging to the aluminate ions. The oxygen atoms in the aluminate ion are most assuredly negatively charged, but the exact numerical charge on these atoms is unknown. We have previously calculated in the spectrum of one water molecule interacting with two neutral, -1, and -2 charged oxygen atoms. In our calculations, the assumed geometry for the water molecule (see Figure 1.4) is the same geometry determined by Bates et al. (44) to be the experimental geometry for water isolated in a crystal of beta-alumina (see Figure 7.2) In addition, the assumed orientation of the charged oxygen atoms in our calculations is the same as determined by the crystallographic studies on the crystal by Bates et al. (44). The structure for our simulation has been previously given in Figure 1.4, where the charge on the oxygen

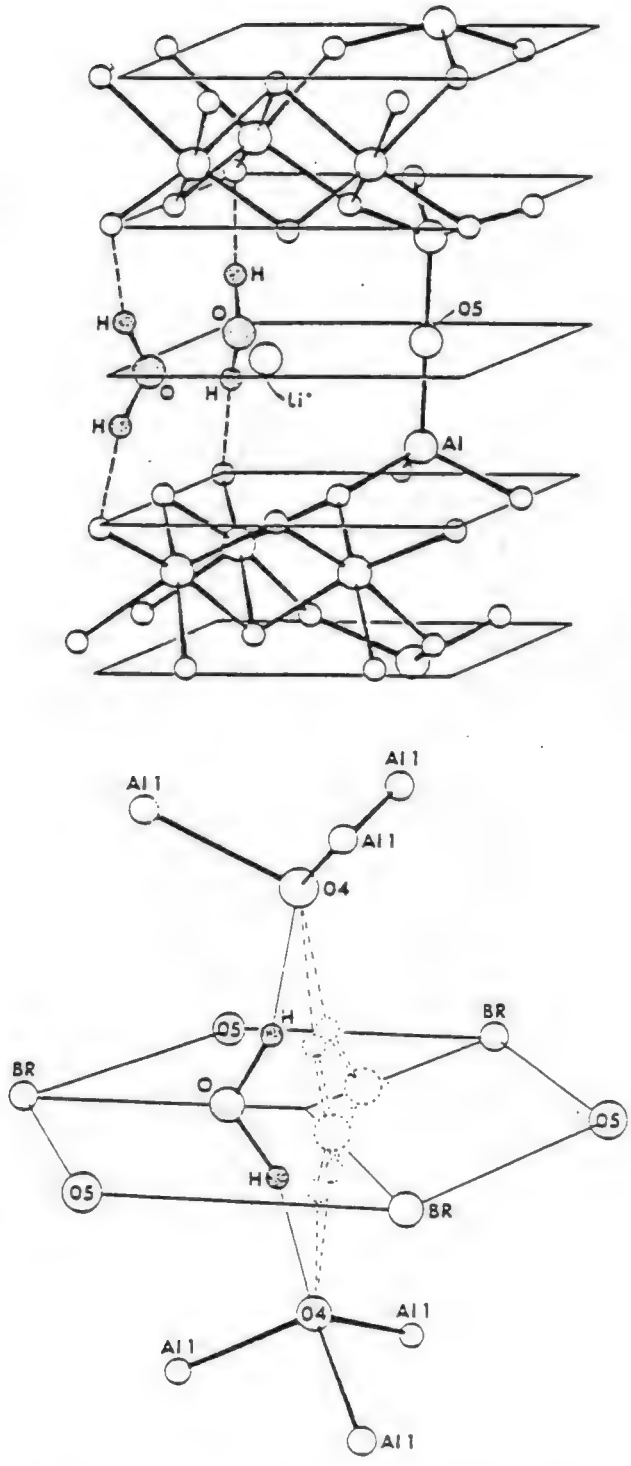

Figure 7.2 Orientation of the H_2O molecule in a hydrated crystal of beta-alumina. (Figure reprinted from reference 44.)

atoms (O_1 and O_5) varies from 0 to -1 to -2. We have seen previously that the spectra calculated using this model are quite different from the spectrum calculated for the isolated water monomer. As a first approximation, we might also expect the experimental spectrum for water isolated in beta-alumina to exhibit some of the predicted changes that were seen in our model; but it must be remembered that our calculation is only a model for what might be expected in the crystal and that the agreement between our calculated results and the experimental results cannot be expected to be exact.

The experimental wavenumbers and intensities for water isolated in beta-alumina have been given in Table 7.2, along with our calculated results for comparison. The best agreement with our calculated results and the experimental results occurs when M = -1, or when the charge on the oxygen atoms in the aluminate ions is -1. The calculated frequencies for the symmetric and asymmetric stretching vibrations are predicted 83 cm^{-1} and 153 cm^{-1} higher than the experimental values, while the bending frequency is predicted 359 cm^{-1} too high. The predicted intensities for these three modes are predicted 203 km/mole too low for the symmetric stretch, and 61 km/mole and 47 km/mole too high for the asymmetric stretching and bending vibrations, respectively. While the agreement between these calculated results and the experimental results is only fair, the differences are greater as the charge on the oxygen atoms is increased to -2. However, as the charge on the oxygen atoms is increased to -2, most of the predicted differences

between the calculated and experimental results change sign relative to the differences predicted when M = -1. This suggests that in the crystal we might expect the charge on these oxygen atoms to be somewhere between -1 and -2, but closer to -1. In our model calculation, the vibrational bands predicted for the complexed water molecule were shifted to lower energy and increased in intensity relative to the isolated monomer. It was also shown that these predicted spectral shifts were due to an electronic interaction bewteen the water molecule and the charged oxygen atoms. The agreement in both frequencies and intensities with the experimental spectrum suggests several important points. First, the assignment of the infrared spectrum made by Bates et al. (44) appears to be correct. Secondly, the large spectral shifts observed experimentally for the vibrations corresponding to the complexed water molecule in the crystal indicate the presence of strong hydrogen bonding in the crystal. Finally, in the crystal, the nearest neighbor oxygen atoms of the aluminate ions appears to be the most important atoms in trying to understand this intermolecular interaction. As a first approximation, these atoms alone are responsible for most of the observed spectral changes for the water molecule in the crystal compared to isolated gaseous water.

CHAPTER 8
IONIZED WATER, H_2O^+

Ionized water, H_2O^+, represents a different challenge for these types of calculations in that it is not an intermolecular complex, but rather an ionic species which may be stable in this form. The calculation of its infrared spectrum is not directly related to the intermolecular complexes previously discussed, but it does represent a spectrum that one might expect for water in a related chemical environment (complete electron donation), and therefore is of interest here.

The geometry, and therefore the principal cartesian coordinates, were taken to be the same as the equilibrium theoretical geometry for neutral water using the 4-31G basis set. The two O-H bond lengths are assumed to be equal and with a value of 0.951 A°, while the H-O-H angle is assumed to be 111.2°. The predicted wavenumbers and absolute intensities for H_2O^+ at this geometry are listed in Table 8.1. In general, the frequencies are predicted to be more or less the same as the frequencies for the neutral molecule, but the intensities are predicted to be considerably larger in the ion.

Table 8.1 Predicted wavenumbers and intensities for H_2O^+ compared to those predicted for H_2O.

Mode	Description	Calculated H_2O^+		Calculated H_2O	
		$\nu(cm^{-1})$	A(km/mole)	$\nu(cm^{-1})$	A(km/mole)
1	Symmetric stretch	4012	350	3983	3.9
2	Bending	1545	303	1676	125
3	Asymmetric stretch	4033	642	4104	54

Since this molecule is charged, the value of the dipole moments depends on the choice of the origin. Since we are interested in calculating dipole derivatives using the method of finite differences, we may fix the origin at the center of mass for consistent estimation of the dipole derivative (see discussion in Chapter 7). As discussed also in Chapter 7, the charge on the molecule requires a "translational correction" (56) to the dipole derivative (APT) before we attempt to compare the APTs of an ion with the APTs of the corresponding neutral molecule. The APTs for ionized water both with and without the translational contribution are reported in Tables 8.2 and 8.3, respectively, together with the corresponding APTs for the neutral molecule in the coordinate system as defined in Table 8.2. By comparing Tables 8.2 and 8.3 it becomes immediately apparent that the APTs reported with and those reported without the translational contribution are considerably different. The "corrected" APTs given in Table 8.3 should be compared with the APTs from neutral water. There are considerable differences between the corrected APTs of the ion and the APTs for the neutral molecule. These differences were analyzed in terms of the CCFO analysis. The charge, charge flux and overlap tensors for the ion and neutral molecule are listed in Tables 8.4, 8.5 and 8.6, respectively.

The charge contribution to the APTs of the ion are listed in Table 8.4 with and without the translational contribution. The values that include the translational contributions are

Table 8.2 Calculated APTS (e) for ionized water, H_2O^+, compared with the calculated APTs for monomeric neutral water (1 e = 1.602 c 10^{-19} C). Atom numbering and coordinate system as defined below. (Includes translational contribution.)

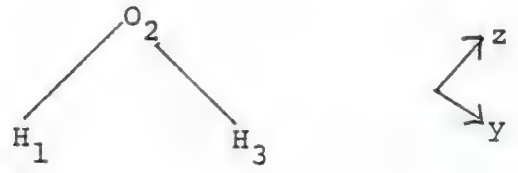

	H_2O^+			H_2O		
$P_x^{H_1}$ =	.479	0	0	.482	0	0
	0	.484	.044	0	.370	-.044
	0	.115	.730	0	.003	.130
$P_x^{O_2}$ =	.043	0	0	-.964	0	0
	0	-.235	-.055	0	-.517	-.045
	0	-.055	-.192	0	-.045	-.482
$P_x^{H_3}$ =	.479	0	0	.482	0	0
	0	.752	.011	0	.148	.089
	0	-.060	.462	0	.042	.352

Table 8.3 Corrected APTs for H_2O^+ compared with the APTs for H_2O (e) (1e = 1.602 x 10^{-19}C). [2]Atom numbering and coordinate system as defined in Table 8.2. (Translational contributions have been removed, see text, Chapter 7.)

	H_2O^+			H_2O		
$P^{H_1}_{x,C}$ =	.423	0	0	.482	0	0
	0	.428	.044	0	.370	-.044
	0	.115	.674	0	.003	.130
$P^{O_2}_{x,C}$ =	-.845	0	0	-.964	0	0
	0	-1.123	-.055	0	-.517	-.045
	0	-.055	-.1080	0	-.045	-.482
$P^{H_3}_{x,C}$ =	.423	0	0	.482	0	0
	0	.696	.011	0	.148	.089
	0	-.060	.406	0	.042	.352

Table 8.4 Calculated charge tensors[a] (e) (1 e = 1.602 x 10^{-19} C) for H_2O^+ compared to H_2O. Atom numbering and coordinate system as defined in Table 8.2.

	H_2O^+	H_2O
	With translational contribution	
H_1	.595	.402
O_2	-.190	-.804
H_3	.595	.402
	With translational contribution removed	
H_1	.539	.402
O_2	-1.078	-.804
H_3	.539	.402

[a]The charge tensors are given by $Q_A\underline{E}$, where Q_A is the Mulliken charge for atom A as listed here.

Table 8.5 Calculated charge flux tensors for H_2O^+ compared to H_2O (e) (1 e = 1.602 x 10^{-19} C). Atom numbering and coordinate system as defined in Table 8.2.

	H_2O^+			H_2O		
H_1 P(CF) =	0	0	0	0	0	0
	0	.060	.200	0	-.043	.039
	0	.186	4.12	0	.106	.052
O_2 P(CF) =	0	0	0	0	0	0
	0	-.556	-.216	0	-.045	-.093
	0	-.216	-.388	0	-.093	.027
H_3 P(CF) =	0	0	0	0	0	0
	0	.496	.016	0	.089	.054
	0	.031	-.024	0	-.012	-.079

Table 8.6 Calculated overlap tensors for H_2O^+ compared to H_2O (e) (1 e = 1.602 x 10^{-19} C). Atom numbering and coordinate system as defined in Table 8.2.

	H_2O^+			H_2O		
$P(O)^{H_1}$ =	-.116	0	0	.080	0	0
	0	-.171	-.156	0	.011	-.083
	0	-.071	-.277	0	-.103	-.324
$P(O)^{O_2}$ =	.233	0	0	-.160	0	0
	0	.511	.161	0	.332	.048
	0	.161	.386	0	.048	.295
$P(O)^{H_3}$ =	-.116	0	0	.080	0	0
	0	-.339	-.005	0	-.343	.035
	0	-.091	-.009	0	.054	.029

simply the Mulliken equilibrium charges on the atoms in the ion. These charges represent the actual distribution of electron density on each of the atoms in the ion, and represent the total contribution of these static charges to the APTs. The charges reported with the translational contribution removed represent the vibrational-rotational contribution to the APTs from only the static Mulliken charges (56).

The charges with the translational corrections included indicate that approximately 0.60 e is removed from the oxygen atom and 0.20 e from each of the two hydrogen atoms as the ion is formed. This suggests that the ion forms primarily by loss of a lone pair electron on the oxygen. The contribution from the uncorrected charge tensor to the APT for the oxygen atom in the ion is therefore less (closer to zero) than the charge contribution in the neutral molecule (-.190 e vs. -.804 e). The charges reported with the translational contribution removed (or the corrected charge tensors) actually show that the charge contribution to the APT of the oxygen atom is greater (more negative) in the ion than in the neutral molecule (-1.078 e vs. -.804 e). This means that the charge contribution to the corrected APT (or vibrational-rotational APT) of the oxygen atom is significantly greater in the ion than in the neutral molecule. This result is important because it is the first time that we have seen a situation where the predicted changes in the APTs contain such a large contribution from anything other than the charge flux tensor.

The charge flux and overlap tensors for the ion and the neutral molecule in the coordinate system defined in Table 8.2 are listed in Tables 8.5 and 8.6 respectively. The two hydrogen atoms are identical by symmetry, but the tensors reported here differ because in the bond coordinate system used here the orientation with respect to the coordinate system is different for these two atoms. We chose to use the bond coordinate system because in this coordinate system the differences in charge flux between the ion and the neutral molecule are isolated to the P_{yy} term for H_3 (and correspondingly to the rotated tensor for H_1). There are almost no differences in the overlap tensors for the ion and the neutral molecule. Therefore, it seems that the biggest contributions to the changes in the total APTs between the ion and the neutral molecule are due to changes in charge and charge flux.

The contribution to the intensity change from the change in normal coordinates as the ion is formed (mechanical effect) and the contributions from each of the three constituent tensors of the APT for ionized water are given in Table 8.7. The differences between the normal coordinates of the ion and the neutral molecule are negligible, and do not account for any significant differences in the intensities of the ion. The difference in charge flux between the ion and the neutral molecule is responsible for the majority of the increase in the asymmetric stretching mode (79%) and for 38% of the predicted intensity increase for the symmetric stretching mode. The overlap contribution is negligible, while the

Table 8.7 Calculated contributions to the predicted intensities of H_2O^+ (km/mole).

Mode	Using Monomer APTs	Add $P_{YY}^{H_3}(CF)$	Add $P_{YY}^{H_3}(O)$	Add $P_{YY}^{H_3}(C)$	Calculated H_2O^+
1	2.1	136	140	233	350
2	126	155	156	167	303
3	54	516	525	788	642

charge contribution actually overestimates (by 146 km/mole) the predicted intensity increase for the asymmetric stretching mode. The predicted intensities in column five of Table 8.7 do not agree with the values predicted for the ion (column six) due to some contributions to the APTs other than the P_{yy} term of H_3. However, the large contributions from both charge flux and charge to the predicted intensity increase in the ion relative to the neutral molecule are important. This will be discussed in more detail in Chapter 9.

The force constants for ionized water compared to those for the neutral molecule are given in Table 8.8. The major differences between the two are the interaction constant between the two stretching coordinates (F_{12}) and the interaction constant between the stretching coordinate and the bending coordinate (F_{13}). These differences are relatively minor, and are responsible for the minor differences predicted in frequencies between the two species. The increased interaction constant would serve to increase the frequency of the symmetric stretching vibration, and decrease the frequency of the asymmetric stretching mode. This is exactly the result shown in Table 8.1. The slight decrease in the bending constant is responsible for the slight decrease in the bending frequency seen in Table 8.1. The fact that the stretching constants are not affected very much would indicate that the electron removed when forming the ion is of nonbonding character. But again, this discussion will be given in more detail in Chapter 9.

Table 8.8 Calculated internal force constants for H_2O^+ compared to H_2O. Internal coordinates are defined as $R_1(O_2\text{-}H_1) = R_2(O_2\text{-}H_3) = d_3(H_1\text{-}O_2\text{-}H_3)$. Atom numbering as in Table 8.2. (Weighting is done with d = 1 A°, see text, Chapter 3).

	Force Constant (md/A°)	
	H_2O^+	H_2O
$F_{11} = F_{22}$	9.03	9.14
F_{33}	.640	.714
F_{12}	.144	-.065
F_{13}	.469	.300

CHAPTER 9
GENERAL COMMENTS AND FINAL SUMMARY

Ab initio self consistent field calculations using the 4-31G basis set have been used to predict and interpret the infrared spectra of water molecules interacting in different chemical environments. These environments have varied with respect to orientation of the electron donor/acceptor pair, with respect to the assumed intermolecular distance, and with respect to the strength of the electron donor. The predicted spectra are strongly dependent upon all these parameters, and by analyzing these spectra we have been able to make some comments concerning the nature of intermolecular interactions.

The predicted spectrum for the linear water dimer (summarized in Table 4.2) compares favorably with experimental spectra (19-22). The symmetric stretching vibration of the electron acceptor molecule is predicted to shift to lower energy and increase in intensity, as is characteristic of hydrogen bonded systems (43) and as is found in the experimental spectra. The frequency and intensity predicted for this vibration are also seen to be rather sensitive to the assumed intermolecular distance. The origin of the predicted frequency shift is the predicted change in the strength of the O-H bond as indicated by the predicted change in O_5-H_4 bond length in the electron acceptor molecule of the dimer

relative to the O-H bond length in the isolated monomer. The origin of the intensity enhancement is predicted to be due entirely to the increase in charge flux for the bonded hydrogen atom of the electron acceptor molecule.

The cyclic and bifurcated forms of the water dimer are predicted to be less stable energetically (40), and the spectra for these two forms are not predicted to exhibit the same drastic spectral changes as for the linear dimer. In both the cyclic and bifurcated configurations previous calculations (36) have indicated that the geometries of the individual monomers in these complexes are not perturbed from the geometry of the corresponding isolated monomer. Therefore, we have fixed the geometries for the individual water molecules in these configurations and calculated the spectra with varying intermolecular distances. In the cyclic configuration, the frequencies of the stretching vibrations shifted only slightly from the corresponding monomer vibrations, and these shifts were due to the presence of increased intramolecular coupling in the complex relative to the monomer. The bending vibrations were predicted to shift slightly more than the stretching vibrations, and these predicted shifts were seen to be due to intermolecular coupling between these vibrations and the low frequency vibrations. The intensities for the cyclic configuration were predicted to be slightly higher than those of the corresponding vibrations in the monomer, but the predicted increases were not nearly as drastic as those for the linear dimer. These predicted changes in intensity were seen

to be a result of two effects in almost equal contributions; first, the mechanical effect due to the symmetry of the cyclic configuration (C_i) and the perturbation of the form of the normal vibration in the complex relative to the same mode in the isolated monomer, and second, the electronic effect (or the increase in charge flux for the bonded hydrogen atom). The predicted changes in the spectral properties (both frequencies and intensities) of the cyclic configuration relative to the isolated monomer were seen to be almost independent of the assumed intermolecular distance. Finally, in order to determine if perhaps these spectral changes were induced by the symmetry of the cyclic complex, the spectrum for the cyclic configuration without a center of inversion was also predicted. This spectrum was predicted to be quite similar to the predicted spectrum for the cyclic configuration with the center of inversion (if the different selection rules for these two symmetry groups are properly accounted for).

The predicted spectrum for the bifurcated form of the water-water complex was found to be very similar to the spectrum one might expect from two noninteracting water molecules. The predicted frequencies in the bifurcated complex agree very well with the predicted frequencies of the corresponding vibrations in isolated monomeric water. The intensities were predicted to change in the complex relative to the monomer, but the predicted changes were due to the mechanical effect coupling the vibrations of the two molecules, and not the result of the electronic effect or change in charge flux. The

predicted spectrum for the bifurcated form of the complex was also almost entirely independent of the assumed intermolecular distance.

The predicted spectra for the water molecule in the $O^{M} \cdot H_2O \cdot O^{M}$ complex, with M varying from 0 to -1 to -2, indicated that the spectral properties of a hydrogen bonded electron acceptor molecule are strongly dependent upon the strength of the electron donor: the stronger the electron donor the larger the predicted changes in the spectrum of the complex (at a particular fixed geometry) relative to the isolated monomer. This was found to be true for both the predicted shifts in frequencies and for the predicted increases in intensities. The frequency shift occured because the O-H stretching force constant was predicted to decrease, while the predicted intensity increases were due primarily to predicted increases in charge flux. The prediction that the intensities of intermolecular complexes are determined by charge flux seems to be ubiquitous in these calculations. The importance of the charge flux tensor will be briefly discussed below.

9.1 Comments on the Charge Flux, Charge, and Overlap Tensors

Previous attempts to parameterize infrared intensities have used various parametric methods such as APTs (7,8) and electrooptical parameters (EOPs)(5,6,9), which include contributions from static charges, charge flux, and overlap.

However, the intensities for intermolecular complexes appear to be determined by the distribution of electrical charge at equilibrium and the changes in these charges during atomic motions (i.e., vibrations). Therefore, it appears to be of some use to attempt to parameterize charge flows in intermolecular complexes. The following discussion of charge flows will focus its attention on the bonded hydrogen atom because at this point it seems clear that this is the most important atom to consider.

Gussoni, Jona, and Zerbi (93) have attempted recently to understand the infrared intensities for vibrations of C-H bonds by measuring what they have termed "charge undeformability." They have defined this term with respect to the invariants of the APTs. This quantity is defined (93) as the ratio of the mean dipole moment, $\bar{p}^A$, to the anisotropy β_A. This parameter measures the resistance to charge flow; it is infinite for completely undeformable charges, and small for highly deformable charges (93).

In the limiting case of a heteronuclear diatomic molecule AB and the EECF model of Decius (68), this ratio takes the following form (93):

$$\left|\frac{\bar{p}^A}{\beta_A}\right| = \left|\frac{q_A^o}{\left(\frac{\partial q_A^o}{\partial r_{AB}}\right) r_{AB}^o} + \frac{1}{3}\right| \qquad (90)$$

where the dipole moment of a heteronuclear diatomic is given by

$$\bar{P} = q_A^{o}\bar{r}_{AB} \tag{91}$$

so that the charge flux and overlap terms of the CCFO model are incorporated into the term $(\partial q_A^o/\partial r_{AB})r_{AB}^o$.

For the same heteronuclear diatomic AB, the CCFO model gives this same ratio in the following form

$$\left|\frac{\bar{p}^A}{\beta_A}\right| = \left|\frac{a}{b-a} + \frac{1}{3}\right| \tag{92}$$

where the APT for atom A is defined below along with the definitions of the terms a and b

$$P_X^A = \begin{pmatrix} a & 0 & 0 \\ 0 & b & 0 \\ 0 & 0 & a \end{pmatrix} = \begin{pmatrix} q_A^o + P^A(O) & 0 & 0 \\ 0 & q_A^o + P'^A(O) + P^A(CF) & 0 \\ 0 & 0 & q_A^o + P^A(O) \end{pmatrix} \tag{93}$$

where q_A^o is the equilibrium charge on atom A, $P^A(O)$ is the overlap contribution along the two degenerate axes perpendicular to the AB bond, $P'^A(O)$ is the overlap contribution along the molecular axis, and $P^A(CF)$ is the charge flux contribution along the molecular axis. Substituting into equation 92 gives the ratio as

$$\left|\frac{\bar{p}^A}{\beta_A}\right| = \left|\frac{q_A^o + P^A(O)}{P^A(CF) + P'^A(O) - P^A(O)} + \frac{1}{3}\right| \tag{94}$$

By representing the ratio $|\bar{p}^A/\beta_A|$ in terms of the CCFO model we see that this ratio is not actually a pure measure of the charge undeformability because it contains contributions

from overlap also. It would be more accurate to represent charge undeformability as

$$\text{Charge undeformability} = \left| \frac{q_A^o}{P_{(CF)}^A} \right| \qquad (95)$$

because this ratio represents the actual resistance to the change in equilibrium charge on atom A without any contribution from overlap.

We attempted to correlate our predicted increased charge flux in the complexes discussed here, and also with other complexes (91), with predicted decreased values of charge undeformabilities using $|\bar{p}^A/\beta_A|$ as defined by Gussoni, Jona and Zerbi (93). These data are presented in Table 9.1; unfortunately they do not seem to correlate well. (For example, the predicted increased charge flux either at shorter intermolecular distances or with stronger electron donors is expected to be reflected in the smaller values of $|\bar{p}^A/\beta_A|$.) We believe that these discrepancies arise in part due to the presence of the overlap contribution in the ratio $|\bar{p}^A/\beta_A|$. As an alternative definition for charge undeformability we propose to use the effective invariants for the CCFO tensors to give a parameter analogous to the ratio expressed by equation 95. This ratio, which is defined in the general case for any polyatomic molecule is given by

$$\text{Charge undeformability} = \left| \frac{\chi_{(C)}^A}{\chi_{(CF)}^A} \right| \qquad (96)$$

Table 9.1 Correlation between different charge undeformability parameters and increased charge flux for different intermolecular complexes. (Smaller ratio should follow larger charge flux.)

Complex	$\chi^{H_b}_{(C)}$ (e)	$\left\lvert \frac{\bar{p}^{H_b}}{\beta_{H_b}} \right\rvert$	$\left\lvert \frac{\chi^{H_b}_{(C)}}{\chi^{H_b}_{(CF)}} \right\rvert$
Linear Dimer			
R = 2.532 A°	.3820	1.212	1.280
R = 2.682 A°	.3158	1.593	1.509
R = 2.832 A°	.2668	2.085	1.739
R = 2.982 A°	.2287	2.55	1.972
R = 3.132 A°	.1998	2.657	2.203
H_2O---CO[a]			
R = 2.832 A°	.1359	1.885	2.927
R = 3.132 A°	.1179	1.543	3.390
R = 3.532 A°	.1021	1.399	3.923
R = 3.732 A°	.0969	1.341	4.133
Cyclic Dimer			
R = 2.74 A°	.1510	1.346	2.855
Bifurcated Dimer			
R = 2.89 A°	.0695	1.305	5.890
$O^{-1}\cdot H_2O\cdot O^{-1}$	.4205	1.065	1.108
$O^{-2}\cdot H_2O\cdot O^{-2}$	.6545	.7279	.6283

[a]Reference 91.

where $\chi^{A}_{(C)}$ and $\chi^{A}_{(CF)}$ are the previously defined effective invariants (see equations 71 and 78) for the charge tensor and the charge flux tensor respectively. From analysis of these data presented in Table 9.1, it appears that this ratio does correlate better with our predicted increased charge flux (i.e., as the charge flux increases, the charge undeformability decreases). Therefore, we suggest that the ratio $|\chi^{A}_{(C)}/\chi^{A}_{(CF)}|$ is a good parameter to measure charge flows in these complexes.

While the charge flux tensor appears to be the most important contribution to the predicted intensities of intermolecular complexes, we have seen that in ions the contributions from the charge and overlap tensors cannot be completely overlooked (when comparing the intensities of these species with the parent or corresponding neutral molecule). Recent calculations on other ions (18) and radicals (94) also point out the importance of these two component tensors in infrared intensities. These results will be discussed below.

The overlap tensor represents the change in the dipole moment due to the rehybridization of charge, without a change in charge on a particular atom, as an atom in the molecule vibrates. The charge tensors are represented by the static equilibrium Mulliken charges (70) on the atoms in a molecule, complex or ion. In general, the charge and overlap contributions to the predicted increases in intensities in an intermolecular complex relative to the isolated monomer are negligible. Therefore, these calculations offer little

insight into the nature of both of these tensors. However, calculations reported recently on molecular ions (18) and radicals (94), and the comparison to the corresponding neutral species have been helpful in characterizing both the charge tensor and the overlap tensor, and their importance in vibrational intensities.

The calculations were all performed in the same manner as previously described (see Chapter 2), and the results are presented elsewhere (18,94). These results will be briefly summarized here. In general, the intensities of the asymmetric stretching vibrations of CO_2^+ (18) and CS_2^+ (18) are predicted to be less than the intensities in the corresponding neutral molecules, while those of H_2O^+ (see Chapter 8) are predicted to be greater than those of H_2O. The differences in charge flux between the ion and the neutral molecule are primarily responsible for these predicted differences in intensity; however, there are also important contributions from both changes in charge and overlap. It is these latter changes which lead to some important conclusions concerning the nature of these tensors in vibrational intensities.

The asymmetric stretching vibrations for these ions have been analyzed in terms of the CCFO theory, and the various contributions to the differences in intensities have been analyzed using the program PXPQ (see Appendix A). For the ions CS_2^+ and H_2O^+ there is a considerable contribution to the predicted changes in intensity (relative to the corresponding neutral molecule) from the charge tensor (21% and

45% respectively). For CO_2^+ the contribution from the charge tensor is minimal, but there is instead a significant contribution (45%) from the overlap tensor.

Presumably, the differences in intensity between an ion and a neutral molecule (for these positive ions) are due to the absence of an electron in the ion. Therefore, the differences in the contributions to the changes in intensity would be found logically in the nature of the electron removed. The contribution from charge flux appears to be ubiquitous and not related to the nature of the electron removed. In the cases of CO_2^+ and CS_2^+ it was found that the differences in the charge flux could be explained on the basis of different resonance structures in the ion relative to the neutral molecule (18). However, the contributions from charge and overlap appear only in certain situations, and therefore comments on the nature of these tensors can be offered.

CS_2^+ and H_2O^+ are both ions which are formed by the removal of a lone pair electron. In CS_2^+ this electron is removed from the S atoms, and in H_2O^+ from the O atom. Consequently, there are subsequent changes in the static Mulliken charges on these atoms in the ions. Therefore, there is a significant contribution to the changes in intensity from the charge tensor. CO_2^+ is formed by the removal of a bonding electron from CO_2 (18). Therefore, the overlap contribution to the APTs in the ion is different from that in the neutral molecule. Based on these results we believe that the importance of the charge tensor lies in the lone pair

effects, and the importance of the overlap tensor more in the bonding electrons.

9.2 Other Applications for These Calculations

While we have used these calculated spectra to investigate some of the more important aspects of intermolecular interactions, these types of predictions may also be useful in other areas. For instance, by comparing the predicted spectral pattern for the linear, cyclic and bifurcated water dimers with experimental spectra (19-21), it is obvious that the spectral pattern for the linear configuration is in best agreement with the experimental spectra. While the agreement between experiment and theory is not perfect, the lack of agreement between experiment and theory for the cyclic and bifurcated forms seems to indicate that the interpretation of the experimental spectrum in terms of a linear dimer is indeed correct. While these calculations do not exclude the presence of the cyclic (or bifurcated) dimers, they strongly support the idea that the linear configuration dominate the spectrum.

As another example, one can determine the relative concentrations of the two species in a given sample (for example in a matrix) by using the predicted values of the integrated intensities for the monomer and for the dimer. This determination is made using equation 97 below where a_M is the integrated absorbance of one of the monomer absorption bands (obtained from the spectrum), A is the calculated integrated

molar absorption coefficient for that band, ℓ is the path-length, and C is the concentration

$$a_M = A_M C_M \ell \tag{97a}$$

or

$$\frac{C_D}{C_M} = \frac{A_M a_D}{A_D a_M} \tag{97b}$$

Using these relative concentrations from equation 97b, the equilibrium constant for the reaction $2\ H_2O = (H_2O)_2$ is

$$K_{eq} = \frac{[\text{dimer}]}{[\text{monomer}]^2} = \frac{C_D}{(C_M)^2} \tag{98}$$

under the experimental conditions of that particular sample can be roughly determined (95).

The calculation of the vibrational spectrum for the $O^M \cdot H_2O \cdot O^M$ complex as a model for the infrared spectrum of water isolated in a crystal of beta-alumina indicated that it is possible to model complicated chemical systems using rather simple theoretical models, at least to a first approximation. This is important because it offers hope that vibrational spectroscopic problems that have in the past not been investigated by theoretical calculations because they were too complicated or too large for economically reasonable and reliable calculations may now confidently be attacked using simpler models.

Finally, we should like to offer some additional comments on the calculations of infrared spectra which have not been

discussed in this thesis but which seem promising for future applications of this work. Vibrational spectroscopy is often used to characterize species which cannot be obtained in a bottle and isolated in pure form (96). In these cases, where standard spectra are often absent, the prediction of these spectra would appear to be of great help in trying to identify these species (for instance in flames, in planetary atmospheres, or on catalytic surfaces). The predictions of the integrated intensities could also be used to estimate roughly the relative concentrations of these species in a particular sample, or if the pathlength is known, the absolute concentration. For example, this is important in the spectroscopy of astrophysical sources (such as evolved stars), where the absolute concentrations of species believed to be important in these sources are important in the development of thermo- and chemical models for these sources (97). Preliminary work has recently been done in this area (18,94), but more detailed investigations are necessary to full understand the capabilities for predictions in this field.

Understanding of the infrared spectra of large (> 10 atoms) biologically important molecules may be an important tool in reaching an understanding of the myeries of living systems. However, the size of these molecules and the even larger ones in living systems often means the spectra are very complicated, with many vibrational infrared absportion bands close in energy to each other. This makes the interpretation of these spectra extremely difficult, and sometimes

impossible, even for isolated 12 atom molecules (17). Ab initio calculations of vibrational force fields (and hence vibrational frequencies and the normal coordinate transformation matrix) can be used in conjunction with ab initio APTs to predict both infrared absorption frequencies and integrated intensities. These predicted spectra must match the experimental spectra (including both frequencies and intensities) if the assignment is correct. Once a reasonable theoretical prediction has been obtained, the corresponding normal modes can then easily be assigned from the calculated normal coordinate transformation and the visual vibrating program VIBRATE (see Appendix A). This has just recently been done for the 12 atom molecule uracil (17), and the results are very encouraging. Work in this area should be continued, as the future prospects seem extremely bright.

APPENDIX A
SUMMARY OF PROGRAMS

1. PRINCIPA
   Disk Input - none
   Operator Input - masses and cartesian coordinates in any arbitrary coordinate system
   Terminal Output- principal cartesian coordinates, principal moments of inertia, transformation matrix from principal cartesian coordinates to the original coordinates.
   Disk output - principal cartesian coordinates
   Description - calculates the moment of inertia tensor in the original coordinate system and then diagonalizes that tensor to find the transformation to principal cartesian axes. Also calculates the center of mass, and then uses this as the origin and the transformation to principal cartesian axes to find the principal cartesian coordinates.

2. ORTHO
   Disk Input - principal cartesian coordinates
   Operator Input - masses, principal moments of inertia, basis vectors
   Terminal Output- *U* transformation matrix (3Nx3N)
   Disk Output - *U* transformation matrix (3Nx3N)
   Description - sets up matrix of basis vectors, where each row corresponds to a different vector. These vectors correspond to the linear combinations of principal cartesian coordinates which reduce as the irreducible representations of the point group of the molecule. Each set of three columns represent the triplet X, Y, Z for each of the N atoms in the molecule. The column coefficients for each row represent the amount of each coordinate in that vector. The first six vectors are set equal to zero since the translations and rotation are explicitly defined and calculated by the program. There are 3N remaining vectors to be defined, and the basis matrix is therefore ((3N+6) x 3N). These vectors are then orthogonalized to the

translations and rotations, with the six redundant coordinates becoming zero. These orthogonal vectors are then normalized, giving the orthonormal U matrix. The first six rows of this matrix are the explicit definitions of the translations and rotations as defined by the Eckart conditions, and the remaining 3N-6 orthonormal rows represent pure vibrational coordinates.

3. PUNCH
   Disk input - U matrix
   Operator input - masses, symmetry block information, routing cards for Gaussian 76
   Terminal output- cartesian coordinates of displaced vibrational coordinates
   Disk input - cartesian coordinates of displaced vibrational coordinates in format suitable for input into Gaussian 76 (including routing cards).
   Description - calculates S_i, then displaces along $\pm\Delta S_i$ for vibrational coordinates. Uses $S_i \pm \Delta S_i$, then $-\Delta S_i$ until all i's in symmetry block are done. Then does off diagonal elements $\sum_{ij>i} \sum (S_i+\Delta S_i, S_j+\Delta S_j)$ in same manner until all complete. Does similar procedure on all symmetry blocks.

4. FORCERIT
   Disk input - none
   Operator input - upper right hand corner of force constant matrix F_S, in row order.
   Terminal output - none
   Disk output - force constant matrix, F_S (3Nx3N)
   Description - simply takes force constant matrix F_S, beginning at row 7 column 7 (first vibrational coordinate) and writes entire 3Nx3N matrix to disk. Automatically fills constants corresponding to translations and rotations to zero. (i.e., $\sum_{i=1}^{6} \sum_{j=6}^{N} F_{ij}$ and $\sum_{i=1}^{6} \sum_{j=7}^{N} F_{ij}$)

5. APTWRITE
   Disk input - none
   Operator input - dipole derivatives in S coordinates, P_S (3x3N), in row order.
   Terminal output - none
   Disk output - P_S matrix (3x3N)
   Description - takes dipole derivatives (in e) in S coordinates, P_S, and writes them to a disk set.

6. FLUXRITE
   Disk input - none
   Operator input - charge derivatives in S coordinates (Nx3N), row order.
   Terminal output - none
   Disk output - charge derivatives in S coordinates (Nx3N).
   Description - takes charge derivatives and writes them to disk. Each row of this matrix corresponds to one of the N atoms in the molecule, and each column represents one of the 3N S coordinates. Therefore, the first six columns are all zero. The operator input begins at atom 1 column 7 (S_7) and is entered in row order.

7. FREQ
   Disk input - U (3Nx3N); F_S (3Nx3N)
   Operator input - masses, transformation from principal cartesians to original cartesians
   Terminal output- frequencies (cm^{-1}) and normal coordinate transformation in original cartesian coordinates, L^{-1} (3Nx3N) in mass weighted principal cartesian coordinates.
   Disk output - normal coordinate transformation matrix, ℓ^{-1} (3Nx3N) in mass weighted principal cartesian coordinates
   Description - using U, F_S are transformed to K, where K is the force constrant matrix in mass weighted cartesians. This matrix is then diagonalized, giving the frequency parameters and normal coordinate transformation. The frequency parameters are converted to wavenumbers, and the normal coordinates are expressed in the original system of cartesian coordinates.

8. INTENSIT
   Disk input - U (3Nx3N), P_S (3x3N), ℓ^{-1} (3Nx3N)
   Operator input - none
   Terminal output- intensities of normal coordinates in km/mole.
   Disk output - none
   Description - transforms P_S to P_X in principal cartesian coordinates by using U, then calculates P_Q by multiplying P_X and ℓ^{-1}. Finally, P_Q are converted to intensities by using the appropriate constants. The numbering of the coordinates corresponds to the numbering of the coordinates from FREQ.

9. ATOMPOLT
   Disk input - U (3Nx3N), P_S (3x3N)
   Operator input - masses and transformation matrix from principal cartesians to original coordinates
   Terminal output- Atomic Polar Tensors in original coordinates with units of e.
   Disk output - APTs in original coordinates
   Description - transforms P_S to tensors in mass weighted principal cartesians by using U. Then uses the masses and transformation matrix to transform these tensors into APTs in the original cartesian coordinate system. Note that the APTs in any coordinate system can be calculated by simply entering the appropriate transformation matrix.

10. FLUX
    Disk input - charge derivatives in S coordinates (Nx3N), U (3Nx3N), principal cartesian coordinates
    Operator input- masses and transformation matrix from principal cartesian coordinates to original coordinates
    Terminal output-atomic charge derivatives in original cartesian coordinates and charge flux tensors in original cartesian coordinates
    Disk output - none
    Description - transforms atomic charge deriatives from S coordinates to mass weighted principal cartesian coordinates by using U. Then, using the transformation matrix and the masses, calculates atomic charge derivatives in original cartesian coordinates. The charge flux tensors are finally calculated by multiplying the charge derivatives by the appropriate cartesian coordinates. These tensors can be calculated in any coordinate system by entering the appropriate transformation matrix from principal cartesians to the coordinate system desired.

11. PXPQ
    Disk input - P_X (3x3N), ℓ^{-1} (3Nx3N), U (3Nx3N), P_S (3x3N)
    Operator input- transformation matrix from principal cartesians to original coordinates, adjustment of APT elements
    Terminal output-intensities using adjuted APTs in km/mole
    Disk output - none
    Description - uses U and P_S to calculate translational and rotational corrections to intensities. Transforms ℓ^{-1} from principal cartesian coordinates to original coordinates using the transformation matrix. Calculates intensities using P_X and transformed ℓ^{-1},

subtracting translational and rotational corrections so that the intensities corresponding to these motions are zero. Allows the operator to adjust any element of any APT in the molecule and then recalculate the intensities. This ma be done as many times as is desired.

12. BMAT
    Disk input - principal cartesian coordinates
    Operator input- internal coordinate definitions
    Terminal output-internal coordinate definitions, B matrix
    Disk output - B matrix
    Description - the little S vector techniques are used to calculate the B matrix elements for the internal coordinates; bond stretching, angle bending, wagging, torsional bending and linear bending. The operator defines the number of the coordinate, the type, and the atoms involved in the coordinate. A weighting factor may be applied, but if none is specified, 1.0 is assumed. If two coordinates are given the same number, then that coordinate is the sum of the two coordinates. A coordinate number of Ø signifies that no more coordinates are to be defined.

13. AMATRIX
    Disk input - B matrix
    Operator input - masses
    Terminal output - A matrix
    Disk output - A matrix
    Description - using the technique described in Chapter 2, a nonredundant set of internal coordinates described by the B matrix is used to calculate the G matrix. G is then inverted and used to calculate the A matrix such that A B = E and B A = E.

14. FORCE
    Disk input - F_S (3Nx3N0, U (3Nx3N), A
    Operator input - masses
    Terminal output - force constants in internal coordinates
    Disk output - force constants in internal coordinates
    Description - F_S are transformed to K (force constants in mass weighted principal cartesians) with U, then further transformed to force constants in principal cartesians with the masses. Finally, A is used to transform into force constants in internal coordinates (F_i).

15. PERTURB
    Disk input - F_i, B matrix
    Operator input - masses, adjustment of force constants
    Terminal output - adjusted force constants, and resulting frequencies
    Disk output - ℓ^{-1} matrix for adjusted frequencies
    Description - allows the operator to adjust any number of any of the internal force constants, then uses the masses and B matrix to transform these adjusted constants to mass weighted principal cartesian force constants. This matrix is then diagonalized to give the frequencies calculated with these adjusted constants. These adjustments can be made as often as desired. Finally, the final calculated ℓ^{-1} matrix corresponding to the final calculated frequencies may be written to disk. A "return" signifies that no more force constants are to be adjusted.

16. VIBCORDS
    Disk input - principal cartesians, ℓ^{-1} matrix (3Nx3N)
    Operator input - masses, displacement increment
    Terminal output - none
    Disk output - cartesian coordinates of displaced normal coordinates, $Q_i \pm \Delta Q_i$
    Description - the values of Q are calculated by multiplying the principal cartesians, the masses and ℓ^{-1}. The Q's are then displaced by $\pm\Delta Q_i$ where the increment is input by the operator. Using these displaced Q's, the displaced cartesians corresponding to these displaced Q's are calculated. This is repeated (both + and - ΔQ_i) for each Q.

17. VIBRATE (written in BASIC)
    Disk input - principal cartesians, cartesian coordinates of displaced normal coordinates
    Operator input - radii of atoms, rotation matrix
    Terminal output- XY projection of molecule, option to vibrate molecule along any normal coordinate
    Disk output - none
    Description - draws a ball and stick model of the XY projection of the molecule with the radii input, then draws bonds between the specified atoms. Allows rotation of the molecule by entering the appropriate transformation matrix. Furthermore, the picture can be labelled. Finally, the molecule can be made to vibrate along any of its normal coordinates. This vibration

can be frozen in either $\pm\Delta Q_i$ phase, or another normal coordinate can be chosen to vibrate along by pressing "C". The bonds are no longer drawn by entering -1, 2, labelling is ended by typing "Control E."

SUBROUTINES (all contained in library MYLIB.REL)

1. FILEREAD - reads a file from disk
2. FILERITE - writes a file to disk
3. MULTIP - multiplies two matrices
4. JACOBI - diagonalizes a square symmetrix matrix
5. SQINUT - inverts a square symmetrix matrix
6. STRET - calculates B matrix elements for stretching coordinate
7. BEND - calculates B matrices elements for bending coordinate
8. OPLA - calculates B matrix elements for wagging coordinate
9. TORS - calculates B matrix elements for torsional bending coordinate
10. LIBE - calculates B matrix elements for linear bending coordinates
11. VECTOR - calculates the vector between two atoms given cartesian coordinates
12. DOTP - calculates the dot product of two vectors
13. CROSS - calculates the cross product of two vectors
14. SINE - calculates the sine of an angle from the cos of an angle

APPENDIX B
NORMAL COORDINATE TRANSFORMATION MATRICES

The normal coordinate transformation matrices used in these calculations have all been stored on 8 inch floppy disks. These disks are formatted single side double density for use with the CP/M operating system, version 2.2 (73). These data sets were created with Microsoft FORTRAN-80 (74) source code. These matrices have been stored as vectors, in row order, one element at a time, and should be read into memory in the same fashion. This appendix contains a list of filenames corresponding to the various normal coordinate transformation matrices used in these calculations, for all of the systems studied here.

1. Theoretical Water Monomer (_MONOT) (N = number of atoms)
   Principal cartesian coordinates XMONOT (3xN)
   U matrix UMONOT (3Nx3N)
   Force constants (K) *S* coordinates FMONOT (3Nx3N)
   Dipole derivatives (P_S) *S* coordinates DMONOT (3x3N)
   Normal coordinate transformation (ℓ^{-1}) principal cartesians LMONOT (3Nx3N)
   Atomic Polar Tensors (P_x) original cartesians PMONOT (3x3N)
   Atomic charge derivatives for calculating charge flux tensors, *S* coordinates CMONOT (Nx3N)
   B matrix (B) principal cartesians BMONOT (# internal coordinates x 3N)
   A matrix (A) principal cartesians AMONOT (3N x # internal coordinates)
   Internal force constants (F_i) IMONOT (# internal coordinates x # internal coordinates)
   Coordinates for picturing normal vibrations NMONOT (dimensions not needed)

The filenaming convention employed here is the same in every case. The system being calculated is given a code name (up to seven letters and/or numbers) and then the appropriate matrices are defined by the one letter prefix, as given above. In some instances (i.e., in the case that redundancies exist in internal coordinates), two additional matrices may have to be defined. These matrices are the transformation matrix from the redundant set of internal coordinates to the nonredundant set of symmetry coordinates, and then the symmetrized B matrix. These matrices are given the prefix codes Q and S respectively.

The code names for the systems studied here are listed below.

2. Linear Dimer R = 2.832 A° (_LINDIMT)
   R = 2.982 A° (_LINDIM1)
   R = 2.682 A° (_LINDIM2)
   R = 3.132 A° (_LINDIM3)
   R = 2.532 A° (_LINDIM4)

3. Cyclic Dimer R = 2.74 A° (_CYCDIM1)
   R = 2.65 A° (_CYCDIM2)
   R = 2.99 A° (_CYCDIM3)
   R = 2.74 A° No inversion center (_CYCDIM4)

4. Bifurcated Dimer R = 2.90 A° (_BIFDIM1)
   R = 3.05 A° (_BIFDIM2)
   R = 2.90 A° perpendicular molecules (_BIFDIM3)

5. H_2O^+ (_H2OP)

6. $O \cdot H_2O \cdot O$ (_H2O3N)

7. $O^{-1} \cdot H_2O \cdot O^{-1}$ (_H2O3-2)

8. $O^{-2} \cdot H_2O \cdot O^{-2}$ (_H2O3-4)

APPENDIX C
REDUNDANT INTERNAL COORDINATES

In the case where more internal coordinates than vibrational degrees of freedom are defined, a redundancy condition exists. This means that the set of internal coordinates are dependent, and the redundancy is the linear dependency between some of the coordinates chosen. The function which describes the redundancy condition does not change throughout vibrational motion and therefore makes no contribution to the solutions of the secular equation. If one chooses to simply eliminate the dependent coordinates then it is often the case that the potential function cannot be properly described in terms of symmetry coordinates. Therefore one usually constructs as many symmetry coordinates as there are internal coordinates where one (or more) of these symmetry coordinates is exactly the redundancy condition and can be easily removed. However, the set of appropriate symmetry coordinates is not unique, and depends in part on both the geometry and the original internal coordinates defined. In addition, it can be shown that while the potential function in symmetry coordinates uniquely defines the vibrational properties of the molecule, the potential function in the original set of internal coordinates is not uniquely defined.

If $\bar{R}$ is the set of redundant interanl coordinates (where in this case we use an example with one redundancy), then the transformation to symmetry coordinates $\bar{S}$ is written

$$\bar{S}(N) = \underline{U}(N \times (N+1))\ \bar{R}((N+1) \times 1) \tag{99}$$

where $\underline{U}$ is a transformation matrix, $\bar{R}$ contains one redundancy condition and is of dimension (N+1), $\bar{S}$ is of dimension (N) because the redundancy has been explicitly defined and removed, and $\underline{U}$ is of dimensions (N x (N+1)). If we assume that $\underline{U}$ represents a unitary transformation matrix, then the following are true:

$$\underline{U}(N \times (N+1))\ \underline{U}^{+}((N+1) \times N) = E(NxN) \tag{100a}$$

$$\underline{U}^{+}((N+1)\ xN)\ \underline{U}(N \times (N+1)) = E((N+1) \times (N+1)) \tag{100b}$$

Using this assumption, equation 99 may be pre-multiplied by $\underline{U}^{+}$ to give

$$\bar{R} = \underline{U}^{+}\bar{S} \tag{101}$$

or by substituting with equation 99

$$\bar{R} = (\underline{U}^{+}\underline{U})\ \bar{R} \tag{102}$$

The set of internal coordinates $\bar{R}$ were originally defined to contain a redundancy condition. Equation 102, in conjunction with equation 100b directly contradicts this statement. If equation 100b is correct, then equation 102 indicates that there is a one-to-one correspondence in the internal coordinate space, or that the internal coordinates are linearly independent. However, the presence of a redundancy condition necessitates that the internal coordinates by linearly

dependent. Thereefore, we may conclude that the assumption that $\underline{U}$ is a unitary transformation matrix is not correct, and subsequently, equation 100b is not true,

$$\underline{U}^{+}((N+1) \times N)\ \underline{U}(N \times (N+1)) \neq E((N+1) \times (N+1)) \tag{103}$$

Therefore we define

$$\underline{C}((N+1) \times (N+1)) = \underline{U}^{+}\underline{U} \tag{104}$$

Using equation 100, we note write

$$\underline{C}\cdot\underline{C} = \underline{U}^{+}\underline{U}\underline{U}^{+}\underline{U} = \underline{U}^{+}\underline{U} = \underline{C} \tag{105}$$

$$\underline{C}^{2} = \underline{C} \quad \text{or} \quad \underline{C}^{2}-C = O\underline{E}((N+1) \times (N+1) \tag{106}$$

$$\underline{C}(\underline{C}-\underline{E}) = 0 \tag{107}$$

where if we premultiply equation 107 by the inverse of $\underline{C}$ we obtain

$$(\underline{C}-\underline{E}) = 0 \quad \text{or} \quad \underline{C} = \underline{E} \tag{108}$$

but equation 108 directly contradicts equation 103, so we must conclude that $\underline{C}$ has no inverse, or in other words

$$|\underline{U}^{+}\underline{U}| = |\underline{C}| = 0 \tag{109}$$

The potential energy of this system can be expressed as

$$2V = \overline{S}^{+}\underline{F_s}\overline{S} = \overline{R}^{+}\underline{U}^{+}\underline{F_s}\underline{U}\overline{R} = \overline{R}^{+}\underline{F_i}F \tag{110}$$

where we have made use of equation 99 and where

$$\underline{F_i} = \underline{U}^{+}\underline{F_s}\underline{U} \tag{111}$$

Alternately, we can write the potential energy as

$$2V = \bar{R}^{+} \underline{F_i} \bar{R} = \bar{S}^{+} \underline{U F_i U}^{+} \bar{S} = \bar{S}^{+} \underline{F_s} \bar{S} \tag{112}$$

where we make use of equation 101. Therefore, we obtain

$$\underline{F_s} = \underline{U F_i U}^{+} \tag{113}$$

By substituting equation 113 into equation 111 and using equation 104 we obtain

$$\underline{F_i}' = \underline{U}^{+} \underline{U F_i U}^{+} \underline{U} \quad \text{or} \quad \underline{F_i}' = \underline{C F_i C} \tag{114}$$

Equation 114 points out the fact that $\underline{F_i}$ cannot be unique, but rather the transformation given by equation 114 can be successively applied an infinite number of times, and each $\underline{F_i}'$ is different, but correctly determines $\underline{F_s}$ via equation 113.

Therefore, we have shown that while the values of $\underline{F_s}$ are determinable and can be used to solve the vibrational secular equation, the transformation of these parameters back to $\underline{F_i}$ in the original redundant coordinates is not uniquely determined.

REFERENCES

1. L.J. Bellamy, Advances in Infrared Group Frequencies (Methuen and Co. Ltd., London, 1968).

2. Vibrational Intensities in Infrared and Raman Spectroscopy (W.B. Person and G. Zerbi, Eds.) (Elsevier, Amsterdam, 1982).

3. W.B. Person and D. Steele, Molecular Spectroscopy (R.F. Barrow, D.A. Long, and D.J. Millen, Eds.) (The Chemical Society, London, 1974), Vol. 2, pp. 357-438.

4. L.M. Sverdlov, M.A. Kovner, and E.P. Krainov, Vibrational Spectra of Polyatomic Molecules (John Wiley and Sons, New York, 1974).

5. M. Gussoni and S. Abbate, J. Chem. Phys., 65 (1976) 3439.

6. L.A. Gribov, Intensity Theory for Infrared Spectra of Polyatomic Molecules (English translation) (Consultants Bureau, New York, 1964.

7. J.F. Biarge, J. Herranz, and J. Morcillo, An. R. Soc. Esp. Fis. Quim., A57 (1961) 81.

8. W.B. Person and J.H. Newton, J. Chem. Phys., 61 (1974) 1040; 64 (1976) 3036.

9. M. Gussoni, Vibrational Intensities in Infrared and Raman Spectroscopy (W.B. Person and G. Zerbi, Eds.)(Elsevier, Amsterdam, 1982), Chapter 5.

10. E.B. Wilson, Jr., J.C. Decius, and P.C. Cross, Molecular Vibrations (McGraw-Hill, New York, 1955).

11. S. Califano, Vibrational States (John Wiley and Sons, New York, 1976).

12. C.E. Blom, P.J. Slingerland, and C. Altona, Mol. Phys., 31 (1976) 1359.

13. C.E. Blom and C. Altona, Mol. Phys., 31 (1976) 1377.

14. C.E. Blom, L.P. Otto, and C. Altona, Mol. Phys., 32 (1976) 1137.

15. C.E. Blom, Ph.D. Dissertation, University of Leiden, The Netherlands, 1976.

16. W.J. Hehre, R.F. Stewart, and J.A. Pople, J. Chem. Phys., 51 (1969) 2657.

17. S. Chin, I. Scott, K. Szczepaniak, and W.B. Person, accepted for publication by J. Am. Chem. Soc.

18. S. Chin and W.B. Person, accepted for publication by J. Phys. Chem.

19. A.J. Tursi and E.R. Nixon, J. Chem. Phys., 52 (1970) 1521.

20. M. Van Thiel, E.D. Becker, and G.C. Pimentel, J. Chem. Phys., 27 (1957) 486.

21. P.V. Huong and J.-C. Cornut, J. Chem. Phys., 72 (1975) 534.

22. B. Mann, T. Neikes, E. Schmidt, and W.A.P. Luck, Ber. Bunsenges Phys. Chem., 78 (1974) 1236.

23. R.E. Barletta, Ph.D. Dissertation, Brown University, 1977.

24. W.A.P. Luck, in The Hydrogen Bond (P. Schuster, G. Zundel, and C. Sandorfy, Eds.) (North Holland Publishing, New York, 1976), Vol. 2, Chapter 11.

25. R.M. Bentwood, A.J. Barnes, and W.J. Orville-Thomas, J. Mol. Spectrosc., 84 (1980) 391.

26. W.A. Hagen and A.G.G.M. Tielenes, J. Chem. Phys., 75 (1981) 4198.

27. A. Behrens and W.A.P. Luck, J. Mol. Struct., 60 (1980) 337.

28. G.P. Ayers and A.D.E. Pullin, Spectrochim. Acta, 32A (1976) 1629.

29. L. Fredin, B. Nelander, and G. Ribbergard, J. Chem. Phys., 66 (1977) 4065.

30. L.A. Curtiss and J.A. Pople, J. Mol. Spectrosc., 55 (1975) 1.

31. A.H. Popkie, H. Kistenmacher, and E. Clementi, J. Chem. Phys., 59 (1973) 1325.

32. J. Del Bene and J.A. Pople, J. Chem. Phys., 52 (1970) 4858.

33. P.A. Kollman and L.C. Allen, J. Chem. Phys., 51 (1969) 3286.

34. K. Morokuma and J.R. Winick, J. Chem. Phys., 52 (1970) 1301.

35. G.H.F. Diercksen, Theoret. Chim Acta, 21 (1971) 335.

36. K. Morokuma and L. Pedersen, J. Chem. Phys., 48 (1968) 3275.

37. P. van Hensbergen, R. Block, and L. Jansen, J. Chem. Phys., 76 (1982) 316.

38. L.L. Shipman, J.C. Owicki, and H.A. Scheraga, J. Phys. Chem., 78 (1974) 2055.

39. B. Zilles and W.B. Person, J. Chem. Phys., 79 (1983) 65.

40. R.C. Kerns and L.C. Allen, J. Am. Chem. Soc., 100 (1978) 6587.

41. B. Zilles, Ph.D. Dissertation, University of Florida, 1980.

42. D. Hadzi and S. Bratos in The Hydrogen Bond (P. Schuster, G. Zundel, and C. Sandorfy, Eds.) (North-Holland Publishing, New York, 1976), Vol. 2, Chapter 12.

43. G.C. Pimentel and A.L. McClellan, The Hydrogen Bond (Freeman, San Francisco, 1960), p. 248.

44. J.B. Bates, M.J. Dudney, G.M. Brown, J.C. Wang, and R. Frech, J. Chem. Phys., 77 (1982) 4838.

45. J.B. Bates, R. Frech, H. Engstrom, J.C. Wang, and T. Kaneda, Solid State Ionics, 1 (1980) 15.

46. I.M. Mills in Infrared Spectroscopy and Molecular Structure (M. Davies, Ed.) (Elsevier, Amsterdam, 1963), Chapter 5.

47. J.D. Rogers, Ph.D. Dissertation, University of Florida, 1980.

48. R.G.A. Maia, Ph.D. Dissertation, University of Florida, 1980.

49. C. Eckart, Phys. Rev., 47 (1935) 552.

50. A. Sayvetz, J. Chem. Phys., 6 (1939) 383.

51. C.L. Perrin, Mathematics for Chemists (Wiley-Interscience, New York, 1970), pp. 177-178.

52. F.A. Cotton, Chemical Applications of Group Theory (Wiley-Interscience, New York, 1963) (Second Edition), pp. 295-339.

53. L.A. Curtiss and J.A. Pople, J. Mol. Spectrosc., 48 (1973) 413.

54. W.J. Hehre, M.D. Newton, J.S. Binkley, R.A. Whiteside, P.C. Hariharan, R. Seeger, and J.A. Pople, "Gaussian 76- An Ab Initio Molecular Orbital Program," Program No. 391, Quantum Chemistry Program Exchange, Indiana University, Bloomington, IN. IBM version translation by C.M. Cook, Department of Chemistry, Princeton University, Princeton, NJ.

55. W.T. King in Vibrational Intensities in Infrared and Raman Spectroscopy (W.B. Person and G. Zerbi, Eds.)(Elsevier, Amsterdam, 1982), Chapter 6.

56. J.D. Rogers and J.J. Hillman, J. Chem. Phys., 77 (1982) 3615.

57. W.B. Person in Vibrational Intensities in Infrared and Raman Spectroscopy (W.B. Person and G. Zerbi, Eds.) (Elsevier, Amsterdam, 1982), Chapter 4.

58. I.W. Lewin and R.A.R. Pearce in Vibrational Spectra and Structure (J.R. Durig, Ed.)(Elsevier, New York, 1975), Vol. 4, Chapter 3.

59. C.L. Perrin, Mathematics for Chemists (Wiley-Interscience, New York, 1970), p. 222.

60. J. Overend in Infrared Spectroscopy and Molecular Structure (M. Davies, Ed.) (Elsevier, Amsterdam, 1963), Chapter 10.

61. J. Overend in Vibrational Intensities in Infrared and Raman Spectroscopy (W.B. Person and G. Zerbi, Eds.)(Elsevier, Amsterdam, 1982), Chapter 2.

62. B. Crawford, Jr., J. Chem. Phys., 29 (1958) 1047.

63. B. Crawford, Jr., J. Chem. Phys., 20 (1952) 977.

64. W.T. King, G.B. Mast, and P.P. Blanchette, J. Chem. Phys., 56 (1972) 4440.

65. G.B. Mast and W.T. King, J. Phys. Chem., 80 (1976) 2004.

66. W.T. King and G.B. Mast, J. Phys. Chem., 80 (1976) 2521.

67. J.C. Decius and G.B. Mast, J. Mol. Spectrosc., 70 (1978) 294.

68. J.C. Decius, J. Mol. Spectrosc., 57 (1975) 348.

69. W.B. Person, B. Zilles, J.D. Rogers, and R.G.A Maia, J. Mol. Struct., 80 (1982) 297.

70. R.S. Mulliken, J. Chem. Phys., 23 (1955) 1833, 1841, 2338, 2343; Ibid., 36 (1962) 326.

71. R. Ditchfield, W.J. Hehre, and J.A. Pople, J. Chem. Phys., 51 (1971) 724.

72. P. Pulay, G. Fogarasi, and J.E. Boggs, J. Chem. Phys., 74 (1981) 3999.

73. Digital Research CP/M Version 2.2 Manual (Digital Research, Los Angeles, CA, 1978).

74. MicroSoft BASIC, MicroSoft FORTRAN, and MicroSoft BASIC COMPLIED User's Guides (MicroSoft, Inc., Seattle, Washington, 1981).

75. W.A. Lathan, W.H. Hehre, L.A. Curtiss, and J.A. Pople, J. Am. Chem. Soc., 93 (1971) 6377.

76. W.S. Benedict, N. Gailor, and E.K. Plyler, J. Chem. Phys., 24 (1956) 1139.

77. S.A. Clough, Y. Beeres, G.D. Klein, and L.S. Rothman, J. Chem. Phys., 59 (1973) 2254.

78. E. Menna, R. Moccia, and L. Randaccio, Theo. Chim Acta, 4 (1966) 408.

79. R.J. Bartlett, private communication.

80. W.B. Person in Vibrational-Rotational Spectroscopy for Planetary Atmospheres, NASA Conference Publication 2223 (M.J. Mumma, K. Fox, and J. Hornstein, Eds.), Vol. I., pp. 89-123 (1982)

81. T.R. Dyke, K.M. Mack, and J.S. Muenter, J. Chem. Phys., 66 (1977) 498.

82. S. Motherwell, "PLUTO (Early Version), A Program for Plotting Molecular and Crystal Structures," University Chemical Laboratory, Lensfield Road, Cambridge, CB2 IEW England. Special thanks to G. Palenik, University of Florida, for providing a copy of the source listing for this program.

83. H. Ratajczak and W.J. Orville-Thomas, J. Mol. Struct. 1 (1967) 449.

84. R. Gold, J.M. Dowling, and A.G. Meister, J. Mol. Spectrosc., 2 (1958) 9.

85. S. Califano and B. Crawford, J., Z. Electrochem., 64 (1960) 571.

86. J.C. Decius, J. Chem. Phys., 17 (1949) 1315.

87. M. Gussoni, G. Dellepiane, and S. Abbate, J. Mol. Spectrosc., 57 (1975) 323.

88. C.E. Sun, R.G. Parr, and B. Crawford, Jr., J. Chem. Phys., 17 (1949) 840.

89. B. Crawford, Jr. and W.H. Fletcher, J. Chem. Phys., 19 (1951) 840.

90. E.B. Wilson, Jr., J. Chem. Phys., 9 (1941) 76.

91. S. Chin, T.A. Ford, and W.B. Person, submitted to J. Mol. Struct.

92. P. Lorrain and D.R. Corson, Electromagnetic Fields and Waves (W.H. Freeman and Company, San Francisco, 1970).

93. M. Gussoni, P. Jona, and G. Zerbi, J. Chem. Phys., 78 (1983) 6802.

94. S. Chin, unpublished work at the University of Florida.

96. S. Chin and W.B. Person, Paper WE-5 presented at the 37th Symposium of Molecular Spectroscopy, Columbus, Ohio, June 14-18, 1982.

96. J. Overend, Applied Spectroscopy, 37 (1983) No. 1, ix.

97. J.J. Hillman, private communication.

BIOGRAPHICAL SKETCH

Steven Chin was born on July 4, 1957, in Flushing, New York. He then did his undergraduate studies at State University of New York at Binghamton, where he received his Bachelor's degree in chemistry in May of 1979. He entered the graduate school at the University of Florida in August of 1979, and is receiving the Ph.D. degree in chemistry in April of 1984.

I certify that I have read this study and that in my opinion it conforms to acceptable standards of scholarly presentation and is fully adequate, in scope and quality, as a dissertation for the degree of Doctor of Philosophy.

Willis B. Person

Willis B. Person, Chairman
Professor of Chemistry

I certify that I have read this study and that in my opinion it conforms to acceptable standards of scholarly presentation and is fully adequate, in scope and quality, as a dissertation for the degree of Doctor of Philosophy.

Earle E. Muschlitz, Jr.

Earle E. Muschlitz, Jr.
Professor of Chemistry

I certify that I have read this study and that in my opinion it conforms to acceptable standards of scholarly presentation and is fully adequate, in scope and quality, as a dissertation for the degree of Doctor of Philosophy.

John R. Eyler

John R. Eyler
Associate Professor of
Chemistry

I certify that I have read this study and that in my opinion it conforms to acceptable standards of scholarly presentation and is fully adequate, in scope and quality, as a dissertation for the degree of Doctor of Philosophy.

James D. Winefordner

James D. Winefordner
Graduate Research Professor
of Chemistry

I certify that I have read this study and that in my opinion it conforms to acceptable standards of scholarly presentation and is fully adequate, in scope and quality, as a dissertation for the degree of Doctor of Philosophy.

Thomas L. Bailey

Thomas L. Bailey
Professor of Physics

This dissertation was submitted to the Graduate Faculty of the Department of Chemistry in the College of Liberal Arts and Sciences and to the Graduate School, and was accepted as partial fulfillment of the requirements for the Degree of Doctor of Philosophy.

April 1984

Dean for Graduate Studies
and Research

UNIVERSITY OF FLORIDA
3 1262 08554 0010